

**MAMMALIAN MSS51 IS A NEWLY DESCRIBED,
SKELETAL MUSCLE-SPECIFIC GENE**

by
Adam L. Moyer

A dissertation submitted to the Johns Hopkins University in conformity with the
requirements of the degree of Doctor of Philosophy.

Baltimore, Maryland
December 2015

© 2015 Adam L. Moyer
All Rights Reserved

Abstract

Skeletal muscle is a complex system with robust ability to repair and regenerate after damage. Modulation of the pathways involved in these processes are very important in the context of muscle disease, where muscle progressively wastes or degenerates and loses its ability to regenerate efficiently. One such pathway relies on nitric oxide (NO) signaling, which we modulated with the phosphodiesterase inhibitor sildenafil and the soluble guanylate cyclase activator BAY 60-2770 in the mouse models of muscle injury and muscular dystrophy, respectively, and showed no benefit from either treatment method.

An additional pathway of interest is the myostatin pathway, whose inhibition leads to muscle hypertrophy and altered muscle metabolism. The altered metabolic program includes changes in mRNA levels of many metabolic genes, including the newly-described skeletal muscle-specific gene *Mss51*, presented here. Expression patterns of *Mss51* were described in various tissues of mice and humans, and in muscles of different fiber type distributions. *Mss51* was predominantly expressed in glycolytic muscle groups, and in humans, the protein product MSS51 localized to the mitochondria.

The effect of ablation of *Mss51* was examined in C2C12 immortal myoblasts as well as in mice and primary myoblasts. Decreased *Mss51* expression resulted in altered myosin heavy chain expression, increased expression of genes involved in fatty acid oxidation, and altered metabolic function as shown with the Seahorse metabolic flux analyzer in C2C12 myotubes and treadmill endurance in *Mss51*^{-/-} mice. Overall, *Mss51* was shown to be a skeletal muscle-specific gene playing a role in the regulation of metabolic processes specifically in glycolytic muscle groups.

Advisor:

Dr. Kathryn Wagner

Thesis Committee:

Dr. Jonathan Pevsner (Chair)

Dr. Thomas Clemens (Reader)

Dr. Eva Chin (2013-present)

Dr. Robert Bloch (2011-2013)

Acknowledgements

First and foremost, I'd like to thank my advisor, Dr. Kathryn Wagner, for years of guidance, support, and motivation. She encouraged me through many failed experiments and contradictory results and trained me to be a better scientist and critical thinker. She demonstrates her passion for her work at all times in a truly inspiring manner. Additionally, my thesis committee members Drs. Jonathan Pevsner, Thomas Clemens, Eva Chin, and Robert Bloch have all provided me with invaluable advice and insight into my thesis project and future career options. I greatly appreciate the time they invested in me across the years. I am also thankful for the guidance and advice of Drs. Alexandra McPherron and Se-Jin Lee.

I would also like to thank the great team that has made up the Center for Genetic Muscle Disorders throughout my time here. In the lab, I've been immensely helped by Jessica Miciak, Leigh Johnson, Naili Liu, Tracy Zhang, Kenneth Estrellas, Courtney Young, Melanie Branagan, Tatiana Cohen, and too many more to list. I could not imagine a better group of people to celebrate significant results and commiserate over the not-so-good outcomes. I'm also thankful to the great people working in the clinic and on clinical trials within the Center for Genetic Muscle Disorders who helped to keep my eyes open to the relevance of my work, no matter how basic my projects seemed.

Before starting graduate school, I had the great opportunity of working for a fellow CMM alumnus, Dr. Christopher Buck. Chris opened my eyes to the world of molecular biology, and I appreciate his patience in teaching me to think scientifically and encouraging me to study at Johns Hopkins. Without him, I'm not sure I would have even

applied to CMM, and I'm so glad I did. As a student in CMM, I've greatly appreciated the support and guidance of Dr. Rajini Rao, Leslie Lichter, and Colleen Graham.

Additionally, my decision to join the CMM program introduced me to several lifelong friends. Laura Gottschalk, Sara Sinclair, Laurene Cheung, and Emily Cousins helped me solve problems in class and in lab, as well as provided me with many great memories to carry with me. We've gone through so much together as a group, and without them the struggles of graduate school would have been a lot more painful.

To the friends I've gathered across the years, the support has been amazing. Living on different coasts and different continents, Kim, Christine, Diana, Natalya, Courtney, and Riana have been staples in my life for over a decade. While it hasn't always been easy to get together, I greatly value every minute I do get to spend with them.

To my family, I appreciate years of patience, love, and support. I appreciate that my parents learned early to not ask me when I was graduating or how my project was going. I'm so glad that finally I have answers and updates on that front. I'll never be able to repay the debts I owe them for everything they have done for me throughout my life. I'm thankful for Amanda and Ash, for being a great sister and soon-to-be brother-in-law – you both are hilarious and I'm lucky to have you as friends.

My greatest discovery in Baltimore did not happen in the lab. I'm so lucky to have met Bill in 2011, and I'm thankful for his companionship, love, and support through this process. He opened my eyes to the world around me and convinced me to leave my comfortable bubble in Mount Vernon and experience life in Hollins Market in Southwest

Baltimore. Making a home with him (and Dino, of course) has been a great experience and I look forward to many years and dogs to come.

I'd also like to acknowledge those who I lost during the Ph.D. process. My grandparents, Dr. and Mrs. Ray Landes, are sorely missed. I'm thankful to my grandfather for introducing me to the world of medical thought at an early age, and to my grandmother for passing on several truly cherished family recipes and teaching me to make pink applesauce – a staple of my Pennsylvania Dutch childhood. In April of 2014, I said goodbye to my first pit bull and best friend, Edgar. He both got me through some of my toughest days and caused some of the others, but I learned a lot about enjoying life and making adult decisions from my time with him, even though it was far too short.

Table of Contents

Abstract	ii
Acknowledgements	iv
Table of Contents	vii
Chapter 1. Introduction	1
<i>Overview</i>	2
<i>Introduction</i>	3
<i>Cells of the immune system initiate the response to injury</i>	4
<i>Muscle cells and their progenitors receive and provide trophic cues</i>	8
<i>Connective tissue cells alter skeletal muscle integrity</i>	12
<i>Conclusion</i>	14
Chapter 2. Modulating Nitric Oxide Signaling in Models of Skeletal Muscle Regeneration and Muscular Dystrophy	17
<i>Abstract</i>	18
<i>Introduction</i>	19
<i>Materials and Methods</i>	22
<i>Results</i>	26
<i>Discussion</i>	29
<i>Figures</i>	32
Chapter 3. Mammalian <i>Mss51</i> is a skeletal muscle-specific gene modulating cellular metabolism	40
<i>Abstract</i>	41
<i>Introduction</i>	43
<i>Materials and Methods</i>	46
<i>Results</i>	54
<i>Discussion</i>	62
<i>Figures</i>	67
<i>Supplementary Data</i>	74
Chapter 4. Generation and preliminary characterization of <i>Mss51</i>^{-/-} mice	77
<i>Abstract</i>	78
<i>Introduction</i>	79
<i>Materials and Methods</i>	82
<i>Results</i>	87
<i>Preliminary Conclusions</i>	91
<i>Future Directions</i>	93
<i>Figures</i>	96
References	102
Curriculum Vitae	117

List of Figures and Tables

Chapter 1. Introduction

<i>Figure 1.1. Stages of muscle regeneration.</i>	16
---	----

Chapter 2. Modulating Nitric Oxide Signaling in Models of Skeletal Muscle Regeneration and Muscular Dystrophy

<i>Figure 2.1. Regeneration after cardiotoxin injury.</i>	32
<i>Figure 2.2. Cross sectional area (CSA) of injured myofibers does not significantly change after sildenafil treatment.</i>	33
<i>Figure 2.3. Cross sectional area of myofibers varies between individual mice after cardiotoxin injury irrespective of sildenafil treatment.</i>	34
<i>Figure 2.4. Gene expression of three myogenic regulatory factors does not significantly change with sildenafil treatment in regenerating TAs 5 days after injury.</i>	35
<i>Figure 2.5. Representative images of quadriceps and triceps from control mice and mice treated BAY 60-2770.</i>	36
<i>Figure 2.6. CSA analysis of mdx mice treated with BAY 60-2770.</i>	37
<i>Figure 2.7. Myofiber CSA varies between individual mice regardless of BAY 60-2770 treatment.</i>	38
<i>Table 2.1. BAY 60-2770 serum levels.</i>	39

Chapter 3. Mammalian *Mss51* is a skeletal muscle-specific gene modulating cellular metabolism

<i>Figure 3.1. <i>Mss51</i> expression in vitro.</i>	67
<i>Figure 3.2. <i>Mss51</i> tissue expression.</i>	68
<i>Figure 3.3. Subcellular localization of <i>MSS51</i>.</i>	69
<i>Figure 3.4. CRISPR/Cas9-disruption of <i>Mss51</i> locus in C2C12 myoblasts.</i>	70
<i>Figure 3.5. <i>Mss51</i>-disrupted myoblasts proliferate and differentiate normally.</i>	71
<i>Figure 3.6. Gene and protein expression in <i>Mss51</i>-disrupted differentiated myotubes</i>	72
<i>Figure 3.7. Glycolysis and Oxidative Phosphorylation in <i>Mss51</i>-disrupted cells.</i>	73
<i>Supplementary Figure 3.1. Proliferation of <i>Mss51</i>-disrupted cells compared to control.</i>	74
<i>Supplementary Figure 3.2. <i>PGC1α</i> expression.</i>	75
<i>Supplementary Figure 3.3. Expression of several metabolic proteins in control versus <i>Mss51</i>-disrupted myotubes.</i>	76

Chapter 4. Generation and preliminary characterization of *Mss51*^{-/-} mice

<i>Figure 4.1. Generation and genetic characterization of <i>Mss51</i>^{-/-} mice.</i>	96
<i>Figure 4.2. <i>Mss51</i> mRNA from <i>Mss51</i>^{-/-} mice is missing exons 1 and 2.</i>	97
<i>Figure 4.3. <i>Mss51</i>^{-/-} primary cells proliferate and differentiate normally.</i>	98
<i>Figure 4.4. Gene expression and ATP content of <i>Mss51</i>^{-/-} primary myotubes.</i>	99
<i>Figure 4.5. <i>Mss51</i>^{-/-} mice do not differ in size from wild-type mice.</i>	100
<i>Figure 4.6. <i>Mss51</i>^{-/-} mice appear to differ metabolically from wild-type mice.</i>	101

Chapter 1. Introduction

Overview

In **Chapter 1**, I will provide an introduction to skeletal muscle regeneration in the context of injuries and disease, including therapeutic strategies such as inhibition of the TGF- β superfamily member myostatin and modulation of nitric oxide signaling, adapted and expanded from a review article we wrote entitled “Regeneration versus fibrosis in skeletal muscle” [1]. In **Chapter 2**, I will present a study that used sildenafil, a phosphodiesterase 5 inhibitor, and BAY 60-2770, a soluble guanylate cyclase activator, to modulate nitric oxide signaling in mouse models of muscle injury and muscular dystrophy, respectively. In **Chapter 3**, I will present the *in vitro* characterization of the gene *Mss5l*, which came to our attention after we showed its expression to be regulated by myostatin inhibition *in vivo*. *Mss5l* is a skeletal muscle-specific gene not previously described in mammals. It is encoded in the nucleus but the protein product was shown to localize to the mitochondria, and it is involved in the modulation of metabolic processes including fatty acid utilization and ATP production. In **Chapter 4**, I will introduce the *Mss5l*^{-/-} mouse model we created. The CRISPR/Cas9 system for genetic engineering was used to delete parts of the first 2 exons of *Mss5l* and we have started to characterize the resulting phenotype. Preliminary results will be presented, as well as plans for the continued characterization of the mouse model.

Introduction

Skeletal muscle repair and regeneration are processes that need to be better understood to provide the best treatment possible for numerous conditions, including traumatic injury and muscular dystrophy. Muscular dystrophy is a group of numerous genetic conditions characterized by progressive skeletal muscle weakness and the death of muscle fibers. In these conditions, muscle fibers initially undergo normal repair processes but with time, normal regeneration is not able to keep up with the pace of degeneration and muscle necrosis, leading to the characteristic pathology including fibrosis, fatty infiltration, increased inflammation, and decreased muscle integrity. Our lab studies the complex processes involved in muscle repair and regeneration.

The process of repairing skeletal muscle balances regeneration and fibrosis with results ranging from complete regrowth of myofibers within their original basal lamina to complete replacement of muscle fibers by fat and fibrosis. Several immune, myogenic, and stromal cell types must interact to direct injured skeletal muscle toward a pathway of complete regeneration. Conversely, in certain environments such as those found in chronic muscle disorders, these same cells direct the establishment of fibrosis. For purposes of discussion, regeneration from an acute injury of skeletal muscle can be divided into three distinct phases, although *in vivo*, these processes are highly interdependent. First, immune cells infiltrate and phagocytose necrotic tissue releasing numerous cytokines. Second, muscle progenitors proliferate, differentiate, and fuse to form new myofibers. Third and finally, the extracellular matrix (ECM) is remodeled and fibroblasts undergo apoptosis or proliferate (see Figure 1.1). The critical roles of immune, myogenic, and stromal cells will first be explored, as well as their key mediators in the

repair of skeletal muscle from injury. Injury models serve as a controlled way to study the regenerative processes that occur continuously in chronic muscle disease. Numerous experimental injury models exist, including mechanical injuries, such as crush and freeze injury, or chemical injuries, such as injection of barium chloride or the snake venom cardiotoxin. While the method by which injury is achieved differs, the general processes that result are similar in each model.

Cells of the immune system initiate the response to injury

Following injury, various cells of the immune system, including macrophages and lymphocytes, are activated within or attracted to skeletal muscle. The functions of these immune cells are crucial to the muscle's successful regeneration. Their activity is carefully mediated by factors that contribute to the final endpoint, which is either regenerated muscle or fibrotic tissue. Both resident and recruited macrophages of a variety of populations, defined by surface marker expression linked to function, appear necessary in the processes, whereas specific T cell response types may also play a role in the balance between fibrosis and regeneration.

Resident macrophages can be found in the connective tissue of muscle, in both the epimysium enveloping the entire muscle and the perimysium surrounding bundles of muscle fibers called fascicles, but rarely in the endomysium surrounding individual fibers [2]. Resident macrophages release cytokine-induced neutrophil chemoattractant and monocyte chemoattractant protein 1 (MCP-1, also called CC chemokine ligand 2, CCL2) after injury, leading to the recruitment of neutrophils and monocytes from vascular

circulation [2]. This initial cellular response is marked by a release of inflammatory mediators including tumor necrosis factor alpha (TNF- α) and an accumulation of neutrophils and subsequent macrophages. The response subsists for several days and is widely accepted as an integral feature of myorepair (as reviewed by Chazaud *et al.* [3]). CCL2 and other chemokines implicated in monocyte/macrophage recruitment signal through the C-C chemokine receptor 2 (CCR2), which is found on a variety of bone marrow-derived cells, as well as non-bone marrow-derived cells such as fibroblasts and endothelial progenitor cells. The importance of CCR2 signaling to skeletal muscle regeneration was first demonstrated in *CCR2*-null mice in which regeneration was shown to be greatly decreased [4]. Bone marrow-derived cells have been implicated as the critical *CCR2* expressing cell type mediating regeneration [5]. Using bone marrow chimeras, *CCR2* expression in bone marrow-derived cells, but not skeletal muscle, was found to be necessary for the mononuclear cell infiltration present at 3 and 7 days after injury [5]. *CCR2* expression in bone marrow-derived cells was also linked to larger myofiber size and smaller areas of residual necrosis 21 days after injury [5]. Interestingly, in animals receiving *CCR2*^{-/-} bone marrow, there were higher numbers of myogenic progenitor cells (MPCs) after 7 days [5]. In a complementary study, Lu *et al.* recently showed that a CCR2 ligand, *CCL2*, must be expressed in both bone marrow-derived cells and muscle tissue for adequate repair [6]. Again using various bone marrow chimeras, recruitment of wild-type macrophages by *CCL2*-deficient injured muscles was markedly impaired whereas wild-type bone marrow completely restored muscle inflammation in *CCR2* null mice [6]. There remain important questions left unanswered, such as which cells of the muscle tissue (e.g. myoblasts, myofibers, endothelial cells, or fibroblasts) are

required to express *CCL2* for full inflammatory response and subsequent regeneration. However, the published studies would suggest that without *CCL2/CCR2*, immune cells are not successfully activated or recruited to injured muscle and MPCs are not able to completely differentiate.

Various macrophage phenotypes and activation states dominate different phases of muscle regeneration. The early immune response to muscle injury is driven by cytokines produced by T helper 1 cells (Type 1 cytokine response), including interferon (IFN) and TNF- α , which stimulate the so-called ‘classically activated’ macrophages (M1). M1 macrophages produce both pro-inflammatory cytokines and nitric oxide, promoting muscle damage. Within 1–3 days after macrophage activation, the dominant macrophage response changes from M1 to an ‘alternatively activated’ M2 phenotype, likely caused by the phagocytosis of both apoptotic and necrotic myofibers [3]. Two subsets of M2 macrophages have been shown to be involved in muscle regeneration and are activated by different cytokines produced by T helper 2 cells (Type 2 cytokine response): M2a by interleukin (IL)-4 and IL-13, and M2c by IL-10 (for an excellent and more extensive review of this subject, see Tidball and Villalta [7]). M2 macrophages both abrogate inflammation by deactivating M1 macrophages and release cytokines that promote tissue repair and nonmyeloid cell proliferation. Additionally, the relative involvement of various macrophage phenotypes has been shown to affect the severity of muscle pathology in muscular dystrophy models, linking nitric oxide of an M1 response with most severe muscle damage [8]. For example, muscle damage can be lessened with the appearance of an M2a response due to competition for L-arginine between inducible nitric oxide synthase (*iNOS*, expressed by M1 macrophages) and arginase (expressed by

M2a macrophages) [8]. Simultaneously, expression of *IL-10* increases, deactivating M1 and stimulating M2c macrophages [8]. To deactivate potentially damaging M1 macrophages in the *mdx* mouse model of Duchenne muscular dystrophy (DMD), Villalta *et al.* treated mice with IL-10, which was linked to decreased *iNOS* expression and increased levels of M2c macrophages [9]. Conversely, when the authors ablated *IL-10* expression, *iNOS* expression and muscle damage increased, and strength and endurance were reduced [9]. These experiments indicate that IL-10 could serve as a potential therapeutic target to reduce harmful aspects of the inflammatory response and subsequent fibrosis.

In addition to secreted cytokines, additional immunoregulatory molecules have recently been found to play critical roles in normal muscle regeneration. One example is stem cell antigen-1 (Sca-1), which is implicated in stem cell self-renewal and expressed on multiple hematopoietic cell types as well as myoblasts following muscle injury [10]. Sca-1 is necessary for the recruitment of soluble IgM and C3 complement to damaged muscle, which results in lysis of the cell followed by phagocytosis of the fragments by macrophages [11]. In the absence of Sca-1, there is reduced recruitment of IgM and B-1a cells, the non-conventional B cell subset that produces autoantibodies recognizing the altered surface patterns of damaged tissue [11]. Long *et al.* showed that TGF- β 1 produced by macrophages in regenerating muscle negatively regulates the expression of *Sca-1* in both myogenic and immune cells, including T cells, B cells, and macrophages [12]. Without Sca-1, the activity of matrix metalloproteinases (MMPs), enzymes responsible for ECM remodeling, is reduced, contributing to increased fibrosis in *mdx* mice [10].

The immune response to skeletal muscle damage is both complex and critical, and must be considered in all studies of muscle regeneration. Lagrota-Candido *et al.* remind us of that fact in a recent study characterizing fibrosis and muscle regeneration in different mouse strains [13]. In a bupivacaine injury model, they showed that C57BL/6 mice, which produce a dominant Type 1 cytokine response, had successful regeneration with limited fibrosis whereas BALB/c mice, with their dominant Type 2 cytokine response, developed both higher levels of fibrosis and increased *TGF-β* expression [13]. BALB/c^{nu/nu} mice developed a similar high deposition of collagen indicating that this fibrotic response is not secondary to T cell activity [13]. These results not only underscore the importance of properly controlling for the genetic background in animal models of muscle regeneration but also the complexity of the cytokine response to muscle injury that is not fully elucidated.

Muscle cells and their progenitors receive and provide trophic cues

Following the initial inflammatory phase dominated by the presence of immune cells, normal muscle regeneration is marked by the proliferation and differentiation of MPCs. Most muscle regeneration occurs through the proliferation of myogenic cells, called satellite cells due to their position on the periphery of the muscle fiber beneath a common basal lamina. However, it is now clear that satellite cells are not a homogeneous population and that other progenitor cells, including those derived from the interstitium and bone marrow, have myogenic potential. Myogenic cells produce growth factors that act in autocrine and paracrine manners, further directing muscle regeneration or fibrosis.

Satellite cells have traditionally been the focus of much research in muscle regeneration. The vast majority of these studies are in murine models. It is challenging to obtain large numbers of primary satellite cells from human muscle, due to their low prevalence in adult tissue and the invasive nature of muscle biopsies. It therefore remains to be shown whether human satellite cells exhibit the same behaviors and antigenic markers as mouse satellite cells. For example, Pax7, a paired box transcription factor, is a reliable marker of quiescent and activated mouse satellite cells but appears to only recognize a subset of human satellite cells as defined by neural cell adhesion molecule positivity and sublaminar position (for a complete review of human versus murine antigenic markers see Boldrin *et al.* [14]). Another difficult aspect in the study of satellite cells is that in both species, satellite cells are heterogeneous populations [15]. Even from satellite cells isolated from the same mouse fiber, a large range of proliferative potential and variability of antigenic markers have been demonstrated.

MPC function is highly dependent on environmental factors as has been demonstrated in elegant heterochronic parabiotic studies. Exposure of old muscle to youthful blood circulation stimulated proliferation of MPCs, enhanced regeneration and reduced fibrosis following injury [16,17]. The local and systemic environmental factors responsible for determining MPC function and their relative importance have not yet been clearly defined. However, the heterochronic parabiotic studies, among others, implicate the Notch signaling pathway as a key determinant of muscle regeneration [16,17]. Pharmacologically increasing Notch signaling, or inhibiting the opposing Wnt signaling pathway, leads to enhanced reparative ability of satellite cells in aged muscle.

Conversely, increased Wnt signaling is associated with increased fibrosis and may induce MPCs to alter their fate from myogenic to fibrogenic lineage [16].

Other important factors in the local environment modulating MPC behavior include IGF-1, TGF- β 1, and myostatin. IGF-1 is likely the major pro-growth factor, stimulating MPC proliferation and differentiation and reducing muscle fibrosis. IGF-1 is expressed from a host of tissues, and within muscle is expressed by myofibers and macrophages [6,18]. Recently, a relationship between IGF-1 and Sonic hedgehog, both known to promote MPC proliferation and differentiation, was proposed [19]. IGF-1 acts cooperatively with Sonic hedgehog and its effector, smoothened, to stimulate the expression of myogenic regulatory factors, and increase the activation of PI3K-Akt and MAPK/ERK pathways in myoblasts [19].

Myostatin, also known as growth differentiation factor 8 (GDF8), is a TGF- β family member expressed predominantly in skeletal muscle. The function of myostatin was first described by Se-Jin Lee and Alexandra McPherron's characterization of myostatin knockout mice, which showed significant increases in body weight and muscle mass [20]. As decreased levels of myostatin lead to increased muscle mass, its inhibition is of high interest in the context of diseases of muscle wasting. Myostatin has been shown to be an autocrine and paracrine inhibitor of muscle growth, and its inhibition results in increased muscle growth and reduced fibrosis in animal models of chronic muscle disease. Conversely, myostatin directly promotes fibroblast proliferation resulting in muscle fibrosis *in vivo* [21].

Myostatin signals by binding a membrane-bound activin type II receptor, which results in the recruitment of the co-receptor ALK4 or ALK5, initiating a signaling cascade within the muscle. Inhibition of myostatin can be achieved using ActRIIB-Fc, a soluble activin type IIB receptor that binds and sequesters myostatin. ActRIIB-Fc treatment leads to rapid and dramatic increases in muscle mass in normal mice [22,23] and decreased fibroblast proliferation and fibrosis in dystrophic muscle (Z.B. Li and K.R. Wagner, unpublished observation). Gene expression profiling in mice treated with ActRIIB-Fc as well as in myostatin knockout mice has shown many changes in gene expression, with altered pathways including oxidative phosphorylation, mitochondrial function, citrate cycle, and pyruvate metabolism [24]. Additionally, in both ActRIIB-Fc treated mice and myostatin knockout mice there is decreased Type I slow fiber myosin heavy chain isoform expression and a trend toward decreased expression of the major slow fiber type determinant peroxisome proliferator-activated receptor- γ coactivator-1 α . *PGC-1 α* [24]. Further understanding of the diverse effects of myostatin inhibition is needed.

ActRIIB-Fc has been developed by Acceleron/Shire as the drug ACE-031 and was eagerly anticipated for the treatment of chronic muscle diseases prior to recent clinical trials in Duchenne muscular dystrophy being terminated for unacceptable side effects unrelated to its action on skeletal muscle (ClinicalTrials.gov Identifier NCT01099761). Pharmacological development of myostatin inhibitors continues, however, with alternative approaches and current high hopes for the introduction of follistatin, a nonspecific biological antagonist of myostatin. Transgenic overexpression of follistatin in mice was recently demonstrated to facilitate regeneration as well as reduce

fibrosis after injury in mice [25]. Follistatin gene delivery via adeno-associated virus serotype-1 induced increases in muscle size and strength without systemic toxicity in cynomolgus macaques, paving the way for clinical trials in inclusion body myositis [26]. As the biology of myostatin continues to be elucidated, additional targets are suggested: myostatin transcripts are subject to microRNA (miRNA)-mediated silencing indicating that it may be possible augment or mimic this biological modulator to inhibit myostatin activity [27]. Additional targets may arise as the effects of myostatin inhibition are better understood, including targets altering metabolic processes.

Connective tissue cells alter skeletal muscle integrity

Muscle is intimately linked to connective tissue, where several cell types are involved in regeneration and referred to collectively as muscle resident stromal cells (mrSCs). These include fibroblasts, responsible for ECM and collagen synthesis, adipocytes which replace muscle fibers in disease and aging, and fibro/adipogenic progenitors (FAPs), bipotential cells that can become either fibroblasts or adipocytes. These cell types play important roles in successful muscle regeneration, but if not kept in check, contribute to a self-perpetuating process of fibrosis.

Recent studies describe important roles for stromal progenitor cells, FAPs, found in the endomysial compartment between myofibers. Following muscle injury, FAPs begin to proliferate among MPCs and damaged myofibers (*in vivo*) and provide trophic factors that stimulate myoblast differentiation (*in vitro*) [28]. When regeneration is effective, FAPs drop back down to their initial population size [28]. It is believed that

when this process goes awry, an inhibitory signal is missed and FAPs differentiate into adipocytes or fibroblasts, increasing fibrosis or fatty infiltration [29]. Conversely, direct cell contact with regenerating myofibers inhibits the differentiation of FAPs into adipocytes [30]. Less is known about the ability of FAPs to differentiate into fibroblasts *in vivo*, as the lack of selective fibroblast markers in skeletal muscle hampers this field in general. However, in skeletal muscle, the expression of the tyrosine kinase platelet-derived growth factor receptor alpha (*PDGFR α*) appears to be selective for FAPs [30]. Conditional *PDGFR α* knock-in mice have diffuse fibrosis in skeletal muscle, as well as other organs, suggesting that proliferation of FAPs may be sufficient to induce endomysial fibrosis and suggesting another therapeutic target for chronic myopathies [31].

Additional evidence of the paracrine regulation of muscle growth by mrSCs is provided in an important study by Mathew *et al.* [32], describing the transcription factor *Tcf4*, which is strongly expressed by muscle tissue fibroblasts. Using Cre-activated expression of diphtheria toxin, the authors genetically ablated *Tcf4*-positive fibroblasts to demonstrate that fibroblasts modulate the determination of muscle fiber type, showing a reduced frequency of type I fibers in mice without *Tcf4*-positive fibroblasts [32]. These studies were performed in developing and normal adult muscle and the effects of *Tcf4* in models of muscle regeneration will be important subsequent studies [32].

Connective tissue cells can be regulated by a variety of mechanisms, presenting some additional targets that may have anti-fibrotic potential. In other organ systems, fibrosis is modulated by miRNAs, which may target TGF- β , tissue inhibitors of metalloproteinases, or other mRNA targets. Depending on the target, the silencing effects

can result in either increased or decreased levels of fibrosis. Such a miRNA-based approach has recently been successfully demonstrated in a murine model of cardiac fibrosis [33]. Further studies in this area are anticipated to lead to new treatments that could be useful in a variety of chronic skeletal muscle diseases.

Conclusion

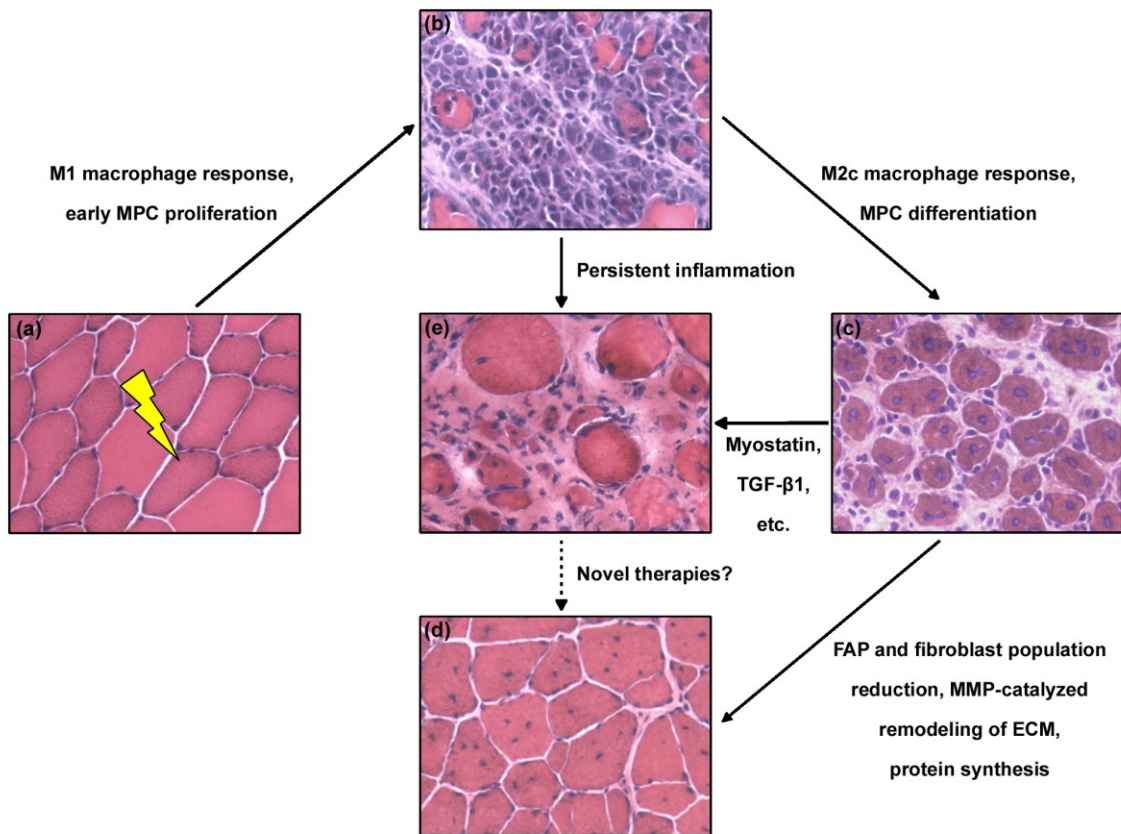
In the past, many studies have focused primarily on muscle precursor cells and the factors that inhibit or stimulate their activities, but recent work has highlighted the interactions of immune and stromal cells with myogenic cells that results in regeneration of the muscle tissue. One theme that is emerging from these studies is that the timing of activation, proliferation, and differentiation of immune, muscle progenitor, and connective tissue cells is critical. Different cell types, as well as the factors that mediate them, may play unique and opposing roles at different times during the regeneration process. This will have implications not only to the design of novel therapeutics but potentially to the implementation of their clinical use.

Two areas of intense interest in the treatment of muscle disease have been modulation of nitric oxide signaling and inhibition of myostatin, both of which will be explored in greater detail in the following chapters. Nitric oxide (NO) is produced by nitric oxide synthase (NOS), an enzyme that, in mammals, exists in three isoforms: eNOS, or endothelial NOS; iNOS, or inducible NOS; and nNOS, or neuronal NOS, which is the predominant form expressed in skeletal muscle. The role of iNOS-produced NO in breaking down injured muscle was previously mentioned, but nNOS-produced NO

is an important signaling molecule within muscle fibers affecting calcium handling [34]. In Duchenne muscular dystrophy, the lack of the dystrophin-glycoprotein complex causes nNOS to mislocalize, decreasing NO production and signaling. Therefore, there is clinical interest in increasing levels or activity of members of the NO signaling pathway, which will be further explored in Chapter 2.

Myostatin inhibition causes numerous changes, including alterations in muscle growth, fat accumulation, and metabolic processes. One of these changes is the downregulation of *Mss5l* (formerly known as *Zmynd17*), a gene that was not previously described in mammalian systems. In Chapters 3 and 4, evidence for the role of *Mss5l* in metabolic regulation will be explored.

Figure 1.1. Stages of muscle regeneration. Normal muscle (a) is injured, inciting an immune response including M1 macrophages and stimulating muscle progenitor cell (MPC) proliferation. Following 1-2 days of muscle fiber necrosis and early inflammation (b), an M1 macrophage response is substituted for an M2c macrophage response, which accompanies MPC differentiation and leads to nascent muscle fibers by 3-5 days post injury (c). Muscle regeneration is completed by 1 month following injury (d) with increased protein synthesis in nascent myofibers, reduction in fibro/adipogenic precursors (FAP) and fibroblast populations, and remodeling of the extracellular matrix (ECM) by matrix metalloproteinases (MMPs). Alternatively, in the presence of persistent inflammation and growth factors such as myostatin and TGF- β 1, fibroblasts continue to proliferate and express collagen and other ECM components and a self-perpetuating process of fibrosis ensues (e). Development of novel therapeutics to resolve fibrosis and rescue surviving muscle progenitor cells to form new myofibers is needed.



***Chapter 2. Modulating Nitric Oxide Signaling in Models of
Skeletal Muscle Regeneration and Muscular Dystrophy***

Abstract

The nitric oxide signaling pathway provides multiple therapeutic targets for modulation of skeletal muscle regeneration and health in contexts including the muscular dystrophies. We treated cardiotoxin-injured wild-type mice with sildenafil and measured changes in cross sectional area and gene expression. We also used the *mdx* model of Duchenne muscular dystrophy (DMD) to examine the effects of treatment with BAY 60-2770, a soluble guanylate cyclase activator, during the first six weeks postnatal, during which the mice undergo massive waves of degeneration and regeneration. In both cases, we did not find significant differences between treated and untreated animals, indicating that modulation of nitric oxide signaling was insufficient to improve the examined outcomes in these model systems.

Introduction

Duchenne muscular dystrophy (DMD) is caused by mutations in the dystrophin gene that result in a lack of functional protein [35]. Becker muscular dystrophy (BMD) is also caused by mutations in dystrophin, though patients with BMD produce some partially functional dystrophin, leading to less severe pathology [36]. Dystrophin is an integral part of the dystrophin-glycoprotein complex (DGC), anchoring many other proteins to the sarcolemma [37]. Without dystrophin, these other members mislocalize, are expressed at lower levels, and are less functionally active. One of the members of the complex known to mislocalize is neuronal nitric oxide synthase (nNOS), which produces nitric oxide (NO) and activates soluble guanylate cyclase (sGC) [38]. sGC catalyzes the production of cyclic guanosine monophosphate (cGMP), which has been linked to changes in intracellular calcium levels that play important roles in muscle contraction and health [34]. As NO signaling is decreased when nNOS mislocalizes away from the sarcolemma, there has been interest in pharmacologically modulating downstream players in the pathway to maximize cGMP levels in the muscle of muscular dystrophy patients.

One way to achieve this is by inhibition of phosphodiesterase 5, which cleaves cGMP. PDE5 inhibitors include sildenafil (Viagra and Revatio) and tadalafil (Cialis). PDE5 is found in various tissues including the corpus cavernosum and vascular smooth muscle, platelets, and skeletal muscle. PDE5 inhibitors cause vasorelaxation by blocking the hydrolysis of cGMP, increasing the cGMP-induced activation of protein kinase G [39]. Sildenafil was initially explored as a drug for the treatment of heart disease and hypertension, but its side effects caused it to be marketed instead for the treatment of

erectile dysfunction [39]. While that remains its most common indication, there has been renewed interest in the use of sildenafil in the treatment of both cardiac and skeletal muscle diseases [34,39,40].

An alternate method to modulate the NO pathway is to use sGC activators that increase the production of cGMP in a NO-independent manner. One such sGC activator is BAY 60-2770, which, like sildenafil, has also been shown to ameliorate erectile dysfunction and cause vasorelaxation in animal models [41–44].

To explore the effects of modulating NO signaling in skeletal muscle, we used two different model systems: sildenafil treatment in a cardiotoxin injury model and BAY 60-2770 treatment in the *mdx* mouse model of DMD. Cardiotoxins are the main component of the venom of cobras. In our injury model, the cardiotoxin used is harvested from *Naja nigricollis*, the black-necked spitting cobra. It specifically affects and destroys muscle fibers by causing depolarization and contraction, leaving the muscle progenitor population, or satellite cells, to survive and regenerate functional muscle [45]. This injury model is commonly studied because it causes a uniform and synchronous wave of degeneration and necrosis followed by complete muscle regeneration. The *mdx* mouse model is commonly used to study dystrophinopathies, though the phenotype is not equivalent to that of a patient with DMD [46]. The *mdx* mice undergo massive waves of degeneration and regeneration early in life. By adulthood (approximately 8 weeks), the muscle appears relatively normal though centrally nucleated, which indicates that it has undergone regeneration [47]. These models allowed us to examine the effect of PDE5 inhibition from acute injury through muscle repair and the effect of sGC activation through the period of major degeneration and regeneration in the *mdx* mouse.

Materials and Methods

Animals

All animal experiments were performed in accordance with the guidelines of the Institutional Animal Care and Use Committee at the Johns Hopkins University School of Medicine. Wild-type (C57Bl/6J) and *mdx* (C57Bl/10ScSn-Dmd^{mdx}/J) were obtained from the Jackson Laboratories (Bar Harbor, ME). Animals were maintained on a 12h:12h light:dark schedule with *ad libitum* access to food and water. Animals were euthanized by inhalation overdose of isoflurane and cervical dislocation. Total blood was removed from *mdx* mice using cardiac puncture, and serum was isolated using serum separator microtainer tubes (BD, Franklin Lakes, NJ, USA).

Administration of sildenafil and BAY 60-2770

For sildenafil treatment, two days before cardiotoxin injury, six-to-eight week old male wild-type mice began drug treatment. Mice were fed transgenic dough diet (Bio-Serv, Flemington, NJ, USA) containing sildenafil at a concentration of 1 mg per gram of dough. 20 mg tablets of sildenafil were generously provided by David Kass (Johns Hopkins University School of Medicine, Baltimore, MD, USA). Tablets were processed into a fine powder using a mortar and pestle. The powder was then carefully kneaded into the dough for thirty minutes at 4 degrees Celsius to ensure even distribution throughout the food. Control mice were fed transgenic dough without drug. Food was replaced every 2 days. Mice ate approximately 5 g of dough each day, which contained 5 mg of sildenafil, corresponding to a dose of 200 mg/kg/day, as the mice were

approximately 25 g. Mice were maintained on control or treated diets until sacrifice 5, 7, or 14 days post-injury.

For BAY 60-2770 treatment, mating cages of *mdx* mice were checked daily for pups. When a litter was born, they were assigned a treatment group, and on p1 (postnatal day 1), treatment was initiated. Mice were divided into three treatment groups: vehicle-only control, low dose (0.1 mg/kg) and high dose (1.0 mg/kg). Powdered BAY 60-2770 was generously provided by David Kass. BAY 60-2770 was dissolved in a solvent mixture of 70% water, 20% Cremophor EL (Sigma-Aldrich, St. Louis, MO, USA), and 10% Transcutol HP (Gattefossé, Saint-Priest, France) at a concentration of 1 mg per 10 mL solvent for the high dose and 0.1 mg per 10 mL solvent for the low dose. Animals were weighed daily and dosed via subcutaneous injection every 24 hours for the first six weeks of life with 10 μ L solution per gram bodyweight. To determine serum BAY 60-2770 concentration, serum was frozen and shipped to Bayer (Wuppertal, Germany) for analysis.

Cardiotoxin injury

To injure the tibialis anterior (TA) and induce complete muscle degeneration and regeneration, 100 μ L of 10 μ M cardiotoxin (EMD Millipore, Darmstadt, Germany) was injected intramuscularly to each TA. To perform the injection, a 25 G needle was used to enter the skin at the distal end of the TA, inserted along the length of the muscle, and 50 μ L was injected as the needle was slowly withdrawn through the muscle. This was repeated once for a total injection volume of 100 μ L.

Morphometric analysis

Muscle was harvested and frozen in pre-cooled isopentane. The muscles were cryosectioned at midbelly at a thickness of 10 μm and stained either with hemotoxylin and eosin (H&E) or with an anti-laminin primary antibody (1:1,000, Sigma-Aldrich). Fiber cross-sectional area (CSA) and central nucleation were determined in non-overlapping areas of muscle using ImageJ (National Institutes of Health, Bethesda, MD, USA). All analysis was performed using blinded samples in randomized order.

qRT-PCR

RNA was isolated from muscle homogenized in TRIzol (Life Technologies, Carlsbad, CA, USA) and extracted using the Direct-zol RNA MiniPrep kit (Zymo Research, Irvine, CA, USA). cDNA was synthesized using the SuperScript II First-Strand Synthesis kit (Life Technologies) and was diluted and used as the template for quantitative reverse transcription polymerase chain reaction (qRT-PCR) analysis, performed on the 7900HT Fast Real-Time PCR System (Applied Biosystems, Waltham, MA, USA). Validated TaqMan Probes for *MyoD*, *Myogenin*, *Myf5*, and the reference gene *Pgk1* (Applied Biosystems) were used with TaqMan Universal Master Mix II (Applied Biosystems) and analyzed using the $\Delta\Delta\text{Ct}$ method.

Statistical analysis

For analysis of CSA data, the R language for statistical analysis was used to perform a one-way nested analysis of variance (ANOVA) to compare groups and also determine the effect of animal-to-animal variability. For qRT-PCR comparisons, two-way Student's *t* tests were performed. To compare central nucleation between three treatment groups, a one-way ANOVA was used. For all comparisons, probability values

(p values) less than 0.05 were considered significant. Additionally, all plots were coded using the R language.

Results

Sildenafil treatment does not improve skeletal muscle regeneration

Mice began treatment with sildenafil two days before injury by cardiotoxin injection into the TA and continued treatment until euthanasia. Control and sildenafil-treated mice were harvested at days 5, 7, and 14 post injury. Representative histological images from each time point show the appearance of small, centrally nucleated myofibers by 5 days post injury which increase in size by 7 days post injury, and appear nearly fully regenerated by 14 days post injury (Figure 2.1). Injured myofibers remain predominantly centrally nucleated for the life of the animal, allowing for determination of efficiency of cardiotoxin delivery and injury.

From the images of H&E-stained sections, we measured cross sectional area of individual myofibers. For each animal, histogram distributions were determined and averaged within each group to allow for comparison of the fiber size distribution, and additionally the grand means \pm S.E.M. for each time point were examined (Figure 2.2). We did not find significant differences between the groups ($p = 0.38$ at day 5, $p = 0.71$ at day 7, and $p = 0.87$ at day 14), though from the histograms it does appear that the sildenafil-treated mice have a slight increase in the proportion of fibers less than 1000 μm^2 in area at days 5 and 7 post injury (Figure 2.2B, E).

Additionally, data for each individual animal were plotted as box-and-whiskers plots (Figure 2.3). As determined by a nested one-way ANOVA, the differences between individual animals were highly significant regardless of group effect ($p < 1.0 \times 10^{-15}$ at all

time points examined), which is made apparent by the fluctuations in median depicted in the box-and-whiskers plots at each time point.

We additionally performed qRT-PCR of three myogenic regulatory factors: *Myogenin*, *MyoD*, and *Myf5*. TAs were harvested 5 days after injury, and the data are displayed as relative abundance compared to the expression level in uninjured TA muscle from age- and sex-matched mice (Figure 2.4). There were no significant differences between groups in any of the examined markers, which is likely attributable to the variability between individual animals. There was a large upregulation of each marker compared to the uninjured controls, as would be expected in an animal undergoing massive skeletal muscle regeneration.

BAY 60-2770 does not ameliorate muscle pathology in young mdx mice

To examine the effect of increased nitric oxide signaling in a model of Duchenne muscular dystrophy, we treated young *mdx* mice with the Bayer sGC activator BAY 60-2770. Mice were treated for the first 6 weeks postnatal with vehicle-only control, low dose (0.1 mg/kg bodyweight) or high dose (1.0 mg/kg bodyweight) BAY 60-2770. After 6 weeks, mice were euthanized, serum was collected, and the triceps and quadriceps were flash frozen for histological analysis.

From the triceps and quadriceps, CSA was determined using laminin-stained muscle sections (Figure 2.5). Histograms and grand means comparing the control, low dose, and high dose-treated animals were plotted (Figure 2.6A-H). There were no statistically significant differences between groups, though there did appear to be a trend towards a dose-dependent decrease in CSA in animals treated with BAY 60-2770 in both

muscle groups. Additionally, we used images of the quadriceps to determine the percent of fibers with centrally located nuclei, an indicator that the fiber has undergone regeneration (Figure 2.6I). Again, there was no significant difference in the percentage of fibers centrally nucleated between the groups, though there did appear to be a slight trend towards decreased central nucleation in BAY 60-2770-treated animals. Intriguingly, 6 week-old control and high dose-treated mice had many very small myofibers as seen in their histograms, but low-dose treated animals did not (Figure 2.6A-F).

As with the sildenafil-treated animals, we also looked at the box-and-whiskers plots for each individual animal (Figure 2.7). From this, there does appear to be a general trend toward smaller fiber area in animals treated with BAY 60-2770, but it is also apparent that the inter-animal variability is large. One-way nested ANOVAs were used to compare the intra-group and inter-group variability, and it was shown that while group-to-group differences were not significant, differences between individual mice given the same treatment were highly significant ($p < 1.2 \times 10^{-26}$ for both muscles), much like what was observed in the sildenafil-treated wild-type mice.

Finally, serum levels of BAY 60-2770 were determined and are presented in Table 2.1 from all mice treated with either dosage of the drug. For all except one of the low dose-treated mice, serum levels were below the limit of detection. In the mice treated with the high dose, three had serum levels below the limit of detection, and the others had an average of 3.44 μg BAY 60-2770 per liter of serum. The variability was large, with a standard deviation of 1.69 $\mu\text{g}/\text{L}$. Additionally, the control serum sample,

which was pooled from 5 mice, gave a reading of 5.08 $\mu\text{g/L}$, which was postulated to be due to carry over from the previous sample from the high dose-treated group.

Discussion

From studies using sildenafil and BAY 60-2770, we presented preliminary data indicating that the modulation of NO signaling in muscle regeneration and a model of muscular dystrophy is not sufficient to alter the pace or magnitude of repair processes. A common concern arising from both methods is that the inter-animal variability is substantial, which may function to mask small but significant treatment effects. With that in mind, although we did not find statistical differences in the parameters examined, it is concerning that there appeared to be a slight decrease in mean myofiber CSA in a dose-dependent manner with BAY 60-2770 treatment in *mdx* mice (Figure 2.6). Simultaneously, there was a non-significant trend toward decreased central nucleation in the quadriceps of mice treated with BAY 60-2770 (Figure 2.6), a positive outcome indicating decreased susceptibility to initial fiber injury.

Many groups have modulated NO signaling in both dystrophic animals and humans using phosphodiesterase inhibitors, and the results presented have been contradictory. In *mdx* mice, sildenafil treatment has been shown to reduce diaphragm weakness and fibrosis as well as reduce functional deficits in the heart [34,40]. In human studies, these results were not replicated. Patients with Becker muscular dystrophy were given sildenafil and improvements in blood flow, maximal work capacity, and heart function were examined, but no differences were found [48]. In that study, there were no adverse effects, but that has not always been the case.

In our group's Phase 2 REVERSE-DBMD clinical trial (ClinicalTrials.gov identifier NCT01168908), adults with Duchenne or Becker muscular dystrophy (DBMD) and cardiomyopathy were recruited and randomized into sildenafil and placebo groups. The primary endpoint measurement was change in left ventricular end-systolic volume (LVESV) using cardiac magnetic resonance imaging (MRI). The trial was terminated early, after preliminary review by an independent data and safety monitoring board determined there was an average worsening of individuals on sildenafil as determined by LVESV [49]. While this may not indicate that PDE5 inhibition is dangerous in patients with DBMD, it demonstrates that it is unlikely to ameliorate the cardiomyopathy present in the patients. As a result of these studies and others, there is interest in using PDE5 inhibitors that more selectively target PDE5 over other PDE family members. Tadalafil is a more specific PDE5 inhibitor than sildenafil which also targets PDE1c.

Since there did not appear to be a benefit of sildenafil treatment in the context of injury, it may be most important to closely examine the cardiac phenotype as well as the development of fibrosis in skeletal muscle. NO signaling is important in many contexts, and we only examined changes in skeletal muscle. One such context is inflammation, which plays a key role in both muscle regeneration and the replacement of muscle with fibrosis. When *nNOS* is ablated in *mdx* mice, there is no compensatory muscle hypertrophy, and there is increased macrophage infiltration and muscle weakness [38].

There may still be hope for the use of a more specific PDE5 inhibitor or a sGC activator to treat cardiomyopathy or prevent skeletal muscle fibrosis in DBMD patients. Studies have shown some functional benefit of sildenafil in skeletal muscle, including increased protein synthesis and reduced fatigue [50]. There may also be metabolic

benefits conferred by treatment with sildenafil or tadalafil by increasing blood flow to muscle during use [51]. Significant work examining the specificity and mechanisms of action of all modulators of NO signaling need to be considered if there is any hope of finding a beneficial and safe drug for the treatment of dystrophinopathies.

Figures

Figure 2.1. Regeneration after cardiotoxin injury. Representative images of H&E stained sections of cardiotoxin-injured tibialis anterior muscles from control and sildenafil-treated mice harvested 5, 7, and 14 days after injury.

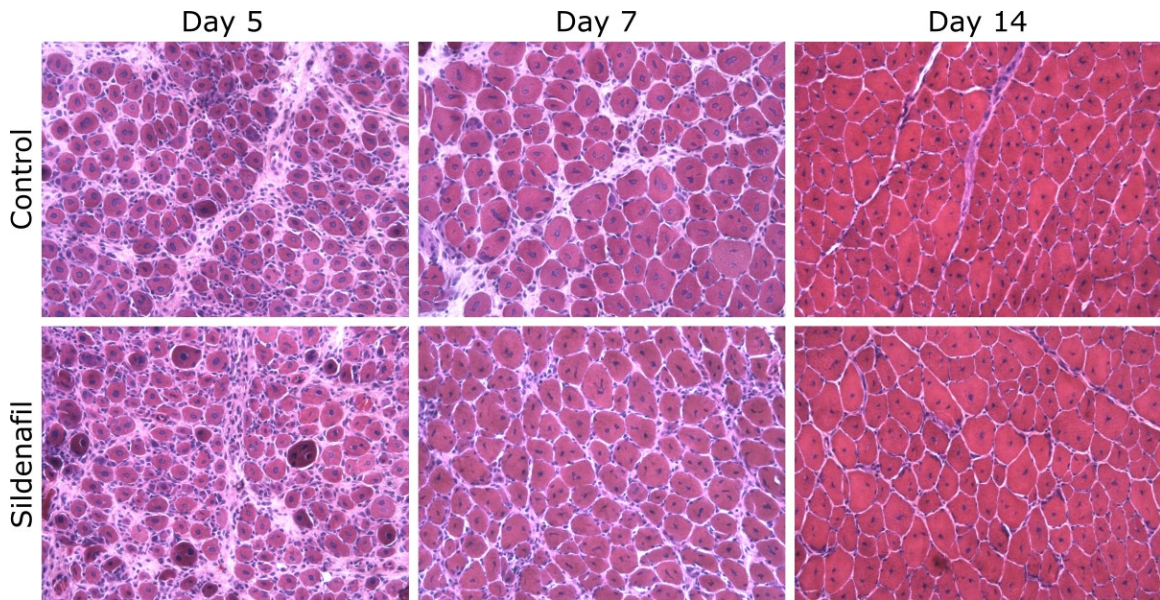


Figure 2.2. Cross sectional area (CSA) of injured myofibers does not significantly change after sildenafil treatment. Control and sildenafil-treated mice were injured and CSA was measured from H&E-stained cryosections collected 5 days (A-C), 7 days (D-F), and 14 days (G-I) post injury. For each time point, average histograms of each treatment group are presented as well as the grand means \pm the standard error of the mean. n = 2-3 mice per group.

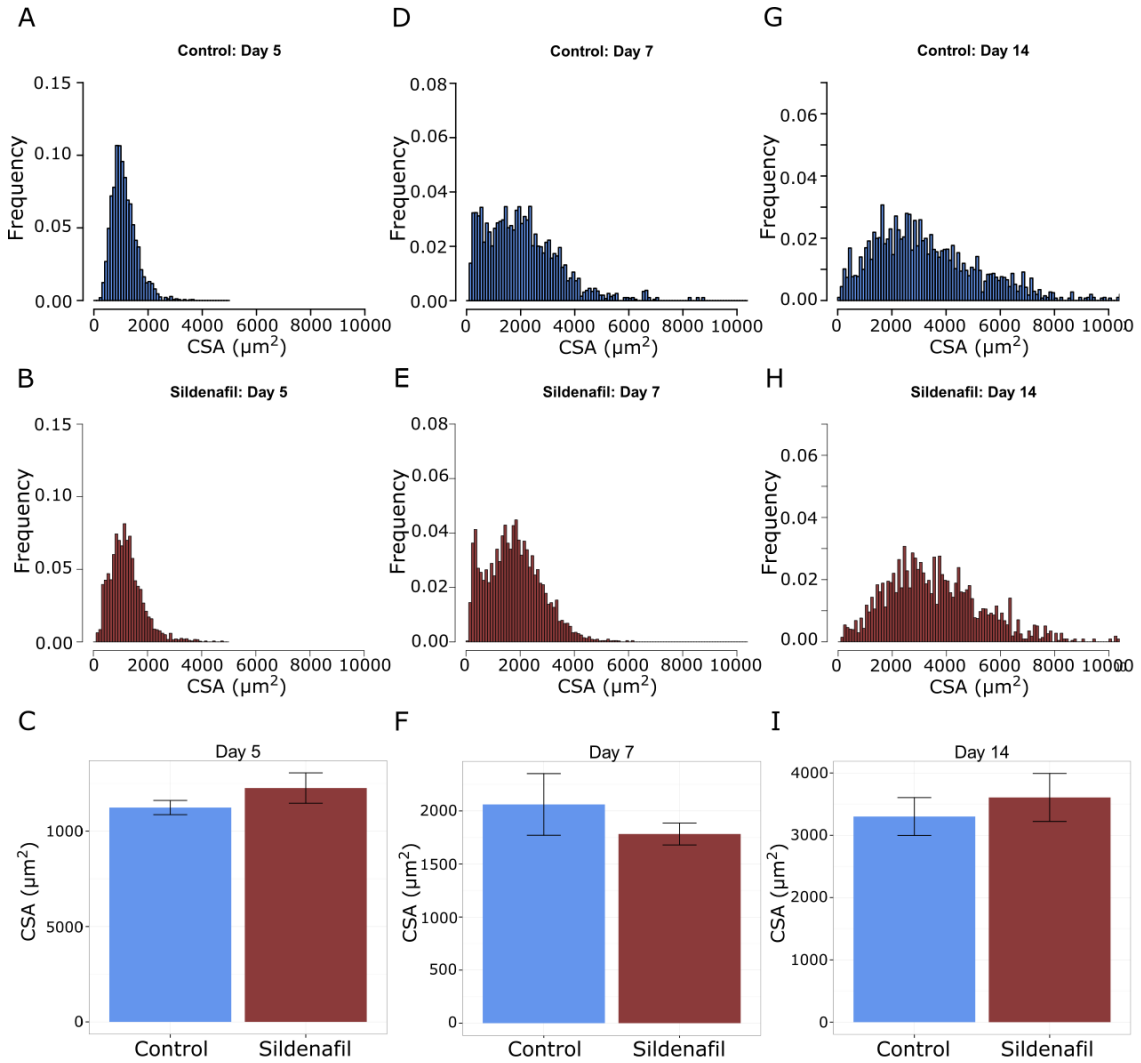


Figure 2.3. Cross sectional area of myofibers varies between individual mice after cardiotoxin injury irrespective of sildenafil treatment. Box-and-whiskers plots comparing myofiber cross sectional area in individual mice either untreated (blue) or treated with sildenafil (red) and harvested 5 (A), 7 (B), and 14 (C) days post-cardiotoxin injury.

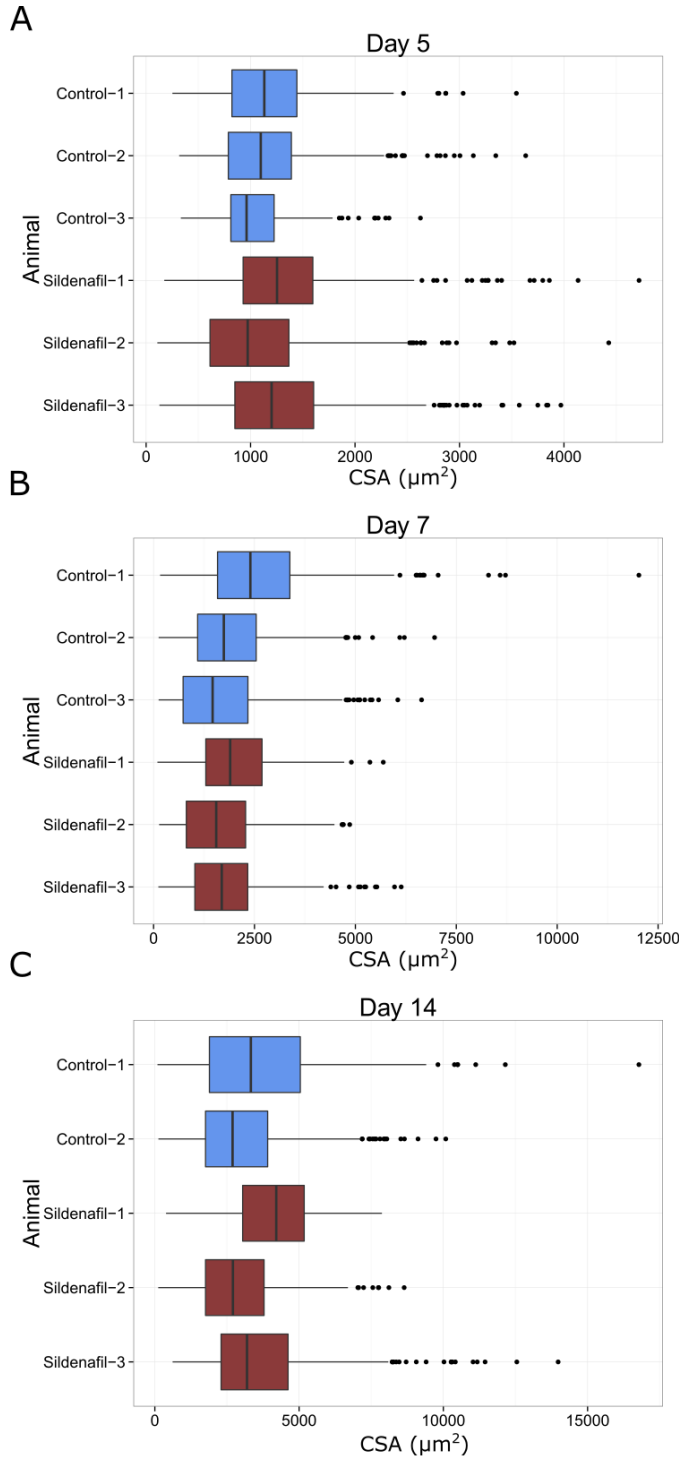


Figure 2.4. Gene expression of three myogenic regulatory factors does not significantly change with sildenafil treatment in regenerating TAs 5 days after injury. (A) *Myogenin*, (B) *MyoD*, and (C) *Myf5* mRNA expression levels were measured using qRT-PCR and normalized to uninjured TAs (not shown, relative mRNA abundance = 1). n = 3 mice per group.

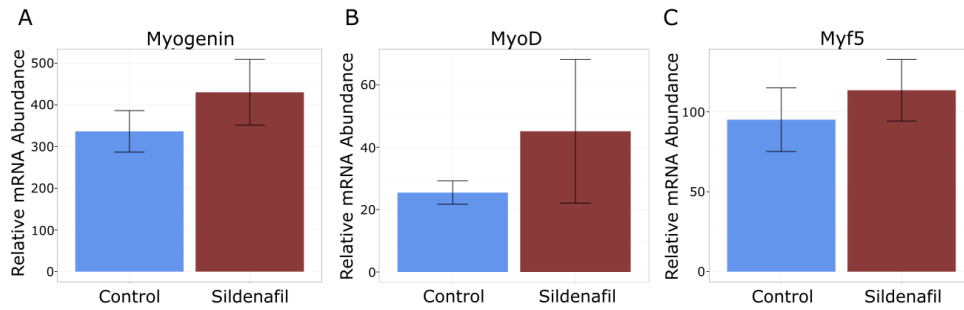


Figure 2.5. Representative images of quadriceps and triceps from control mice and mice treated BAY 60-2770. *mdx* mice were treated for 6 weeks postnatal with control (vehicle only) or a low (0.1 mg/kg) or high (1.0 mg/kg) dose of BAY 60-2770 and harvested. Laminin is shown in red, nuclei are shown by DAPI staining in blue.

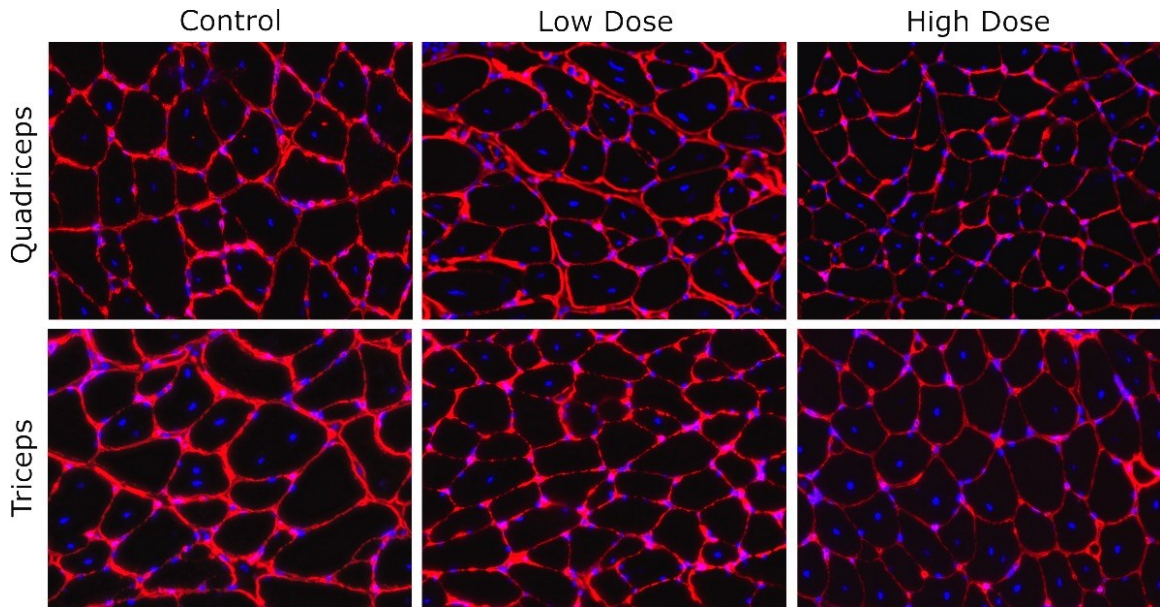


Figure 2.6. CSA analysis of *mdx* mice treated with BAY 60-2770. (A-C) Average histograms of CSA from the quadriceps of control (A), low dose (B), and high dose (C) treated mice. (D-F) Average histograms of CSA from the triceps of control (D), low dose (E), and high dose (F) treated mice. (G, H) Grand means \pm standard error of the mean of quadriceps and triceps, respectively. (I) The percent of myofibers displaying central nucleation were determined from the quadriceps, and there was a trend towards decreased central nucleation in BAY 60-2770 treated mice, though it was not statistically significant. n = 4-6 mice per group.

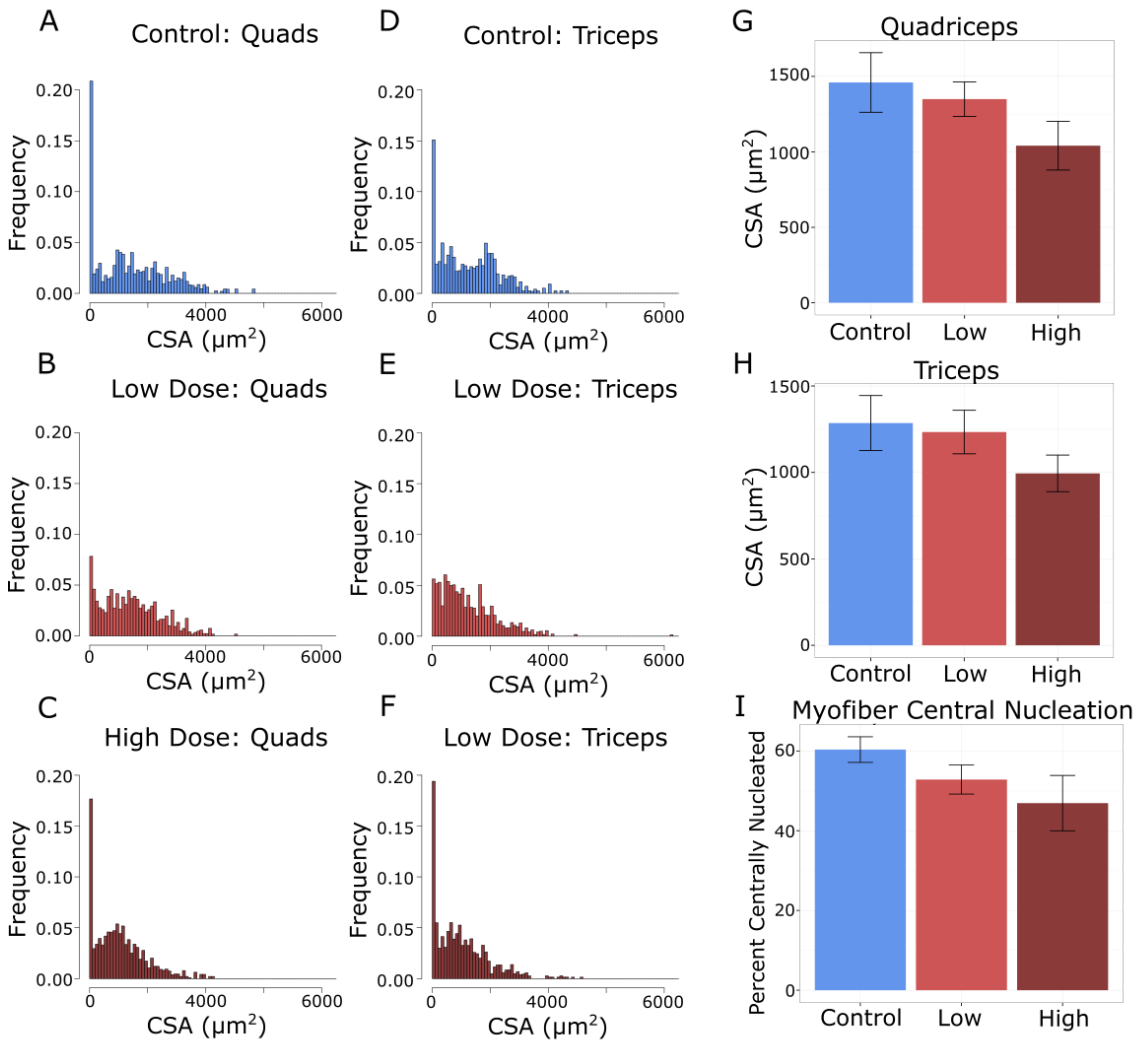


Figure 2.7. Myofiber CSA varies between individual mice regardless of BAY 60-2770 treatment. CSA determined from the quadriceps (A) and the triceps (B) shown as box-and-whiskers plots for each individual animal treated. Control animals are shown in blue, low dose-treated animals in light red, and high dose-treated animals in dark red.

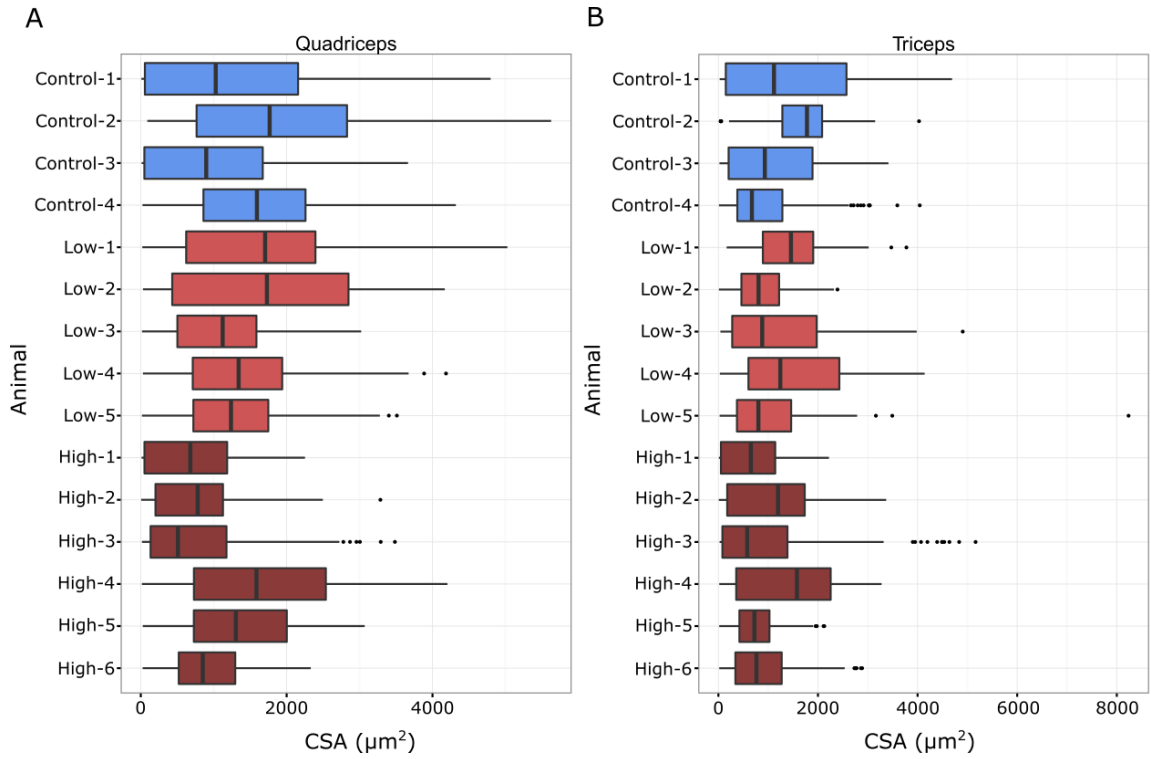


Table 2.1. BAY 60-2770 serum levels. Determined in control, low dose, and high dose-treated *mdx* mice.

BAY 60-2770 sGC-Activator

lc = 1µg/L

KJ110049	Mouse male	6 Weeks s.c.	0.1mg+1mg/kg	Serum
Concentration	Sample	µg/L	Meangeo	Sdgeo
0.1 mg/kg	Kontrolle	5,08		
	B1	4,21		
	B2	<lc		
	B3	<lc		
	B4	<lc		
	B5	<lc		
	B6	<lc		
	B7	<lc		
	B8	<lc		
	B9	<lc		
	B10	<lc		
1 mg/kg	A1	3,46		
	A2	3,17		
	A3	2,28		
	A6	2,17		
	A8	3,28	3,44	1,69
	A9	9,33		
	A4	<lc		
	A5	<lc		
	A7	<lc		

***Chapter 3. Mammalian Mss51 is a skeletal muscle-specific gene
modulating cellular metabolism***

Adam L. Moyer and Kathryn R. Wagner

Published: *J Neuromuscul Dis*, Preprint, 2015. doi: 10.3233/JND-150119

Abstract

Background

The transforming growth factor β (TGF- β) signaling pathways modulate skeletal muscle growth, regeneration, and cellular metabolism. Several recent gene expression studies have shown that inhibition of myostatin and TGF- β 1 signaling consistently leads to a significant reduction in expression of *Mss5l*, also named *Zmynd17*. The function of mammalian *Mss5l* is unknown although a putative homolog in yeast is a mitochondrial translational activator.

Objective

The objective of this work was to characterize mammalian *Mss5l*.

Methods

Quantitative RT-PCR and immunoblot of subcellular fractionation were used to determine expression patterns and localization of *Mss5l*. The CRISPR/Cas9 system was used to reduce expression of *Mss5l* in C2C12 myoblasts and the function of *Mss5l* was evaluated in assays of proliferation, differentiation and cellular metabolism.

Results

Mss5l was predominantly expressed in skeletal muscle and in those muscles dominated by fast-twitch fibers. *In vitro*, its expression was upregulated upon differentiation of C2C12 myoblasts into myotubes. Expression of *Mss5l* was modulated in response to altered TGF- β family signaling. In human muscle, MSS51 localized to the mitochondria.

Its genetic disruption resulted in increased levels of cellular ATP, β -oxidation, glycolysis, and oxidative phosphorylation.

Conclusions

Mss51 is a novel, skeletal muscle-specific gene and a key target of myostatin and TGF- β 1 signaling. Unlike myostatin, TGF- β 1 and IGF-1, *Mss51* does not regulate myoblast proliferation or differentiation. Rather, *Mss51* appears to be one of the effectors of these growth factors on metabolic processes including fatty acid oxidation, glycolysis and oxidative phosphorylation.

Keywords: *Mss51*, myostatin, TGF- β , mitochondria, metabolism, myotube, skeletal muscle

Introduction

Myostatin, or growth/differentiation factor 8 (GDF-8), is a member of the TGF- β superfamily and a negative regulator of muscle growth [20]. Myostatin inhibition has been shown to increase regeneration and decrease fibrosis of skeletal muscle and is thus of high interest for the treatment of acquired and inherited conditions where muscle is not able to regenerate efficiently [21,52–56]. An important additional feature of myostatin inhibition that may indicate potential therapeutic use in insulin resistance and obesity is its modulation of skeletal muscle metabolism [57]. Constitutive deletion of myostatin leads to changes in fiber type composition of skeletal muscle with a decrease in type I/type IIA oxidative fibers and an increase in type IIB glycolytic fibers [58–60]. Myostatin deletion or postnatal inhibition improves insulin sensitivity, increases glucose uptake into skeletal muscle and decreases total body fat [61–63]. Myostatin deletion suppresses fat accumulation and abnormal glucose metabolism in agouti lethal yellow (A(y)) and obese (ob/ob) mice and transgenic overexpression of a dominant negative activin receptor type IIB resolves the severe diabetes of the lipodystrophy A-ZIP mouse [64,65]. Treating mice fed high-fat diets with postnatal inhibitors of myostatin reduces the development of insulin resistance and fat accumulation [66,67]. However, the specific targets of myostatin and other TGF- β family members on genes producing these metabolic effects have not been clarified.

In a previous study, we profiled gene expression in skeletal muscle of mice treated with a soluble activin type IIB receptor (ActRIIB-Fc), the putative receptor of myostatin and activin A [24]. One of the genes whose expression was most significantly altered was *Mss5l* mitochondrial translational activator, named after its putative yeast

homolog *Mss51* and previously known as *Zmynd17*. *Mss51* was downregulated 4.3-fold in response to acute, and 3.3-fold in response to chronic treatment with ActRIIB-Fc, suggesting that *Mss51* might be an effector or downstream target of myostatin or activin A [24].

Similar results have been seen in numerous other published studies. *Mss51* was downregulated 2.7-fold in skeletal muscle of mice where the myostatin gene was deleted post-developmentally [68], 2.8-fold when mice were treated with myostatin neutralizing antibody JA16 [69] and 4.8-fold in transgenic mice expressing a skeletal-muscle specific, myostatin inhibitory pro-peptide [70]. Additionally, *Mss51* expression decreased 2.2-fold in skeletal muscle of transgenic mice expressing a skeletal muscle-specific dominant negative TGF- β receptor [71]. The consistent downregulation of *Mss51* expression in response to numerous methods of postnatal, TGF- β superfamily inhibition suggested that *Mss51* might have a unifying role in skeletal muscle function.

The function of *Mss51* in mammals has not been previously reported. In the yeast *Saccharomyces cerevisiae*, *Mss51* couples the synthesis of cytochrome *c* oxidase subunit 1 (COX1) to the assembly of the cytochrome *c* oxidase complex of the respiratory chain in the mitochondria [72]. Yeast *Mss51* also senses heme and oxygen availability to regulate cytochrome *c* oxidase biogenesis [73]. Iterative orthology prediction using Ortho-Profile demonstrated that the human MSS51 protein is a putative homolog of the yeast *Mss51* protein, and that human MSS51 has a mitochondrial localization signal [74]. However, a global pairwise alignment (using the Needleman-Wunsch algorithm) between yeast *Mss51* [NCBI RefSeq: NP_013304.1] and mouse *Mss51* [RefSeq: NP_083380.1] revealed only 19% amino acid identity (91/490 residues). This suggested that *Mss51*, a

newly recognized target of myostatin and other TGF- β family member signaling, may have a novel function in mammals. Here we investigate the expression and function of *Mss51* in skeletal muscle.

Materials and Methods

Cell Culture

C2C12 cells (ATCC, Manassas, VA) were maintained in Dulbecco's Modified Eagle's Medium (DMEM, Life Technologies, Carlsbad, CA, USA) supplemented with 10% fetal bovine serum (Sigma-Aldrich, St. Louis, MO). Differentiation was induced when cells reached approximately 80% confluence by switching to differentiation medium, DMEM supplemented with 2% horse serum (Life Technologies). Cells were treated with growth factors or inhibitors after three days of differentiation. For treatment with the inhibitors ActRIIB-Fc (generously provided by Qian Wang, Stony Brook University Medical Center, produced as previously described [23]) and TGF- β 1/2/3 neutralizing antibody 1D11 (R&D Systems, Minneapolis, MN), media was changed to DMEM supplemented with 0.1% bovine serum albumin 24 hours before the addition of the inhibitors. For treatment with recombinant myostatin, activin A, TGF- β 1 and insulin-like growth factor 1 (IGF-1) (all obtained from R&D Systems), media was changed to DMEM supplemented with 0.1% bovine serum albumin and the indicated growth factor on the third day post differentiation media change. For all treatments, cells were incubated for 5 hours and harvested in TRIzol (Life Technologies) for qRT-PCR analysis.

Skeletal Muscle Acquisition

Skeletal muscle was obtained from mice for qRT-PCR and humans for subcellular fractionation and Western blots. All animal experiments were conducted in accordance

with the guidelines prescribed by the Institutional Animal Care and Use Committee at the Johns Hopkins University School of Medicine. Ten to twelve week-old female C57BL/6J mice (The Jackson Laboratory, Bar Harbor, ME, USA) were maintained under a 12:12 hour light:dark schedule with *ad libitum* access to food and water. Mice were euthanized by inhalation overdose of isoflurane followed by cervical dislocation. From three mice, the brain, heart, kidney, liver, small intestine, diaphragm, and quadriceps were harvested. From three other mice, the soleus, diaphragm, long head of the triceps, extensor digitorum longus (EDL), and white vastus lateralis (WVL) were harvested. Tissues were minced and frozen in TRIzol for qRT-PCR analysis.

Acquisition of human skeletal muscle was approved by the Johns Hopkins Medicine Institutional Review Board. Written informed consent was obtained for the collection and use of human tissue samples. Human samples of deltoid muscle were obtained by open muscle biopsy of a living volunteer and from an autopsy donor and were stored frozen prior to subcellular fractionation.

CRISPR/Cas9-mediated Disruption of *Mss51* Locus in C2C12 Cells

In order to decrease *Mss51* expression, the *Mss51* genomic locus was disrupted in C2C12 cells using the clustered regularly interspaced short palindromic repeats (CRISPR)/Cas9 system for genome engineering [75]. Guide RNA (gRNA) target sequences and plasmids were designed and synthesized through the University of Massachusetts Medical School's Mutagenesis Core, which provided a plasmid expressing both the CRISPR gRNA and the RNA-guided DNA endonuclease Cas9 under

independent promoters, as well as a reporter plasmid containing a non-functional GFP ORF, disrupted by homology arms flanking DNA sequence containing the *Mss5l*-specific CRISPR target sequence [76]. Proliferating C2C12 cells were transfected with the CRISPR/Cas9 plasmid and disrupted GFP reporter plasmid using an Amaxa Nucleofector II and Cell Line Nucleofector Kit V (Lonza, Walkersville, MD, USA) according to manufacturer's instructions. The target sequence within *Mss5l*, depicted in Figure 3.4A, was cleaved by the CRISPR/Cas9 complex and re-sealed by non-homologous end joining. Simultaneously, the CRISPR/Cas9 complex also cleaved the disrupted GFP reporter plasmid, which was re-sealed by homology-directed repair using the homology arms flanking the cut site, allowing for functional expression of GFP only when the CRISPR/Cas9 complex was present. After 24 hours, transfected cells were isolated by fluorescence-activated cell sorting using a FACSAria IIu (BD Biosciences, Franklin Lakes, NJ, USA), shown schematically in Figure 3.4B. In parallel, control cells were transfected with a plasmid expressing functional GFP and subjected to the same cell sorting process as the *Mss5l*-disrupted cells. Pooled populations of *Mss5l*-disrupted and control cells were collected and expanded for comparative analysis. Cells were allowed to differentiate into myotubes for six days before analysis unless otherwise stated.

Cell Proliferation and Differentiation

To compare rates of cell proliferation, incorporation of the nucleoside analog 5-ethynyl-2'-deoxyuridine (EdU) was measured using the Click-iT EdU Alexa Fluor 594 Imaging Kit per manufacturer's instructions (Life Technologies). To compare myotube

differentiation, cells were stained with anti-sarcomeric myosin (MF20-s, DSHB, Iowa City, IA, USA, 1:1) after fixing with 4% paraformaldehyde (Electron Microscopy Sciences, Hatfield, PA, USA), permeabilizing with 0.1% Triton X-100 (Fisher Scientific, Hampton, NH, USA), and blocking with 5% normal goat serum (Vector Laboratories, Burlingame, CA, USA). For both proliferation and differentiation, images were acquired using an EVOS FL Cell Imaging System equipped with a 20x/0.45 NA objective (Life Technologies). Images were analyzed using ImageJ (National Institutes of Health, Bethesda, MD, USA). The myofusion index was calculated as the percentage of nuclei that were found in MF20-positive fibers. As an additional measure of differentiation, creatine kinase (CK) activity was compared between control and *Mss51*-disrupted cells using the EnzyChrom Creatine Kinase Assay Kit (BioAssay Systems, Hayward, CA, USA) following the manufacturer's instructions.

Subcellular Fractionation and Western Blot

In order to separate nuclear, cytosolic, and mitochondrial fractions from human tissue, subcellular fractionation was performed as previously described [77] with minor modification. Tissue homogenization was performed with a Poltyron PT 10-35 benchtop homogenizer (Kinematica, Luzern, Switzerland) and 20 passes through a 20G needle. Human tissue was used because at the time of these experiments, there were no available antibodies that selectively recognized mouse *Mss51*. The resulting fractions were then heat-denatured and reduced.

For Western blotting, cells were harvested in RIPA lysis buffer. Heat-denatured and reduced protein samples were separated by SDS-PAGE and transferred to PVDF membranes by standard techniques. To ensure equal protein loading, sample concentrations were measured using the bicinchoninic acid (BCA) assay. Membranes were blocked with 5% nonfat milk in TBS with 0.1% Tween 20 (TBS-T), probed with primary antibodies, washed, incubated with appropriate horseradish peroxidase-conjugated secondary antibodies in TBS-T, and developed using X-ray film and Amersham ECL Prime Western Blotting Detection Reagent (RPN2232; GE Healthcare Life Sciences, Pittsburgh, PA, USA). Primary antibodies used were anti-puromycin (PMY-2A4-s; Developmental Studies Hybridoma Bank (DSHB), Iowa City, IA, USA; 1:200), anti-GAPDH (G9545; Sigma-Aldrich; 1:10,000), anti-Histone H3 (H0164; Sigma-Aldrich; 1:10,000), anti-VDAC (4866; Cell Signaling Technology (CST), Danvers, MA, USA; 1:1,000), anti-AMPK α (5831; CST; 1:1,000), and anti-phospho-AMPK α (2535; CST; 1:1,000). At the time of publication, the only Mss51 antibody available is a human-specific, “anti-Zmynd17” (AP54659PU-N; Acris Antibodies, San Diego, CA, USA; 1:500).

Quantitative RT-PCR

Cells and tissues were homogenized in TRIzol, total RNA was isolated using the Direct-zol RNA MiniPrep Kit (Zymo Research, Irvine, CA, USA) and cDNA was synthesized from 1 microgram of RNA per sample using the iScript cDNA Synthesis Kit (Bio-Rad, Hercules, CA, USA). cDNA was diluted and used as the template for real-time

PCR using a CFX Connect Real-Time PCR Detection System (Bio-Rad) and SYBR Green PCR Master Mix (Life Technologies). Relative gene expression was determined using the $\Delta\Delta C_t$ method normalized to the indicated reference genes through the analytical software qbase+ (Biogazelle, Ghent, Belgium). At least three reference genes were included in each qRT-PCR experiment, and qbase+ was used to run the geNorm algorithm to select the most stable and suitable reference gene(s) for each experiment. Primer sequences are available upon request.

SUnSET Assay

To assay relative rates of protein synthesis, the surface sensing of translation (SUnSET) assay was used as previously described [78]. Cells were incubated with 1 μ M puromycin for 30 minutes before lysis in RIPA buffer with protease inhibitors, allowing for Western blot analysis of puromycin incorporation as a marker of protein synthesis. In addition to the gel that was used for Western blot analysis, a duplicate gel was stained with SYPRO Ruby protein gel stain (Life Technologies) following manufacturer's instructions for use in densitometry analysis normalization using ImageJ.

Metabolic Assays

For determination of cellular ATP content, cells were differentiated for 6 days and lysed in Reporter Lysis Buffer (Promega, Madison, WI, USA). The ATP Determination

Kit (Life Technologies) was used according to manufacturer's instructions and data were normalized to the protein content of each well as determined by BCA assay.

β -Oxidation of [1-¹⁴C]palmitic acid (C16:0, Moravek Biochemicals Inc., Brea, CA, USA) to water-soluble products was measured in intact myotubes grown in 6-well plates. Fatty acid in benzene solution was dried under a stream of nitrogen in a glass tube and solubilized with 10 mg/ml α -cyclodextrin (Sigma-Aldrich) in 10 mM Tris-Cl⁻, pH 8.0, to a final concentration of 0.1 mM and a specific activity of ~30,000 dpm/nmol. After 6 days of differentiation, the culture medium was replaced with serum-free DMEM containing 10 μ M solubilized radiolabeled palmitate and 2 mM L-carnitine. After 2 hours at 37°C, the reaction was stopped by adding ice-cold HClO₄ (final concentration 3%) to the medium. Plates were kept on ice for 1 hour before extraction of water soluble products using Folch partition as previously described [79]. The aqueous phase was mixed with Budget-Solve (RPI, Mount Prospect, IL, USA) and radioactivity was determined using a Beckman LS 6500 liquid scintillation spectrometer. Protein was determined in 5-6 wells of parallel 6-well plates by the method of Lowry *et al.* [80]. Results are presented as nmol/2 hr/mg protein \pm SEM.

Extracellular acidification and oxygen consumption rates were measured using a Seahorse XF24 Flux Analyzer (Seahorse Bioscience, Billerica, MA, USA) according to manufacturer's instructions for the glycolysis stress test and mitochondrial stress test. Cells were seeded at equal densities and differentiated for 6 days at which point metabolic flux analysis was performed. For the glycolysis stress test, cells began in glucose-free stress test medium, to which glucose, oligomycin (an ATP coupler), and 2-deoxy-D-glucose (a glucose analog) were added sequentially to final concentrations of 10

mM, 1 μ M, and 100 mM, respectively. For the mitochondrial stress test, cells began in stress test medium containing 10 mM glucose, to which oligomycin, carbonyl cyanide-p-trifluoromethoxyphenylhydrazone (FCCP, an ATP uncoupler), and rotenone/Antimycin A (mitochondrial inhibitors) were added to final concentrations of 1 μ M, 1 μ M, and 0.5 μ M/0.5 μ M, respectively. In both tests, between the addition of each component, the oxygen consumption rate and extracellular acidification were measured as previously described [81].

Statistical Analysis

The data are presented as mean \pm standard error of the mean with the exception of Figure 3.2C, which presents data in box-and-whiskers format with the median, quartiles, and outliers depicted. For qRT-PCR analysis, statistical analysis was performed using qbase+. For all other experiments, statistical analysis was performed using SigmaPlot 11 (SyStat Software, Chicago, IL). When two groups were compared, differences were analyzed with a two-way Student's *t* test. For more than two groups, differences were compared using one-way analysis of variance (ANOVA) with Bonferroni *post hoc* comparisons. Probability (*p*) values less than 0.05 were considered statistically significant.

Results

Mss51 gene expression is modulated by TGF- β Superfamily Signaling

To examine modulation of *Mss51* expression, we first determined the time course of its expression *in vitro*. *Mss51* was expressed at low levels in proliferating C2C12 myoblasts, and significantly higher levels as cells differentiated into myotubes (Figure 3.1A). Myotubes were then differentiated for three days and treated with various TGF- β superfamily members as well as various inhibitors (Figure 3.1B). TGF- β superfamily members (myostatin, TGF- β 1 and activin A) all increased *Mss51* expression in myotubes. The TGF- β 1/2/3 neutralizing antibody 1D11 decreased *Mss51* expression and there was a trend toward decreased expression with ActRIIB-Fc treatment. IGF-1, which has several similar effects on skeletal muscle as myostatin inhibition including increasing proliferation and differentiation *in vitro* and muscle growth *in vivo* [82], also decreased *Mss51* expression. We examined other time points and saw the greatest effects on *Mss51* expression levels when the myotubes were differentiated for three days and no significant change seen when proliferating myoblasts were treated (data not shown). This may be because during differentiation, the cells are actively increasing *Mss51* expression and are therefore more responsive to exogenous signaling cues.

Mss51 is predominantly expressed in glycolytic skeletal muscle

To determine the tissue specificity of *Mss51*, we performed qRT-PCR using RNA isolated from the brain, heart, kidney, liver, small intestine, diaphragm, and quadriceps of

10-12 week-old female C57BL/6J mice. There were no significant differences between brain, heart, kidney, and liver, while expression was higher in the small intestine and diaphragm, approximately 20-fold above the expression level found in the brain. In the quadriceps, expression was approximately 150-fold higher compared to brain (Figure 3.2A).

We also examined the relative expression of *Mss51* in different skeletal muscle groups, selected based on their established fiber type distributions [83–85], listed from more oxidative to more glycolytic: soleus, diaphragm, long head of the triceps brachii, extensor digitorum longus (EDL), and white vastus lateralis (WVL) (Figure 3.2B). There were significant differences between muscle groups, with lower expression in the more oxidative soleus and diaphragm muscles, intermediate in the mixed-type long head of the triceps brachii, and higher expression in the glycolytic EDL and WVL. *Mss51* was highly expressed in muscles that are more glycolytic and dominated by type IIB fibers, while lowly expressed in predominantly oxidative muscles dominated by type I/IIA fibers.

To determine if the expression pattern was similar in humans, we examined the Genotype-Tissue Expression (GTEx) Portal database (<http://www.gtexportal.org>). The GTEx Portal includes searchable RNA-seq data from over 40 tissue types of 175 humans [86]. Our search revealed MSS51 to be expressed at much higher levels in skeletal muscle than any other tissue examined (Figure 3.2C).

MSS51 is localized to the mitochondria

To determine cellular localization of MSS51, human deltoid muscles from an open muscle biopsy of a living donor and from an autopsy were used to perform subcellular fractionation. Fractions of nuclear, cytoplasmic, and mitochondrial proteins were collected and used for SDS-PAGE and Western blotting. These data showed that MSS51 protein co-fractionated with the mitochondrial fraction (Figure 3.3).

Mss51 does not regulate proliferation and differentiation

Using the CRISPR/Cas9 system for genome engineering, a double-strand break was introduced into the first exon of *Mss51* in C2C12 cells at the locus depicted in Figure 3.4A. Pooled populations of sorted cells, control (transfected with a plasmid encoding GFP) versus *Mss51*-disrupted (CRISPR/Cas9 dual expression plasmid co-transfected with a GFP reporter plasmid that only expressed GFP when CRISPR/Cas9 is expressed in the same cell), were collected and enriched as represented in Figure 3.4B. In the resulting cell populations, differentiation was induced and RNA was collected for analysis by qRT-PCR. Relative *Mss51* expression was determined using primers flanking the predicted double strand break, which demonstrated a significant decrease in *Mss51* in differentiating *Mss51*-disrupted myotubes when compared to control cells (Figure 3.4C). The *Mss51*-disrupted myotube population is a pool of many unique mutants that likely also includes cells that have at least one wild-type allele. Because of the nature of this system, we did not achieve total knockout of *Mss51* but instead a significant decrease in total *Mss51* transcript abundance in the study population.

Myostatin, TGF- β , and IGF-1 all modulate myoblast proliferation and differentiation and, as shown in Figure 3.1B, also are associated with altered *Mss5l* gene expression. For this reason, we examined cell proliferation and differentiation in *Mss5l*-disrupted cells. Proliferation was unchanged compared to control cells, as measured by EdU incorporation (Figure 3.5A, B) and alamarBlue assay (Supplementary Figure 3.1). Differentiation was also equivalent in *Mss5l*-disrupted and control cell populations by myofusion index, the proportion of nuclei found in myosin heavy chain-positive fibers at day 5 post differentiation media (Figure 3.5C, D). Creatine kinase enzyme activity, a marker of differentiation, did not differ significantly between control and *Mss5l*-disrupted myotubes after six days of differentiation (Figure 3.5E). Myotubes were differentiated for six days to ensure that stable levels of *Mss5l* transcript and protein were present in control cells, corresponding to the greatest difference between control and disrupted populations. We also looked at expression of myogenic regulatory factors by qPCR and did not see meaningful differences between control and *Mss5l*-disrupted cells (data not shown). Protein synthesis, as measured by puromycin incorporation using the SUNSET assay, was not altered in *Mss5l*-disrupted myotubes after 6 days of differentiation (Figure 3.5F, G).

***Mss5l*-disrupted myotubes are more metabolically active than wild-type myotubes**

Myostatin knockout and IGF-1 transgene expression lead to an alteration in fiber-type composition with a decrease in type 1 slow oxidative fibers and an increase in type IIB fast glycolytic fibers [24,58,59,87–90]. We therefore examined whether

CRISPR/Cas9-mediated disruption of the *Mss51* locus altered expression of the various myosin heavy chain isoforms (MyHCs) expressed by C2C12 myotubes. In *Mss51*-disrupted C2C12 myotubes, embryonic MyHC (*Myh3*), neonatal MyHC (*Myh8*), and MyHC IIX (*Myh1*) were significantly decreased, MyHC IIB (*Myh4*) was significantly increased, and MyHC IIA (*Myh2*) and MyHC I (*Myh7*) were unchanged (Figure 3.6A). The changes exhibited in *Mss51*-disrupted myotubes indicated a shift towards more fast-twitch MyHC expression.

Since expression of MyHC isoforms typically coincide with metabolic properties of muscle, we evaluated whether *Mss51* modulates the mRNA expression of several key regulators of metabolism (Figure 3.6B). Consistent with a shift toward MyHC IIB expression, *Mss51*-disrupted myotubes displayed a downregulation of *PGC1 α* , which among its many functions is the major factor in type I fiber type determination [91]. Cytochrome *c* oxidase subunit 2 (*Cox2*) gene expression was minimally increased but other genes involved with mitochondrial biogenesis (including *Nrf1*, *Nfe2l2*, *citrate synthase*, *ESRR α*) and genes of mitochondrial respiration (including *Atp5o*, *Alas1*, *Cox5b*, *Cyts*) were unchanged. *PGC1 α* is a major player in mitochondrial biogenesis, and it is intriguing that we did not see greater alterations in other genes involved in mitochondrial biogenesis, indicating that the decreased *PGC1 α* expression may be primarily linked to the shift in fiber type profile in cells deficient in *Mss51*. We evaluated *PGC1 α* expression in proliferating and differentiating *Mss51*-disrupted myotubes and found similar levels in proliferating *Mss51*-disrupted myoblasts versus controls but lower levels in differentiated *Mss51*-disrupted myoblasts compared to controls (Supplementary Figure 3.2).

Expression of the glycolytic gene hexokinase 2 (*Hk2*), which has been shown to be more active in the glycolytic EDL muscle than the oxidative soleus muscle [92], was significantly increased in *Mss51*-disrupted myotubes (Figure 3.6B). Other genes that had significant changes in expression with decreased *Mss51* expression were *Cd36* (fatty acid translocase), *Fasn* (fatty acid synthase), and *Pdk4* (pyruvate dehydrogenase lipoamide kinase isozyme 4), which were all increased. The products of these genes are all critical in fatty acid utilization. Other genes involved in fatty acid oxidation (FAO) including *HSL* (hormone sensitive lipase) and *Acadl* (long chain specific acyl-coA dehydrogenase) were also increased to a lesser extent while other genes involved in FAO were unchanged.

Since yeast *Mss51* is a translational activator, we examined changes in protein expression via immunoblotting. We examined several mitochondrial markers, including cytochrome *c*, VDAC, CoxI, CoxIV, and pyruvate dehydrogenase, and did not detect any differences between *Mss51*-disrupted and control myotubes (Supplementary Figure 3.3). We also examined markers of peroxisome proliferator-activated receptor gamma (PPAR γ)-regulated fatty acid metabolism, including AMP-activated protein kinase (AMPK α), SirT1, and GCN5L2 (Figure 3.6C and Supplementary Figure 3.3). Of these, only AMPK α was increased in *Mss51*-disrupted myotubes. Activated, phosphorylated AMPK α (p-AMPK α) is a marker of cellular energy [93], and both total protein expression and p-AMPK α (relative to total AMPK α) were increased in myotubes with reduced *Mss51* expression (Figure 3.6C, D).

AMPK α activation switches off ATP consuming pathways and switches on ATP generating processes (glucose uptake and fatty acid oxidation) [94]. To determine if the increases in gene expression of fatty acid utilization and p-AMPK α described above resulted in increased ATP generation, we measured ATP content of populations of differentiated myotubes. Cellular ATP content was significantly increased in *Mss51*-disrupted myotubes (Figure 3.7A). To determine if fatty acid utilization was altered in *Mss51*-disrupted myotubes, we measured β -oxidation of radiolabeled palmitic acid in intact control and *Mss51*-disrupted myotubes (Figure 3.7B). *Mss51*-disrupted myotubes were shown to have a significantly higher β -oxidation activity.

To confirm the finding that reduced *Mss51* expression resulted in increased cellular metabolism as suggested by increased ATP production and increased β -oxidation of palmitic acid, glycolysis stress and mitochondrial stress tests were performed using the Seahorse XF24 Flux Analyzer. In the glycolysis stress test, the extracellular acidification rate was measured as an indicator of glycolysis when differentiated myotubes were perturbed. Baseline measurements were taken in glucose-free media before glucose, oligomycin, and 2-deoxy-D-glucose were injected to begin glycolysis, shut down the electron transport chain, and inhibit glycolysis, respectively. Between each treatment, the extracellular acidification rate was measured and plotted (Figure 3.7C), allowing for the calculation of several key parameters: glycolysis under normal conditions, maximal glycolytic capacity when the electron transport chain is disrupted, and glycolytic reserve. Comparing *Mss51*-disrupted and control myotubes, we found that *Mss51*-disrupted myotubes had significantly higher glycolysis, glycolytic capacity, and glycolytic reserve than wild-type myotubes (Figure 3.7D). We also performed a mitochondrial stress test,

where cells were treated with oligomycin, carbonyl cyanide-p-trifluoromethoxyphenylhydrazone, and Rotenone/Antimycin to inhibit Complex V, uncouple the proton gradient, and inhibit Complexes I and III, respectively. This allowed for the calculation of basal respiration, ATP production, maximal respiration, and spare respiratory capacity, all measured by changes in oxygen consumption rate (Figure 3.7E). We found that all metrics of mitochondrial respiration excluding proton leak were significantly increased in *Mss51*-disrupted cells (Figure 3.7F), indicating that cells that expressed less *Mss51* had higher metabolic activity, resulting in higher levels of respiration, glycolysis, and ATP production.

Discussion

In this report, we introduce mammalian *Mss5l* as a muscle-specific gene regulated by members of the TGF- β superfamily. Mammalian *Mss5l* initially came to attention as one of the most consistently downregulated genes in gene profiling studies of myostatin inhibition [24,68–71]. Given myostatin's role in skeletal muscle development, postnatal growth and regeneration, we originally postulated that *Mss5l* might have a role in myoblast proliferation or differentiation but this was not supported by assays on C2C12 myoblasts in which *Mss5l* was genetically disrupted (Figure 3.5). Rather, *Mss5l* appears to modulate other aspects of TGF- β signaling in skeletal muscle including fiber type determination and metabolism. The observation that myostatin, TGF- β 1, activin A and IGF-1 all modulate expression of *Mss5l* suggest that it may be a common effector of these growth factors which converge to regulate metabolic adaptations (Figure 3.1).

Mss5l is expressed almost exclusively in skeletal muscle in mice and humans. In mice, it is expressed most abundantly in muscles rich in glycolytic type II fibers and 20- to 25-fold less in those rich in oxidative type I fibers (Figure 3.2). Genetic disruption of *Mss5l* shifts the myosin heavy chain expression profile toward a more glycolytic phenotype dominated by Type IIB myosin heavy chain (Figure 3.6). This is consistent with the effects of myostatin gene deletion and IGF-1 transgene overexpression on fiber type composition which cause a similar shift toward a more glycolytic phenotype *in vivo* [58–60,87–90]. *PGC1 α* , which is a major determinant of type 1 fiber formation, has been shown to be decreased in myostatin-null mice and muscle-specific IGF-1 transgenic mice [60,88,95]. Further, in a transgenic model of overexpression of activated Akt1, a

shift toward increased type IIB fibers was shown to accompany an increase in *Hk2* expression and a decrease in *PGC1 α* expression alongside increased metabolic parameters [96]. Consistent with these findings, *PGC1 α* is downregulated and *Hk2* is upregulated in *Mss51*-disrupted myotubes which have increased MyHC IIB expression compared to control myotubes (Figure 3.6).

Although mammalian Mss51 has a limited similarity to its yeast ortholog Mss51 (19% amino acid identity shared only across the zf-MYND domain), both proteins co-localize with mitochondria (Figure 3.3, [72]). Yeast Mss51 is a translational activator of Cox1 but *Mss51*-disrupted myotubes did not show a reduction in CoxI or CoxIV protein, suggesting its function is not conserved across species (Supplementary Figure 3.3). Conversely, myotubes deficient in *Mss51* displayed increased ATP production, β -oxidation and activation of AMPK α , a marker of cellular metabolic state (Figures 3.6 and 3.7). Glycolysis and mitochondrial respiration are both increased after *Mss51* disruption (Figure 3.7). While the specific actions of Mss51 on cellular metabolism remain to be determined, it appears possible that there is a shift from glucose to fatty acid utilization occurring when there is less Mss51 present. β -oxidation is increased in *Mss51*-disrupted cells (Figure 3.7B) and several genes involved in fatty acid metabolism (*HSL*, *Acadl*, *Cd36*, *Fasn*) are upregulated. Further, increased expression of *Pdk4* and activation of AMPK α would predict a shift toward fatty acid utilization. Although the relationship between lipid balance and muscle insulin sensitivity continues to be explored, one model of obesity-associated insulin resistance posits intramyocellular lipid content as a principal contributor [97]. Myostatin inhibitors have been shown to prevent diet-induced obesity and insulin resistance in a number of models [66,67,98,99]. The possibility that these

effects are in part mediated by *Mss51* is consistent with the downregulation of *Mss51* by myostatin inhibitors and corresponding upregulation of genes involved in fatty acid metabolism.

Multiple myostatin inhibitors are currently in clinical trials for the treatment of neuromuscular disease (ClinicalTrials.gov Identifiers: NCT012310763, NCT02515669, NCT01519349 and NCT01423110). While these trials hope to increase muscle function by stimulating muscle growth and regeneration, inhibition of myostatin is also likely to have metabolic effects on skeletal muscle. Preclinical work by our group and others suggest that *Mss51* will be downregulated by myostatin inhibition [24,68–70]. The current study suggests that this will have positive effects on bioenergetics, increasing cellular ATP. However, there are limitations to the current *in vitro* study in which, necessarily, only basal states are assayed and glucose and glutamine are the primary fuels of cellular metabolism. Additionally, the cell population characterized in this present study does still express functional *Mss51*, albeit significantly less than control populations, which may obscure the changes that would occur in its complete absence. *In vivo* studies using stimuli that modulate fatty acid oxidation and mitochondrial biogenesis will be necessary to further elucidate *Mss51* function.

List of abbreviations

2-DG, 2-deoxy-D-glucose; *Acadl*, acyl-CoA dehydrogenase, long chain (also called *LCAD*); *Acads*, acyl-CoA dehydrogenase, short chain (also called *SCAD*); *Acadvl*, acyl-CoA dehydrogenase, very long chain (also called *VLCAD*); ActRIIB-Fc, soluble Activin

receptor type IIB; *Alas1*, delta-aminolevulinic acid synthase 1; AMPK α , AMP-activated protein kinase alpha; ANOVA, analysis of variance; *Atp5o*, ATP synthase, H⁺ transporting, mitochondrial F1 complex, O subunit; β 2m, β -2-microglobulin; BCA, bicinchoninic acid; Cas9, CRISPR-associated protein 9; *Cd36*, cluster of differentiation 36; CK, creatine kinase; *Cox*, cytochrome c oxidase; *Cpt*, carnitine palmitoyltransferase; CRISPR, clustered regularly interspaced short palindromic repeats; *Cs*, citrate synthase; *Cycs*, cytochrome c, somatic; DAPI, 4',6-diamidino-2-phenylindole; DMEM, Dulbecco's modified Eagle's Medium; ECAR, extracellular acidification rate; ECL, electrochemiluminescence; EDL, extensor digitorum longus; EdU, 5-ethynyl-2'-deoxyuridine; *Eno3*, enolase 3 (beta, muscle); *Esrr*, estrogen related receptor; FACS, fluorescence-activated cell sorting; *Fasn*, fatty acid synthase; FCCP, carbonyl cyanide-p-trifluoromethoxyphenylhydrazone; *GAPDH*, glyceraldehyde 3-phosphate dehydrogenase; *GCN5L2*, general control of amino acid synthesis, yeast, homolog-like 2; GDF-8, growth/differentiation factor 8 (myostatin); GDF-11, growth/differentiation factor 11; gRNA, guide RNA; GTEX, Genotype-Tissue Expression; *Hk2*, hexokinase 2; IGF-1, insulin-like growth factor-1; *Lipe*, hormone sensitive lipase (also called *HSL*); *Mss51*, Mss51 mitochondrial translational activator; *Mstn*, myostatin; MyHC, myosin heavy chain; *Nfe2l2*, nuclear factor, erythroid 2-like 2 (also called *Nrf2*); *Nrf1*, nuclear respiratory factor-1; OCR, oxygen consumption rate; ORF, open reading frame; *Pdk4*, pyruvate dehydrogenase lipoamide kinase 4; *Pfk-1*, phosphofructokinase 1; *PGC1*, peroxisome-proliferator activated receptor gamma coactivator 1; *Pgk1*, phosphoglycerate kinase 1; *PPAR*, peroxisome-proliferator activated receptor; PVDF, polyvinylidene fluoride; qRT-PCR, quantitative reverse transcription polymerase chain reaction; RPKM,

reads per kilobase per million reads mapped; SDS-PAGE, sodium dodecyl sulfate polyacrylamide gel electrophoresis; *Sirt1*, sirtuin 1; *Slc2a4*, solute carrier family 2 member 4 (also called *Glut4*); *Socs7*, suppressor of cytokine signaling 7; *Srebf1*, sterol regulatory element binding transcription factor 1; SUnSET, Surface Sensing of Translation; *TBP*, TATA box binding protein; TBS, Tris-buffered saline; *Tfam*, transcription factor A, mitochondrial; TGF- β , transforming growth factor β ; *Ucp*, uncoupling protein; VDAC, voltage-dependent anion channel; WVL, white vastus lateralis; *Zmynd17*, zinc-finger MYND-domain containing protein 17.

Acknowledgements

The authors thank Qian Wang for ActRIIB-Fc, Alexandra McPherron for helpful comments on the manuscript, Jonathan Pevsner for scientific and technical advice, Paul Watkins for FAO assay assistance and Naili Liu, Alexis Norris, Xiaohai Shi and Gwynn Marsh-Armstrong for technical assistance. Funding for the study was provided by the Hugo W. Moser Research Institute of Kennedy Krieger.

Conflict of Interest

The authors have no conflict of interest to report.

Figures

Figure 3.1. *Mss51* expression in vitro. (A) *Mss51* mRNA expression measured by qRT-PCR in proliferating and differentiating C2C12 cells. Expression level is normalized to proliferating (Day 0) cells using the reference gene *TBP*. (B) *Mss51* expression in differentiated C2C12 myotubes treated with various growth factors and inhibitors: 300 ng/mL myostatin, 5 μ g/mL ActRIIB-Fc, 50 ng/mL TGF- β 1, 10 μ g/mL TGF- β neutralizing antibody 1D11, 20 ng/mL Activin A, and 100 ng/mL IGF-1. Expression level is normalized to control (untreated) cells using reference genes *β 2m* and *TBP*. For (A) and (B), significant differences between groups were determined by a one-way ANOVA ($n=3$, $p < 0.01$) with Bonferroni *post hoc* comparisons. The annotation above each bar indicates statistically significant differences between the means in each group at $p < 0.05$: Groups sharing a letter designation were not significantly different from each other, while groups not sharing a letter were significantly different.

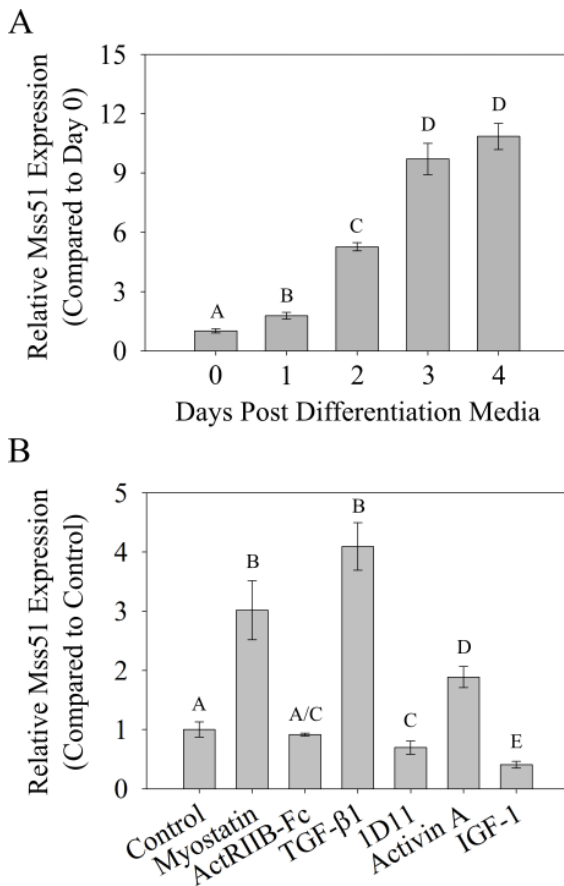


Figure 3.2. *Mss51* tissue expression. (A) *Mss51* mRNA expression measured by qRT-PCR in brain, heart, kidney, liver, small intestine, diaphragm, and quadriceps of 10-12 week-old female C57BL/6J mice, normalized to the quantity found in the brain using the reference gene *Pgkl* (n=3). (B) *Mss51* mRNA expression in soleus, diaphragm, long head of triceps brachii, extensor digitorum longus, and white vastus lateralis of the quadriceps of 10-12 week-old female C57BL/6J mice, normalized to the expression levels found in the soleus using reference genes *Pgkl* and *TBP* (n=3). (C) *MSS51* expression across human tissue types determined by RNA-seq from the Genotype-Tissue Expression (GTEx) Portal showing *MSS51* reads per kilobase per million reads mapped (RPKM). Data were downloaded from GTEx Portal on June 17, 2015. For qRT-PCR experiments, groups were significantly different from each other as determined by a one-way ANOVA (n=3, $p < 0.01$) and Bonferroni *post hoc* comparisons. Different letters above each bar signify statistically significant differences between the means in each group at $p < 0.05$.

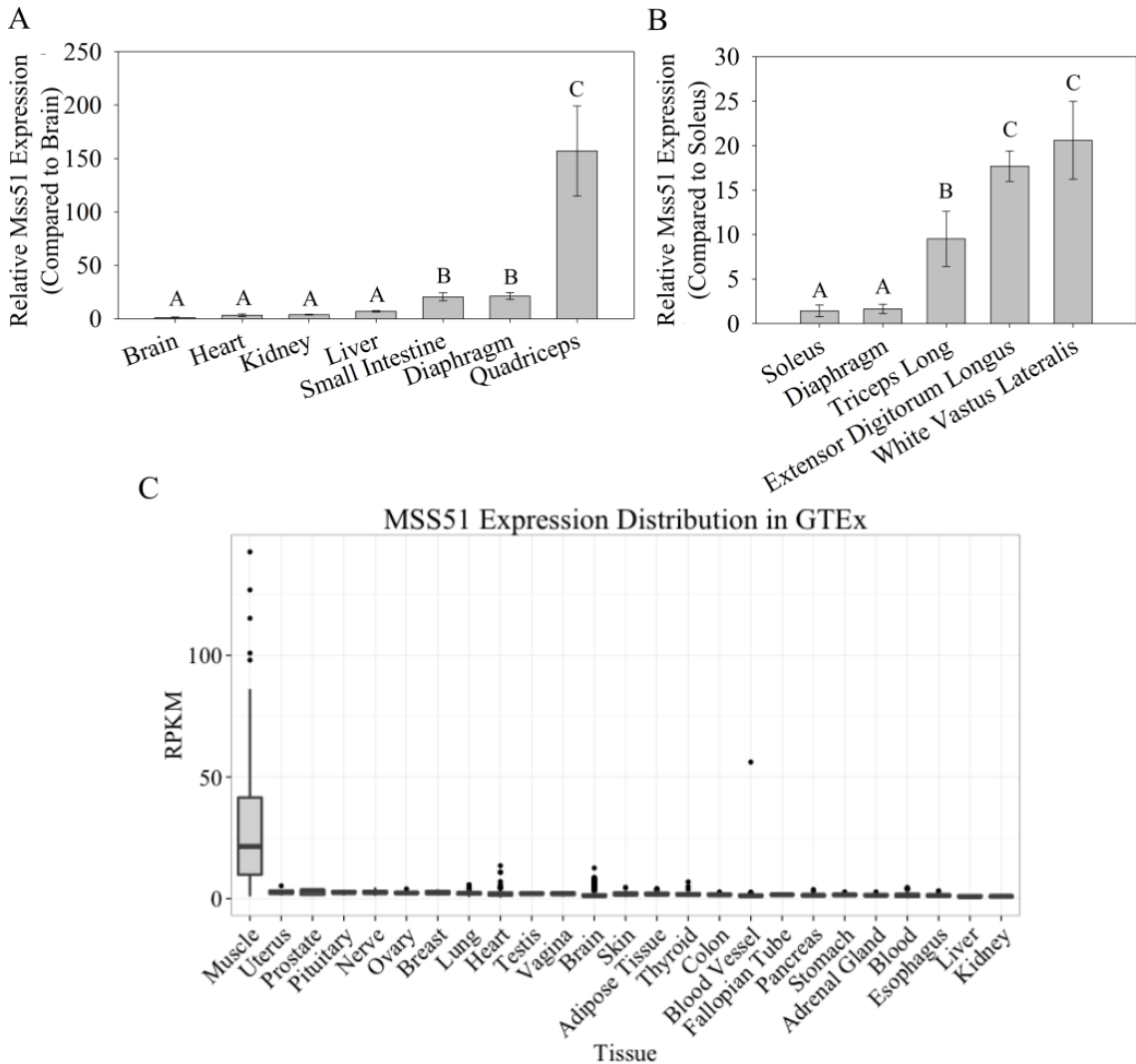


Figure 3.3. Subcellular localization of MSS51. Subcellular fractionation was performed on human deltoid samples from a biopsy and an autopsy and resulting fractions were subjected to SDS-PAGE. Immunoblotting was performed with the only current antibody specific to MSS51 (anti-ZMYND17, Acris Antibodies, San Diego, CA, USA) showing a band in the mitochondrial fraction of the predicted protein product size, 51 kDa. Loading controls were VDAC (mitochondrial), GAPDH (cytoplasmic), and Histone H3 (nuclear).

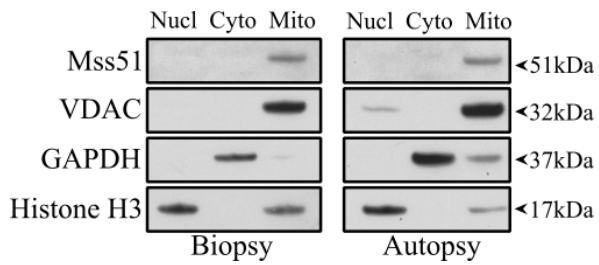


Figure 3.4. CRISPR/Cas9-disruption of *Mss51* locus in C2C12 myoblasts. (A) Schematic of the *Mss51* genomic locus with the CRISPR guide RNA (gRNA) target sequence enlarged, predicted cut site marked in red, exons marked in black, UTRs in white. At the cut site, a double-strand break occurred and was re-sealed by non-homologous end joining. (B) Production of *Mss51*-disrupted cells was achieved by co-transfection of a dual-expression plasmid encoding the CRISPR gRNA (red) and the Cas9 endonuclease (blue), and a reporter plasmid encoding a disrupted GFP with two homology arms (dark green) flanking the CRISPR target site (red), which was cleaved by Cas9, re-sealed by homology-directed repair, and expressed functional GFP. Two populations of GFP-positive cells were collected by FACS sorting and expanded for further analysis – *Mss51*-disrupted cells were collected as shown and in parallel, control cells were transfected with a GFP expression plasmid and subjected to the same FACS process. (C) *Mss51* expression measured by qRT-PCR in control and *Mss51*-disrupted populations over 6 days of differentiation, normalized to expression in proliferating control cells (Day 0) using reference genes *Tfam* and *TBP* (n=3). ** $p < 0.01$, *** $p < 0.001$.

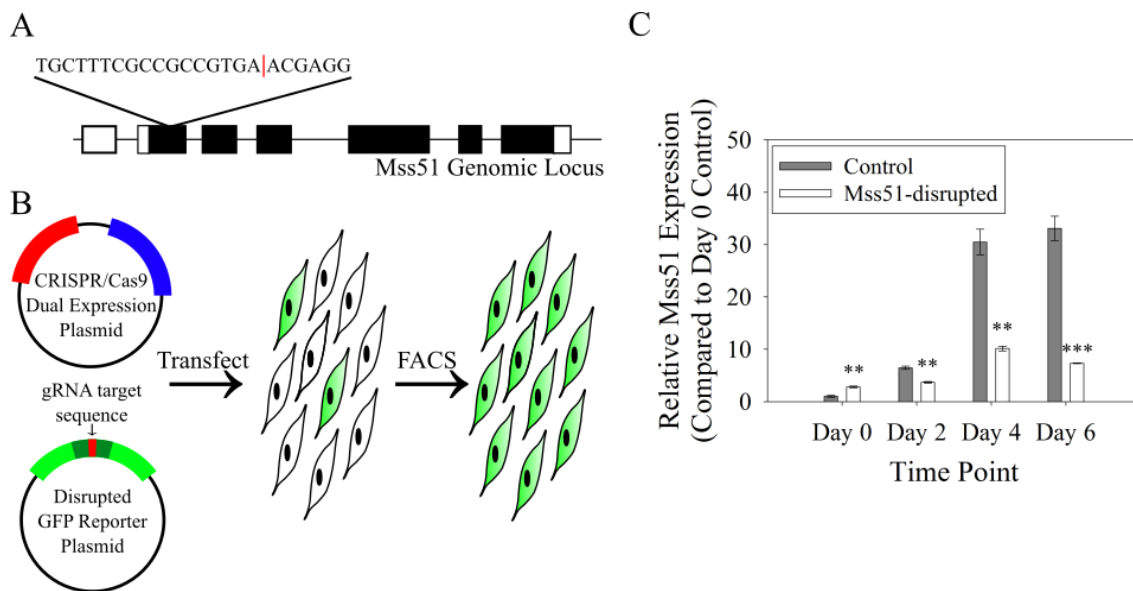


Figure 3.5. *Mss51*-disrupted myoblasts proliferate and differentiate normally. (A) Proliferating control and *Mss51*-disrupted myoblasts labeled with EdU (red) and Hoechst 33342 (blue). (B) Quantification of EdU staining (n=6 wells imaged per sample). (C) Representative myosin heavy chain (MF20, green) staining of control and *Mss51*-disrupted myotubes 2 days after induction of differentiation with nuclei stained by DAPI (blue). (D) Quantification of fusion index (percentage of nuclei found in MF20+ myotubes, n=6). (E) Creatine kinase (CK) activity in myotubes after 6 days of differentiation. (F) Protein synthesis rates as measured by puromycin incorporation on the left and total protein stained by SYPRO Ruby on the right after 6 days of differentiation. (G) Densitometric analysis of SUnSET assay as shown in F, normalized to SYPRO Ruby-stained total protein (n=3). Differences between groups were not statistically significant.

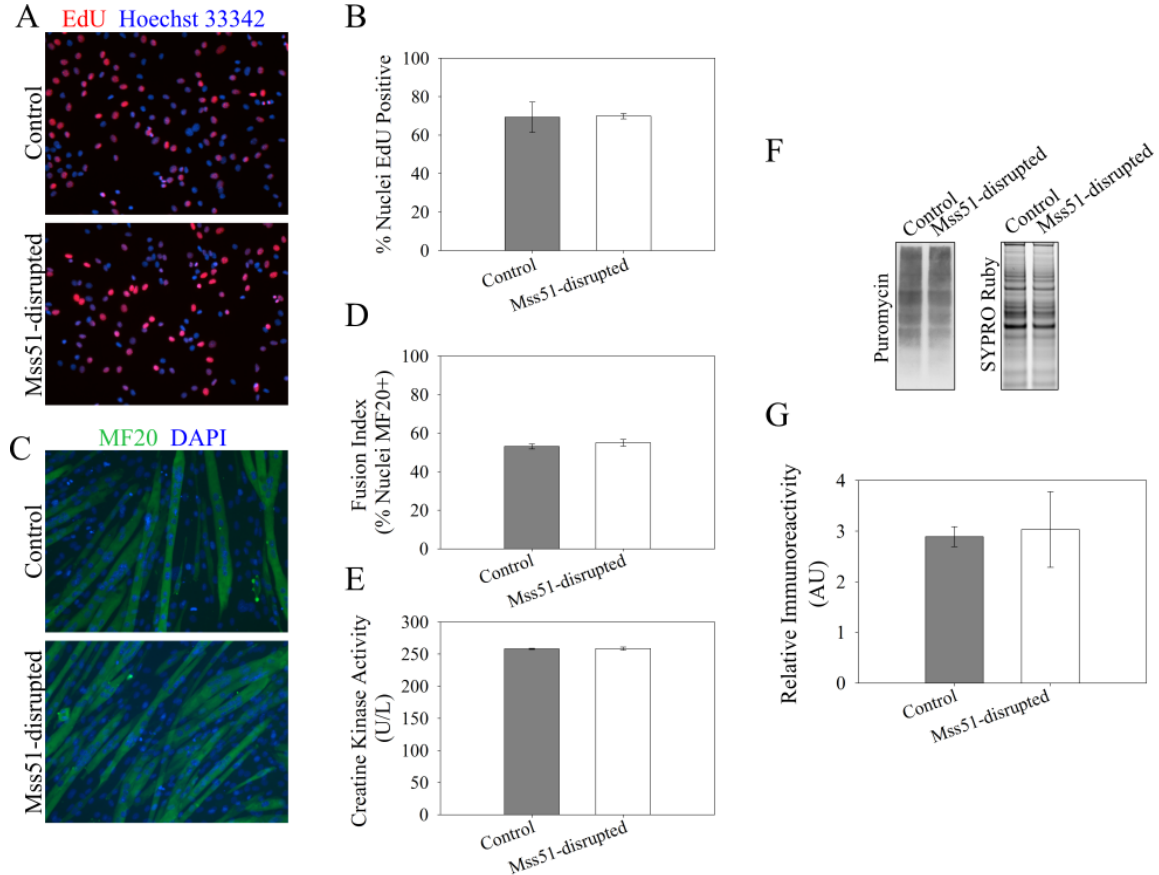


Figure 3.6. Gene and protein expression in *Mss51*-disrupted differentiated myotubes
 (A) Myosin heavy chain expression measured by qRT-PCR in control and *Mss51*-disrupted C2C12 myotubes, normalized to expression levels in control myotubes using reference genes *Tfam* and *TBP* (n=3). (B) Expression of metabolic genes in control and *Mss51*-disrupted C2C12 myotubes, normalized to expression levels in control myotubes using reference genes *Tfam* and *TBP* (n=3). (C) Western blots of control and *Mss51*-disrupted C2C12 myotubes examining expression and phosphorylation of AMPK α . (D) Densitometric analysis of AMPK α expression normalized to GAPDH and of AMPK α phosphorylation normalized to both GAPDH and total AMPK α (n=3). * $p < 0.05$, ** $p < 0.01$.

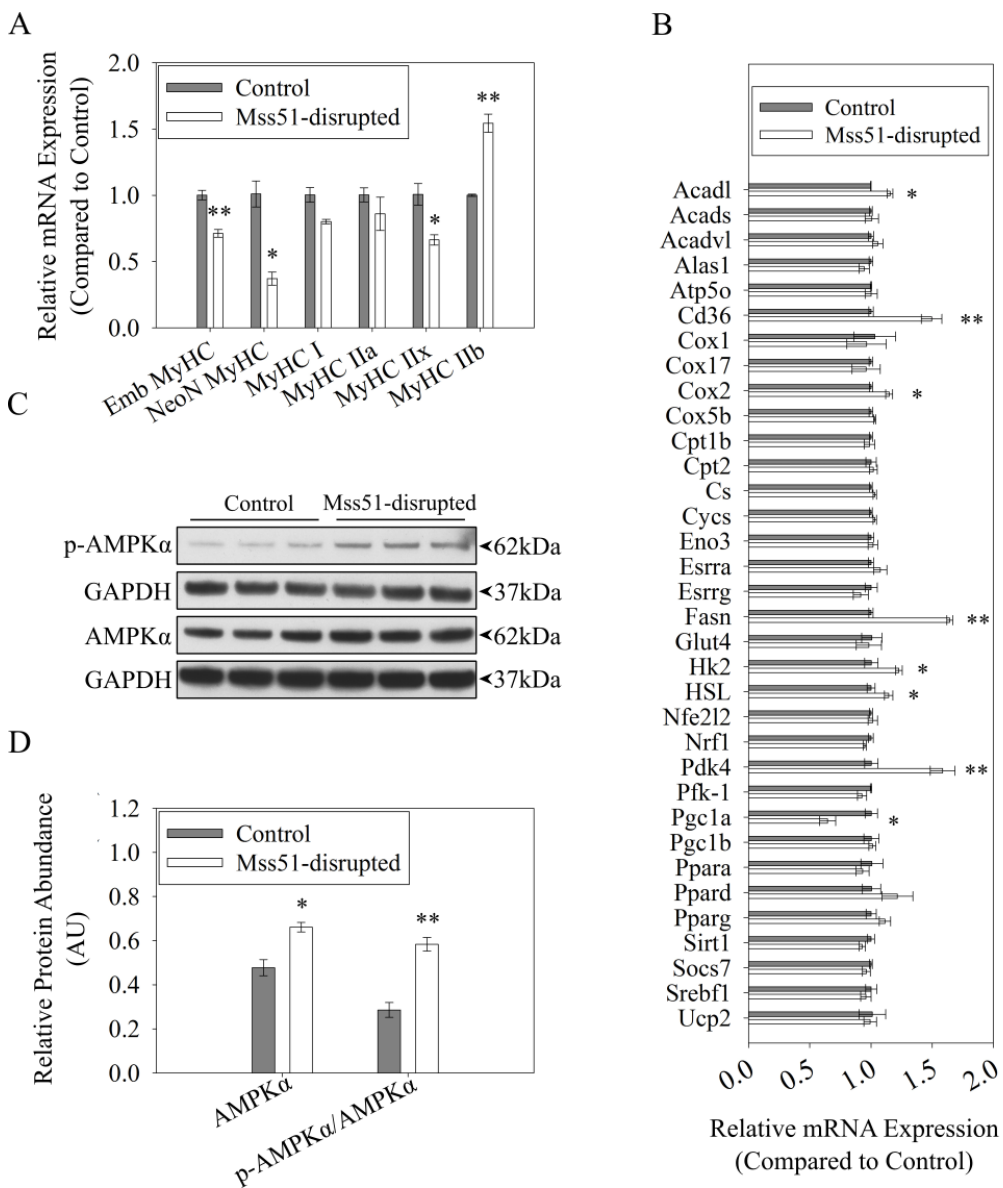
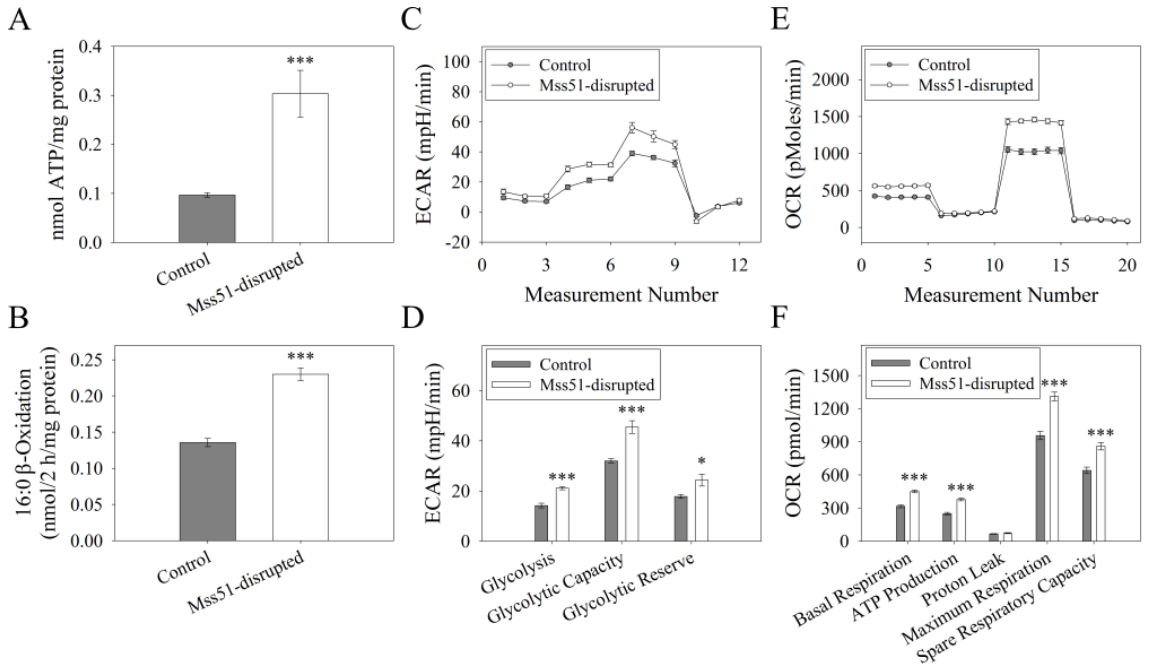
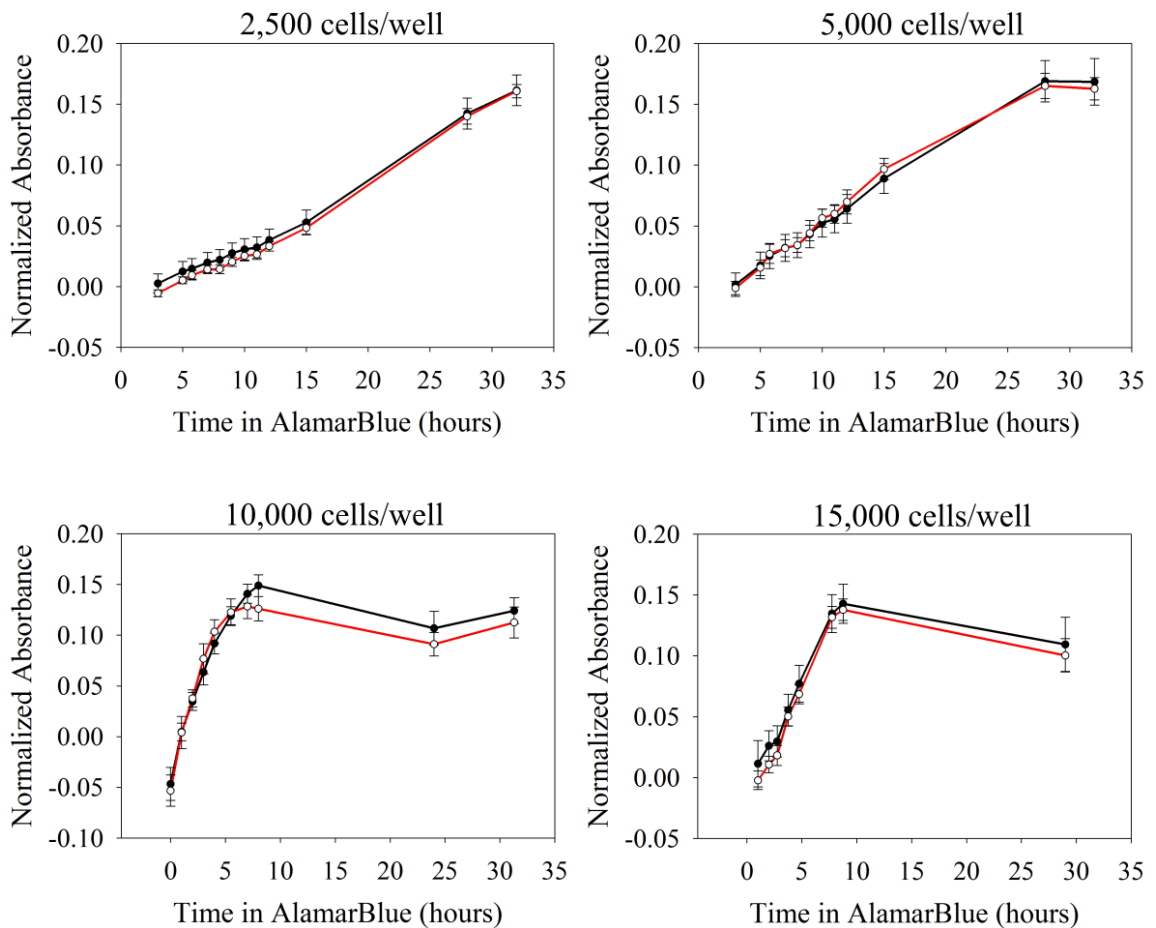


Figure 3.7. Glycolysis and Oxidative Phosphorylation in *Mss51*-disrupted cells. (A) ATP production in control and *Mss51*-disrupted myotubes (n=6). (B) Activity of C_{16:0} fatty acid β -oxidation in control and *Mss51*-disrupted myotubes (n=6). (C) Glycolysis stress test measuring the extracellular acidification rate (ECAR) in control and *Mss51*-disrupted myotubes treated with glucose, oligomycin, and 2-deoxy-D-glucose. (D) Glycolysis, glycolytic capacity, and glycolytic reserve calculated from the glycolysis stress test (n=10). (E) Mitochondrial stress test results comparing oxygen consumption rates (OCR) between control and *Mss51*-disrupted myotubes treated with oligomycin, carbonyl cyanide-p-trifluoromethoxyphen (FCCP), and Antimycin A/Rotenone. (F) Basal respiration, ATP production, proton leak, maximum respiration, and spare respiratory capacity as calculated from the mitochondrial stress test (n=10). * $p < 0.05$, *** $p < 0.001$.

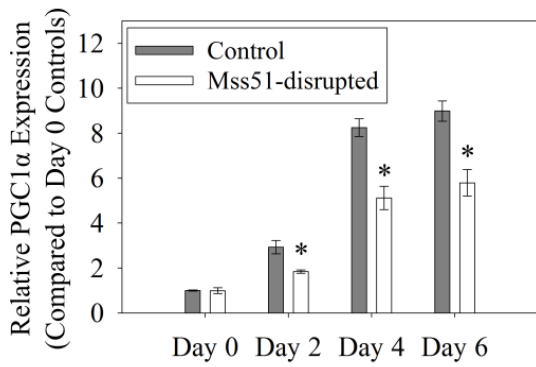


Supplementary Data

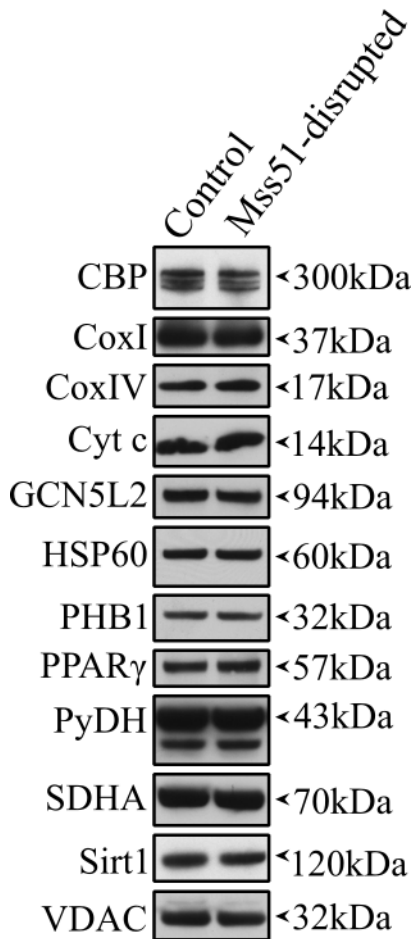
Supplementary Figure 3.1. Proliferation of *Mss51*-disrupted cells (red) compared to control (black). Cells were plated at indicated densities in 96-well plates and proliferation was measured over 1.5 days using the alamarBlue assay (Life Technologies, n = 12).



Supplementary Figure 3.2. PGC1 α expression. *PGC1 α* mRNA expression was measured in control and *Mss51*-disrupted myotubes through the first 6 days of differentiation. Expression was normalized to expression levels in proliferating (Day 0) control cells using reference genes *TBP* and *Tfam* (n=3). * $p < 0.05$.



Supplementary Figure 3.3. Expression of several metabolic proteins in control versus *Mss51*-disrupted myotubes. Protein levels were compared by Western blot in control and *Mss51*-disrupted myotubes differentiated for 6 days.



*Chapter 4. Generation and preliminary characterization of
Mss51^{-/-} mice*

Abstract

Mss5l^{-/-} mice were generated using the CRISPR/Cas9 system for genetic engineering to introduce double strand breaks into the first two exons of *Mss5l*, and several resulting mutants were backcrossed onto the C57BL/6J background. The CRISPR/Cas9 system was delivered efficiently, with 48 of the 104 pups screened showing genomic deletions at least several hundred base pairs in size. Heterozygote crosses generated wild-type and knockout homozygotes, which were used for preliminary studies. Primary cells were derived and showed no difference in rates of proliferation or differentiation, though there were significant alterations in gene expression of metabolic markers and myosin heavy chain isoforms. Muscle and fat weights did not differ between wild-type and knockout animals, though there appear to be trends towards altered metabolic gene expression and treadmill endurance. Further challenges will be required to elucidate the phenotype resulting from genetic ablation of *Mss5l*.

Introduction

Our previous work with *Mss5l* elucidated several important clues regarding its function and mechanism, but there is still much work to be done before the gene's role is fully understood. It is known that *Mss5l* is skeletal muscle-specific and its expression can be regulated by modulating TGF- β superfamily signaling [100]. Additionally, its expression is enriched in muscle groups that are dominated by fast-twitch fibers such as the extensor digitorum longus and the white vastus lateralis [100]. When it was genetically disrupted, cellular proliferation and differentiation were unaltered but cellular metabolism increased, as determined by increased ATP content and β -oxidation of fatty acids. Both gene and protein expression changed as well, with an upregulation of genes involved in fatty acid oxidation, a switch in myosin heavy chain expression to more glycolytic, and increased expression and activation of AMPK α [100]. In a recent analysis of human gene expression data, expression of *Mss5l* was shown to be inversely correlated to physical capacity as determined by VO_{2MAX} in a highly significant manner [101].

The mechanism of action is still poorly understood and there are no known binding partners. In humans, MSS51 localizes to the mitochondrial fraction by subcellular fractionation [100], but it is unknown if it is binding other proteins or mitochondrial transcripts. *Mss5l* was previously known as *Zmynd17*, named for its predicted zinc finger MYND domain. The MYND domain is named for proteins myeloid, Nervy, and DEAF-1, each of which contain a zinc binding domain rich in cysteine and histidine. Numerous studies have shown MYND domain-containing proteins to bind other proteins and form co-repressor complexes, inhibiting the

expression of target genes [102–106]. If *Mss51* is part of a co-repressor complex and localizes to the mitochondria, it would follow that its function is to inhibit transcription of one or more genes in the mitochondrial genome.

In order to elucidate the function of *Mss51*, it was an early priority to generate a knockout mouse line. We initially attempted to generate a conditional knockout mouse using traditional cloning techniques to insert loxP sites into intronic regions of *Mss51*. The constructs would then undergo embryonic stem cell targeting to achieve germline transmission of the mutation, followed by backcrossing mutants to inbred mice, and crossing to mice expressing skeletal muscle-specific Cre recombinase to disrupt *Mss51* only in skeletal muscle. We were in the process creating this construct, specifically introducing loxP sites incorporated into *Mss51*, when the CRISPR/Cas9 system was introduced.

By 2013, investigators adapted the clustered regularly interspaced short palindromic repeat (CRISPR) prokaryotic immune system to manipulate DNA in eukaryotes [107–109]. In prokaryotes, the CRISPR/Cas9 complex functions to recognize and cleave foreign DNA, injected into the organism by bacteriophage. CRISPR guide RNAs (gRNAs) are complementary to known antigenic sequence, and they associate with the CRISPR-associated endonucleases (Cas) to cleave the target sequence. Researchers have been able to hijack the system and use it widely to modify DNA in a variety of settings using CRISPR and Cas9. In this setting, gRNAs are selected based on the uniqueness of sequence upstream of a protospacer adjacent motif (PAM) of the sequence form NGG. The CRISPR/Cas9 system introduces a double strand break three nucleotides upstream of the PAM, which must then be repaired by non-homologous end joining or

homology-directed repair. Now, all that is required to manipulate the genome is a plasmid expressing Cas9 and a gRNA, which can be easily synthesized and cloned due to its short length. The system has drastically decreased the time and energy required to generate knockout animals.

Using the CRISPR/Cas9 system, we derived several mutant mouse lines and have started to characterize the resulting phenotype. As *Mss5l* came to attention in the context of myostatin inhibition, we started looking for changes that have already been shown to occur when myostatin is inhibited, especially those linked to metabolic changes. These include altered fiber type distribution with less Type I fibers, increased muscle mass, and decreased fat accumulation [24,58–60]. We have started by examining both primary myoblasts and mice, comparing results to our previous work and further exploring the effects of ablation of *Mss5l*.

Materials and Methods

*Generation of *Mss51*^{-/-} Mice*

All animal experiments were performed in accordance with the guidelines of the Institutional Animal Care and Use Committee at the Johns Hopkins University School of Medicine. Using the University of Massachusetts Medical School's Mutagenesis Core, two CRISPR gRNAs were selected, targeting exons 1 and 2 of the *Mss51* locus, depicted in Figure 4.1. Selection was based on the CRISPRseek software, scoring potential gRNAs to predict offtarget effects. The Mutagenesis Core synthesized plasmids and provided *in vitro* transcribed RNA of the *Cas9* endonuclease and each gRNA.

An injection mix was created with *Cas9* mRNA at a concentration of 50 ng/ μ L and each gRNA at 20 ng/ μ L, which was delivered to the Johns Hopkins Transgenic Mouse Core facility. There, microinjection was performed to deliver the RNA cocktail to single cell B6SJL/F2 embryos. 11 pseudopregnant mice were implanted each with 25 embryos and resulting litters were transferred to our animal facility. At the time of weaning, tail snip biopsies were taken and DNA was isolated using QuickExtract DNA solution (Epicentre, Madison, WI, USA). Genotyping was performed by PCR using Platinum *Pfx* Polymerase (Life Technologies) with primers spanning both predicted cut sites, allowing for simple screening of deletions (Forward: 5'-GGGCCTTAGAGAGACTTGAATG-3'; Reverse: 5'-GCAGAGGCAGATGGATTTCT-3').

For mice whose genotyping showed discernible deletions, the smallest sized bands were cut from the gel and purified using the QIAquick Gel Extraction Kit (Qiagen, Venlo, Netherlands). DNA was sequenced using the same primers used for PCR, and

from the sequence, protein products were predicted. Based on these results, founder mice were selected for backcrossing to C57BL/6J mice, and we now have 5 different lines that have been backcrossed 6 generations. During the backcrossing process, heterozygote siblings were mated to produce homozygous offspring to ensure viability and allow for preliminary characterization of phenotype. Additionally, RNA was isolated from homozygous knockout mice using the Direct-zol RNA MiniPrep kit (Zymo Research) and cDNA was synthesized using the SuperScript III First-Strand synthesis system with oligo-dT (Life Technologies). The cDNA was used as the template for PCR using primers flanking the deleted region (Forward: 5'-CTTGGAGGAAAGAGAAGGAAGG-3'; Reverse: 5'-TGAGGGATGCGAAAGGATTAG-3') and the resulting sequence was analyzed to ensure that the mutant transcript would not produce functional Mss51 protein.

Animals were euthanized by inhalation overdose of isoflurane and cervical dislocation. Body, muscle, and fat pad weights were obtained and muscle was flash frozen in pre-cooled isopentane.

Primary Cell Culture

Primary cells were isolated from the limb muscles of two mice as previously described [110]. One wild-type and one *Mss51* knockout mouse, generated from crossing N4 mice of line 41, were used to isolate wild-type and *Mss51*^{-/-} myoblasts. Briefly, muscles were harvested, tendons and fat were removed, and the remaining muscle was minced and digested in digestion cocktail containing 2.4 U/mL Dispase II (Roche, Basel, Switzerland), 100 mg/mL Collagenase A (Roche), 50 mM CaCl₂ (Sigma-Aldrich, St. Louis, MO), and 2 U/mL DNase I (Roche) for 1.5 hours at 37 degrees Celsius with

frequent agitation. Cells were washed with PBS with 0.2% BSA and 0.1% DNase I and sequentially passed through 100 μm , 70 μm , and 40 μm cell strainers. Cells were plated in DMEM supplemented with 20% fetal bovine serum (Sigma-Aldrich), 2% chick embryo extract (USBiological, Salem, MA, USA), 2.5 ng/mL bFGF-2 (BioPioneer, San Diego, CA, USA) and 1% penicillin streptomycin (Life Technologies). To eliminate fibroblasts from the culture, cells were pre-plated for 3 hours, during which time many fibroblasts attached while most myoblasts remained in suspension. The media was then transferred to plates coated with Geltrex (Life Technologies) and allowed to attach and proliferate. When cells approached 60% confluence, they were split and subjected to the pre-plating process again. To induce differentiation, media was replaced with DMEM containing 5% horse serum (Life Technologies), 2% chick embryo extract, and 1% penicillin streptomycin.

Determination of Cell Proliferation, Differentiation, and ATP Content

To assay the rate of proliferation, cells were labeled for four hours with 10 μM 5-ethynyl-2'-deoxyuridine (EdU, a thymidine analogue) using the Click-iT EdU Alexa Fluor 594 Imaging Kit (Life Technologies), following manufacturer's instructions. The percentage of nuclei positive for EdU was determined using ImageJ software (National Institutes of Health, Bethesda, MD, USA).

To assay changes in differentiation, cells were allowed to differentiate for two days and then fixed using 4% paraformaldehyde (Electron Microscopy Sciences, Hatfield, PA, USA) and stained with anti-sarcomeric myosin (MF20-s, 1:1, Developmental Studies Hybridoma Bank (DSHB), Iowa City, IA, USA). The percentage of nuclei found within MF20-positive myotubes was determined using ImageJ software.

For both proliferation and differentiation, images were acquired using an EVOS FL Cell Imaging System equipped with a 10x/0.3 NA objective (Life Technologies). Additionally, creatine kinase (CK) enzyme activity was measured in myotubes differentiated for three days using the EnzyChrom Creatine Kinase Assay Kit (BioAssay Systems, Hayward, CA, USA) following manufacturer's instructions.

To determine cellular ATP content, cells were differentiated for three days and lysed in Reporter Lysis Buffer (Promega, Madison, WI, USA). The ATP Determination Kit (Life Technologies) was used according to manufacturer's instructions and data were normalized to protein content as determined by the bicinchonic acid (BCA) assay.

Quantitative RT-PCR

Cells and tissues were homogenized in TRIzol, total RNA was isolated using the Direct-zol RNA MiniPrep Kit (Zymo Research) and cDNA was synthesized from 1 microgram of RNA per sample using the iScript cDNA Synthesis Kit (Bio-Rad, Hercules, CA, USA). cDNA was diluted and used as the template for real-time PCR using a CFX Connect Real-Time PCR Detection System (Bio-Rad, Hercules, CA, USA) and SYBR Green PCR Master Mix (Life Technologies). Relative gene expression was determined using the $\Delta\Delta C_t$ method normalized to the indicated reference genes through the analytical software qbase+ (Biogazelle, Ghent, Belgium). At least two reference genes were included in each qRT-PCR experiment, and qbase+ was used to run the geNorm algorithm to select the most stable and suitable reference gene(s) for each experiment. Primer sequences are available upon request.

Western blot

Primary myotubes differentiated for three days were lysed and stored frozen.

Samples were heat denatured and reduced. They were separated by SDS-PAGE and transferred to PVDF using standard techniques. Membranes were blocked with 5% nonfat milk in TBS with 0.1% Tween 20 (TBS-T), probed with primary antibodies (1:1,000 anti-phosphoAMPK α , Cell Signaling Technology, Danvers, MA, USA; 1:10,000 anti-Histone H3, Sigma-Aldrich), washed, incubated with horseradish peroxidase-conjugated anti-rabbit secondary antibody, and developed using X-ray film and Amersham ECL Prime Western Blotting Detection Reagent (GE Healthcare Life Sciences, Pittsburgh, PA, USA).

Exercise Endurance

Exercise endurance was compared using an Exer 6 rodent treadmill (Columbus Instruments, Columbus, OH, USA) as previously described [111]. Animals were acclimated to the treadmill set at a 10° incline for a 5 minute 0 m/min period, after which the speed was increased to 6 m/min and raised by 2 m/min every 5 minutes until exhaustion, which was defined as 10 consecutive seconds on the shock pad. Time to exhaustion was recorded for each animal, and from that, total distance run was calculated.

Statistical Analysis

For qRT-PCR analysis, the software qbase+ (Biogazelle, Ghent, Switzerland) was used to determine statistical differences. For other experiments, two groups were compared using Student's *t* tests. Probability values (*p* values) less than 0.05 were considered statistically significant.

Results

Genetic Characterization of Founder Generation

The CRISPR/Cas9 system for genetic engineering was used to create *Mss51*^{-/-} mouse lines. Double strand breaks were introduced in the first two exons of the *Mss51* gene in single cell mouse embryos, which were implanted into pseudopregnant mice (Figure 4.1A, B). 104 pups from 11 litters were screened for deletions by genotypic PCR, which showed at least 48 pups with an easily detected deletion (Figure 4.1C). From these 48 mice, the smallest band was isolated, purified, and subjected to Sanger sequencing to determine the sequence of the mutant allele. Based on these results, eight lines were selected for backcrossing to C57BL/6J mice.

Heterozygous offspring of the second backcross generation and subsequent generations were crossed to each other to generate homozygotes, both to check for viability and to isolate RNA and perform reverse transcription PCR of *Mss51*. The amplicons were sequenced to ensure that the transcribed mRNA could not be translated to produce *Mss51*. Interestingly, while the genetic sequences of each mutant line are distinct, the cDNA sequencing results of each line showed that the mutations resulted in the same mRNA sequence. The consensus mutant transcript omits exons 1 and 2, joining the 5' untranslated region (UTR) to exon 3 (Figure 4.2). From this, the first ATG start site reached after the UTR results in a short peptide followed by a stop codon. If that start site were skipped, it is possible that a truncated peptide without the N-terminus could be produced, though it would lack the zf-MYND functional domain (Figure 4.2). Additionally, the ratios of genotypes resulting from each heterozygote cross were compared to determine if the *Mss51* alleles were being inherited in the frequencies

expected by Mendelian genetics. From 13 litters, we determined ratios of 0.174 ± 0.149 *Mss51*^{-/-} : 0.554 ± 0.159 *Mss51*^{+/-} : 0.272 ± 0.165 *Mss51*^{+/+} which were not significantly different from the expected ratio of 0.25 : 0.5 : 0.25.

Characterization of Mss51^{-/-} Primary Myoblasts

Primary myoblasts were isolated from one wild-type mouse and one *Mss51*^{-/-} mouse for characterization. To verify that these cells do not express *Mss51*, gene expression was measured in cells differentiated for 3 days (Figure 4.3A). Previously, we showed that decreased *Mss51* expression had no effect on proliferation and differentiation of C2C12 cells [100]. In the primary cells, we found no difference in proliferation as determined by incorporation of the thymidine analogue EdU (Figure 4.3B, C). Additionally, there were no differences in markers of differentiation, including fusion index after 2 days of differentiation (Figure 4.3D, E) or CK activity after 3 days of differentiation (Figure 4.3F).

We also used primary cells differentiated for 3 days to measure gene expression of numerous metabolic genes that were previously shown to be modulated by decreased *Mss51* expression [100]. In C2C12 myotubes, we showed a shift towards more fully mature, glycolytic myotubes expressing more MyHC IIb and less embryonic, neonatal, and MyHC IIx when *Mss51* expression was decreased. In *Mss51*^{-/-} primary myotubes, the MyHC expression pattern was again altered, but not in the same direction (Figure 4.4A). In this setting, there was again a decrease in neonatal MyHC, but this time, MyHC IIb mRNA levels also decreased in the absence of *Mss51*. Additionally, the expression levels of the oxidative types MyHC I and MyHC IIa were significantly increased in the *Mss51*^{-/-} myotubes (Figure 4.4A).

We examined the expression of some metabolic genes shown to be altered in C2C12s with disrupted *Mss5l*. Long chain acyl-CoA dehydrogenase (*Acadl*) and fatty acid translocase (*Cd36*) mRNA levels were significantly increased in *Mss5l*^{-/-} myotubes, in concordance with our previous results (Figure 4.4B). Peroxisome proliferator-activated receptor gamma coactivator 1-alpha (*PGC1α*) mRNA levels were significantly decreased in *Mss5l*^{-/-} myotubes, also in concordance with our previous results (Figure 4.4B). Unlike our previous results, fatty acid synthase (*Fasn*) was slightly but significantly decreased (Figure 4.4B), whereas in C2C12 myotubes we saw an increase when *Mss5l* was disrupted. *Glut4* (or *Slc2a4*, a glucose transporter) was also slightly but significantly decreased, while in C2C12 myotubes we saw no difference between control and *Mss5l*-disrupted myotubes. In *Mss5l*-disrupted C2C12 myotubes, we saw increased pyruvate dehydrogenase lipoamide kinase 4 (*Pdk4*) and hormone sensitive lipase (*HSL*), while in wild-type and *Mss5l*^{-/-} primary myotubes, there were no significant differences (Figure 4.4B).

We also examined ATP levels in wild-type and *Mss5l*^{-/-} primary myotubes. Previously, we found *Mss5l*-disrupted C2C12 myotubes to have significantly higher levels of ATP, while the opposite was found in the *Mss5l*^{-/-} primary myotubes, which had significantly lower levels of ATP (Figure 4.4C). Finally, we examined the activating phosphorylation of AMP-activated protein kinase alpha (AMPKα), which increased significantly in *Mss5l*-disrupted C2C12 myotubes. In primary myotubes, we found no evidence of increased phosphorylated AMPKα (Figure 4.4D).

We examined changes in body weight in several litters of mice born to heterozygous parents from approximately one week of age through six weeks of age

(Figure 4.5A, B). We found no differences in the growth rate of male or female wild-type, heterozygote, or knockout mice. We used two wild-type and two *Mss51*^{-/-} female mice to determine tissue mass of several muscles, including the extensor digitorum longus (EDL), soleus, tibialis anterior (TA), quadriceps, triceps, gastrocnemius, and pectoralis major, as well as the gonadal white fat pads and subcutaneous brown fat pad (Figure 4.5C,D). We found no significant differences in any of the tissues examined.

We examined expression of the genes encoding the myosin heavy chain isoforms in the quadriceps and EDL using qRT-PCR, and found the altered pattern of myosin heavy chain expression to lead to a more oxidative phenotype, with a non-significant trend towards increased expression of the genes encoding Type I and Type IIa myosin heavy chain, in agreement with the results in *Mss51*^{-/-} primary myotubes (Figure 4.6A, B). Additionally, gene expression of *Acadl* and *Cd36*, previously shown to be upregulated in both *Mss51*-disrupted C2C12 myotubes and in *Mss51*^{-/-} primary cells, was measured and showed a non-significant trend towards increased expression (Figure 4.6C, D). As a whole-organism functional measure, we compared treadmill endurance between 6 week old wild-type and *Mss51*^{-/-} mice, and saw a non-significant trend toward increased endurance as measured by time (Figure 4.6E) and distance (Figure 4.6F).

Preliminary Conclusions

Mss51^{-/-} mouse lines were generated and have been backcrossed onto the C57BL/6J inbred background (Figure 4.1). From those mouse lines, preliminary characterization has been performed. While each line carried a unique mutation in the *Mss51* genomic locus, the sequence of the resulting mRNA transcripts produced were shown to be identical, with the first two exons skipped and the 5' UTR spliced directly to the third exon. The coding sequence produced therefore was predicted to result in a short frame-shifted peptide resulting in an early stop codon. Even if an alternate start site is used and a truncated Mss51 protein is expressed, it would lack the zf-MYND functional domain, likely ablating all protein function (Figure 4.2).

We have demonstrated that *Mss51*^{-/-} primary myoblasts do not differ from wild-type primary myoblasts in their ability to proliferate or differentiate (Figure 4.3), though they did show altered gene expression (Figure 4.4). Unlike *Mss51*-disrupted C2C12 myotubes, their shift in fiber type distribution does not lead to a more glycolytic phenotype but instead to a more oxidative one. Additionally, the *Mss51*^{-/-} myoblasts from these preliminary studies appeared to possess lower cellular ATP levels, contrary to what we previously have shown in the *Mss51*-disrupted C2C12 myotubes. Phosphorylation of AMPK α was not altered in primary myotubes, indicating that the metabolic phenotype differed significantly between the immortal myotube model and the primary myotube model.

Primary myoblasts may be a better system for characterization of *Mss51*, as they are closer to what occurs physiologically *in vivo*. Fiber type expression also appeared to shift in the quadriceps, where by qRT-PCR we showed a trend toward increased

expression of the genes encoding MyHC I and MyHC IIa, which are the most oxidative fiber types (Figure 4.6). This was concordant with the trend toward increased treadmill endurance that we reported in preliminary studies using both male and female wild-type and *Mss5l*^{-/-} mice. Increased treadmill endurance and expression of the oxidative fiber type genes in *Mss5l*^{-/-} mice was consistent with reported human gene expression that shows that individuals with higher physical capacity express significantly less *Mss5l* [101]. This also was in agreement with increased expression of *Cd36* and *Acadl*, both of which are involved with the oxidation of fatty acids as an energy source. These mice did not differ in overall body weight or in the relative weight of a variety of muscles and fat deposits, indicating that phenotype resulting from *Mss5l* knockout is significantly different than that of myostatin-null mice (Figure 4.5).

An additional phenotype observed during preliminary characterization of one of increased spontaneous activity in *Mss5l*^{-/-} mice. *Mss5l*^{-/-} mice were often seen running about in their cages, often in small circles, while their wild-type littermates rested. It is currently unknown if this phenotype is primarily behavioral/neurological or metabolic. Additional tests and measures will be required to fully understand this and the broader metabolic phenotype resulting from ablation of *Mss5l*.

Future Directions

Muscle is a major regulator of metabolic homeostasis, and *Mss5l* appears to be involved in the regulation of several metabolic processes. Decreased expression of *Mss5l* has been linked to increased fatty acid oxidation, increased physical capacity, and a trend toward increased endurance (Figure 4.6, [100,101]). To fully elucidate the role of *Mss5l* in mouse muscle, *Mss5l*^{-/-} mice will be subjected to a battery of metabolic challenges, including altered diets and measures of exercise endurance and strength.

Six week-old wild-type and *Mss5l*^{-/-} mice will be fed a high fat diet for up to 12 weeks. These mice have been backcrossed onto the C57BL/6J strain, which has a well-established predisposition to diet-induced obesity [112]. While on this high fat diet, mice will be weighed twice per week and changes in weight will be compared between wild-type and *Mss5l*^{-/-} mice. Additionally, their body compositions will be compared by EchoMRI, which allows for the determination of the percentage of lean, fat, and water mass [113]. The intraperitoneal glucose tolerance test (IPGTT) will be performed to test for changes in glucose metabolism. To perform this standard test, 2 g glucose per kg body weight will be injected into fasted mice, and at the time of injection as well as at timed intervals, blood glucose levels will be determined from a tail nick using a handheld glucose meter.

Wild-type and *Mss5l*^{-/-} mice will be subjected to additional exercise tests, including repeated endurance testing using the treadmill. Treadmill endurance will be examined in mice at additional ages, and changes in endurance will be measured over time. Additionally, endurance differences can be examined in mice fed a high fat diet, to

examine if changes are altered by the change in metabolic fuels in wild-type and knockout mice.

To examine differences in spontaneous activity, open field behavior monitoring will be performed. In this test, mice are placed in a chamber that records their movement over time, allowing for the quantification of differences between the activity levels of wild-type and *Mss5l*^{-/-} mice. Activity has previously been shown to change in response to metabolic changes including the stimulation of AMPK by 5-Aminoimidazole-4-carboxamide ribonucleotide (AICAR) treatment [114], and we predict we will see increased locomotion in the *Mss5l*^{-/-} mice. We can also perform the Rotarod test to determine if the mice have altered motor coordination, which may help us to determine if *Mss5l*^{-/-} mice have an altered neurological phenotype. Voluntary wheel running may also be measured using rodent wheels (Bioseb, Pinellas Park, Florida, USA) attached to sensors that record activity. We hypothesize that the *Mss5l*^{-/-} mice will use the wheel significantly more than the wild-type mice.

Indirect calorimetry, reviewed in [115], will be useful in determining basal fuel utilization as well as numerous other potential metabolic differences between wild-type and *Mss5l*^{-/-} mice. In indirect calorimetry, changes in oxygen and carbon dioxide levels in the air are measured as indicators of respiration, allowing for the calculation of the respiratory exchange ratio (RER). The RER, determined by dividing the CO₂ exhaled (*V*CO₂) divided by the O₂ inhaled (*V*O₂), varies depending on the substrate being metabolized, from a value of 1.0 for pure carbohydrate metabolism down to 0.7 for pure fat metabolism [115]. The Johns Hopkins Centralized Services for Metabolism Research has a 16-animal Oxymax indirect calorimeter (Columbus Instruments, Columbus, OH),

which can be used for 5-day experiments that allow for acclimation, calibration, and experimental data collection. Due to the trends we have observed in *Acadl* and *Cd36* mRNA expression, we hypothesize that *Mss5l*^{-/-} mice will have a lower RER, indicating that they metabolize fats more efficiently than wild-type mice.

To examine the effects of ablation of *Mss5l* in dystrophic muscle, mice are currently being bred to produce *Mss5l*^{-/-} *mdx* double mutants. These mice will lack both *Mss5l* and dystrophin, allowing for the examination of metabolic benefits in a mouse model of muscular dystrophy without altered muscle mass, as occurs with ablation or inhibition of myostatin. Myostatin-null *mdx* mice demonstrate less severe pathology than *mdx* mice expressing normal levels of myostatin, including increased strength and myofiber diameter and less fibrosis and fatty remodeling of the diaphragm [116,117]. Simultaneously, muscle hypertrophy resulting from myostatin inhibition may increase stress on dystrophic fibers, as demonstrated recently by the accelerated degeneration observed after myostatin inhibition in a mouse model of dysferlinopathy [118]. It is possible that some of the benefits offered with myostatin ablation or blockade in *mdx* are due, in part, to metabolic changes linked to decreased *Mss5l* expression. To explore this, we will examine the muscle of *Mss5l*^{-/-} *mdx* mice compared to *mdx* mice that express wild-type *Mss5l*, looking for changes in strength, endurance, and markers of degeneration and regeneration.

Figures

Figure 4.1. Generation and genetic characterization of *Mss51*^{-/-} mice. (A) CRISPR gRNA target sites located in exons 1 and 2 of the *Mss51* genomic locus. (B) Diagram of procedures including injection of gRNAs and *Cas9* mRNA into mouse zygotes, which develop into blastocysts and are transferred into pseudopregnant females. The resulting pups are potential *Mss51* mutants. (C) Results of *Mss51* genotyping show at least 48 of 104 pups had easily detected deletions in exons 1 and 2 of *Mss51*. The red dotted line indicates the expected size for wild-type *Mss51*. Mice 523 and 524 were mothers of founders serving as wild-type controls, and NTC indicates no template control. Mice were identified by numbers 1 through 104.

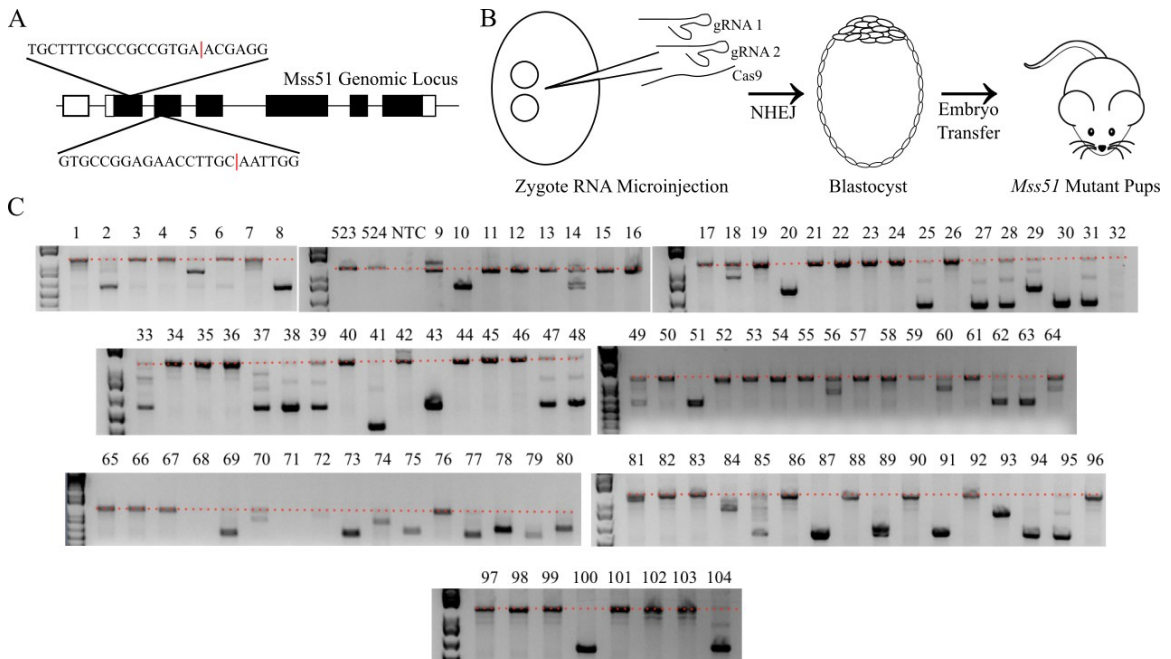


Figure 4.2. *Mss51* mRNA from *Mss51*^{-/-} mice is missing exons 1 and 2. RNA was isolated from knockout mice and used to make cDNA, which served as the template for RT-PCR of *Mss51*. The amplicon was purified, sequenced, and compared to the wild-type *Mss51* transcript. All mouse lines analyzed produced the same transcript, joining the 5' UTR to exon 3.

```

wildtype  GAGTCTTGAGCCCTTTGGCAGAGAATAAGAGTCAGAAAGAGAAGCTCCAGCAGGTGCCAGTCTGACTGTCTCGTTAGGGAGAATTCACTCTGTCTGT
knockout  GAGTCTTGAGCCCTTTGGCAGAGAATAAGAGTCAGAAAGAGAAGCTCCAGCAGGTGCCAGTCTGACTGTCTCGTTAGGGAGAATTCACTCTGTCTGT

wildtype  CTGGTTGGCAGGGCAGCTTAGTCACTGAGACCCAGCATTTCAGCAGTTTGACAGAAAAGTGATGTGAACAGACAGCTGCAAGTGAGACACAGCCTAGGTCTG
knockout  CTGGTTGGCAGGGCAGCTTAGTCACTGAGACCCAGCATTTCAGCAGTTTGACAGAAAAGTGATGTGAACAGACAGCTGCAAGTGAGACACAGCCTAGGTCTG

wildtype  AAGAGATGAAGCATTTACTTCACTTGGAGAAAAGAGAAGGAAGCCTTAGGGCTTAACAGGCAGCTGGTCCCAAGTTCATTGGTCAATGGCTCCTCGTTCA
knockout  AAGAGATGAAGCATTTACTTCACTTGGAGAAAAGAGAAGGAAGCCTTAGGGCTTAACAGG-----

wildtype  CGGGCGGAAAGCACAAGAAACCCCAAGTATTCCCATGATTGAATCCCAAGCAGAGTGTCTCCAGTATCTCCAGCCCTCTCAAACTGGCCCT
knockout  -----

wildtype  AGCATTGATGCATTTGGCTTCACTTCTTGGACAATAATGTACCAGTCTGTCCCAAGTGTACCTCCAAAAGCTGAACATGAAAACATAGAGAATACAAG
knockout  -----

wildtype  TTGGTGATAAATGGGGGAACCCCAAGTATCAAGCTTTGGATAGAATACAAGTTGGTGATAAATGGGGGAACCCCAAGTATCAAGCTTTGGATTTCGATGTCAACA
knockout  -----

wildtype  AGAATGTCCAGAAGATGGAGACACATTCAAGTTCATGCTTAAATGCTCCCTCAAGGCTTCCAAATGCAAGGTTCTCCGGCACTGTAAAG
knockout  -----

wildtype  GTGCAGAAATGCTTACTTACTGTGATACAGAGTCCAGAGGCTCAGATTTGCCAGCACATAGGAAGGTTTGTGGAGAGCTCCGCTCTGTGGCTGTAGTCTGT
knockout  GTGCAGAAATGCTTACTTACTGTGATACAGAGTCCAGAGGCTCAGATTTGCCAGCACATAGGAAGGTTTGTGGAGAGCTCCGCTCTGTGGCTGTAGTCTGT
Predicted knockout coding sequence

wildtype  CATGGAATGGCTTCTGGTACAGGTGATTTTGTCTCAACCTCAGGACCTTGGCCATGGCTACCTGAAGATATACAGAATTGGGATACCTGGTTTCTATGAG
knockout  CATGGAATGGCTTCTGGTACAGGTGATTTTGTCTCAACCTCAGGACCTTGGCCATGGCTACCTGAAGATATACAGAATTGGGATACCTGGTTTCTATGAG
Alternate knockout start site

wildtype  GGGTTTACAGCTAGAATCTACATTGAATGCTCTTCTGGGTAGTCACTCTATGACATGCTTTGGGCAAGCTTAGGAAGGCCACGGCCAGACCCAGATGTCTT
knockout  GGGTTTACAGCTAGAATCTACATTGAATGCTCTTCTGGGTAGTCACTCTATGACATGCTTTGGGCAAGCTTAGGAAGGCCACGGCCAGACCCAGATGTCTT

wildtype  GCATGGCTCTTTGAAGCGGTTGATGACAGATGTTCTGTACAGCCCTTGACCTGGGCTTAGGGCTTCGGACTGTGGCAATAGATGTTGGGAAGACTGGAGG
knockout  GCATGGCTCTTTGAAGCGGTTGATGACAGATGTTCTGTACAGCCCTTGACCTGGGCTTAGGGCTTCGGACTGTGGCAATAGATGTTGGGAAGACTGGAGG

wildtype  AAGCAGATTGCATGGTGGTGGTCTCCCAAGTAGAGACATTTCTTATCGTTCTGGAGATTATGATGAGCTTGGCTACATGTTTCTGAAACCTTGGCTT
knockout  AAGCAGATTGCATGGTGGTGGTCTCCCAAGTAGAGACATTTCTTATCGTTCTGGAGATTATGATGAGCTTGGCTACATGTTTCTGAAACCTTGGCTT

wildtype  TCATGTGATCATGGTGGTGGTGGATGTGGCTACTGACCTTTTACAGAGTCTTCACTTTATCCTTGGAGCTGGAAACAATTAGCTTATGGCCACAGGGC
knockout  TCATGTGATCATGGTGGTGGTGGATGTGGCTACTGACCTTTTACAGAGTCTTCACTTTATCCTTGGAGCTGGAAACAATTAGCTTATGGCCACAGGGC

wildtype  CCTGTATCATGACTTCTGGAGGAGCAATAGAGACTGGGATTTGGCCATCCAGATTGGTGGCTGCATTCCATCCAGGTTTCCATGCTCCCAAGGCTT
knockout  CCTGTATCATGACTTCTGGAGGAGCAATAGAGACTGGGATTTGGCCATCCAGATTGGTGGCTGCATTCCATCCAGGTTTCCATGCTCCCAAGGCTT

wildtype  GATGGAAGCTTGGTACCCACCTGCTACTTCTGACTATGAGATTCACAGATTGATTAAGTGTTTACAGCCAAAGGAACTGGAGCCCTTTGAGAT
knockout  GATGGAAGCTTGGTACCCACCTGCTACTTCTGACTATGAGATTCACAGATTGATTAAGTGTTTACAGCCAAAGGAACTGGAGCCCTTTGAGAT

wildtype  TCTGGTGAATTTGATACACACATCACTGCTGTGGAGCTAATCCTTTCGCATCCCTCAAACAGACAGTCTATTCTAATCCCAACAGCAACAGTATA
knockout  TCTGGTGAATTTGATACACACATCACTGCTGTGGAGCTAATCCTTTCGCATCCCTCAAACAGACAGTCTATTCTAATCCCAACAGCAACAGTATA

wildtype  CAGCAGTGCCTACTACATCATGTTCTTGGAGTTCCCTGCAATTAGATAAGAGACACAGAGGAAAAAAGAAAAAACAACACAGATGATTTTCA
knockout  CAGCAGTGCCTACTACATCATGTTCTTGGAGTTCCCTGCAATTAGATAAGAGACACAGAGGAAAAAAGAAAAAACAACACAGATGATTTTCA

wildtype  GTAATTGAACCAAGCTTTTACTGAATGCTGGAAAATGAAAGCTTAATCAACTTACCCCTGTGATGTGAGATTTTGGCAGCTTGAACCCCTGTGGTATGCT
knockout  GTAATTGAACCAAGCTTTTACTGAATGCTGGAAAATGAAAGCTTAATCAACTTACCCCTGTGATGTGAGATTTTGGCAGCTTGAACCCCTGTGGTATGCT

wildtype  AAACCTTATTCAGATTCAAATAAAGATGTTTAAACCAATGG 1829
knockout  AAACCTTATTCAGATTCAAATAAAGATGTTTAAACCAATGG 1431

```

Figure 4.3. *Mss51*^{-/-} primary cells proliferate and differentiate normally. (A) Differentiated primary cells from *Mss51*^{-/-} mice do not express *Mss51*, as determined by qRT-PCR normalized to reference genes *TBP* and *Tfam* (n=3). (B) Representative images of EdU incorporation (red), with Hoechst 33342 nuclear counterstain (blue). (C) Wild-type and *Mss51*^{-/-} cells proliferate at the same rate as determined by EdU incorporation (n=9). (D) Representative images of MF20-stained myotubes differentiated for 2 days. (E) Fusion index indicates there is no difference in differentiation of wild-type and *Mss51*^{-/-} myotubes (n=6). (F) Wild-type and *Mss51*^{-/-} myotubes differentiated for 3 days have equivalent creatine kinase (CK) activity (n=6).

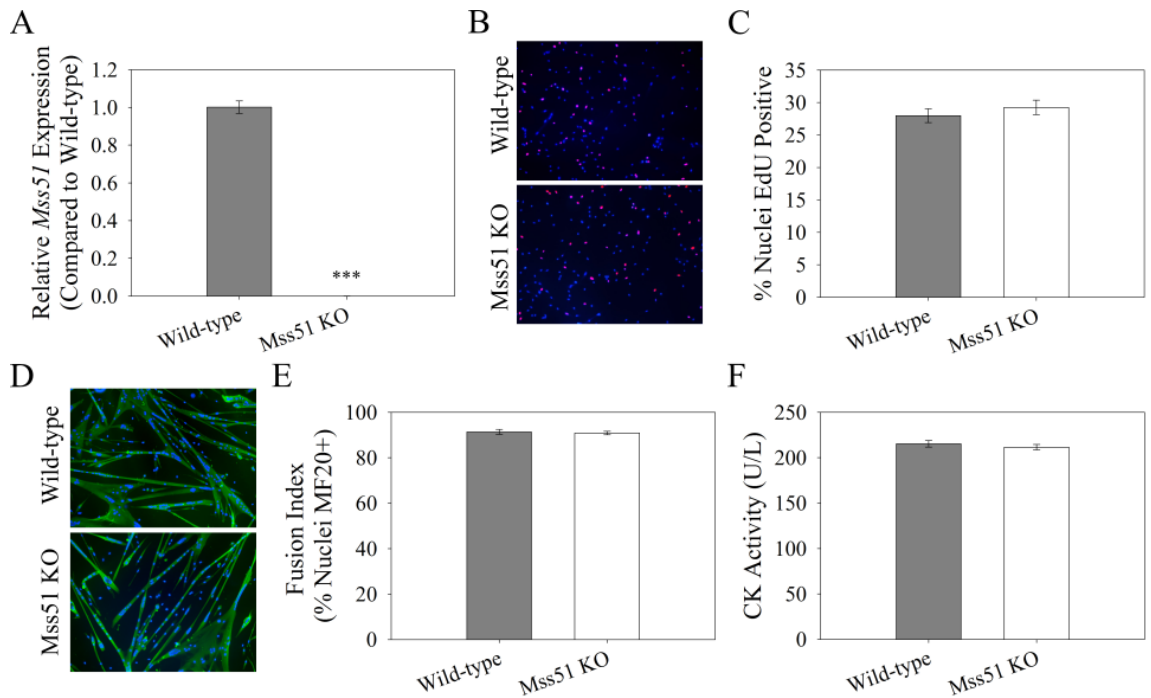


Figure 4.4. Gene expression and ATP content of *Mss51*^{-/-} primary myotubes. (A) Myosin heavy chain and (B) metabolic gene mRNA levels determined by qRT-PCR, normalized to wild-type mRNA abundance using reference genes *TBP* and *Tfam* (n=3). (C) ATP content of wild-type and *Mss51*^{-/-} myotubes, normalized to protein content (n=6). (D) Levels of phosphorylated AMPK α determined by Western blot with loading control Histone H3 (n=4).

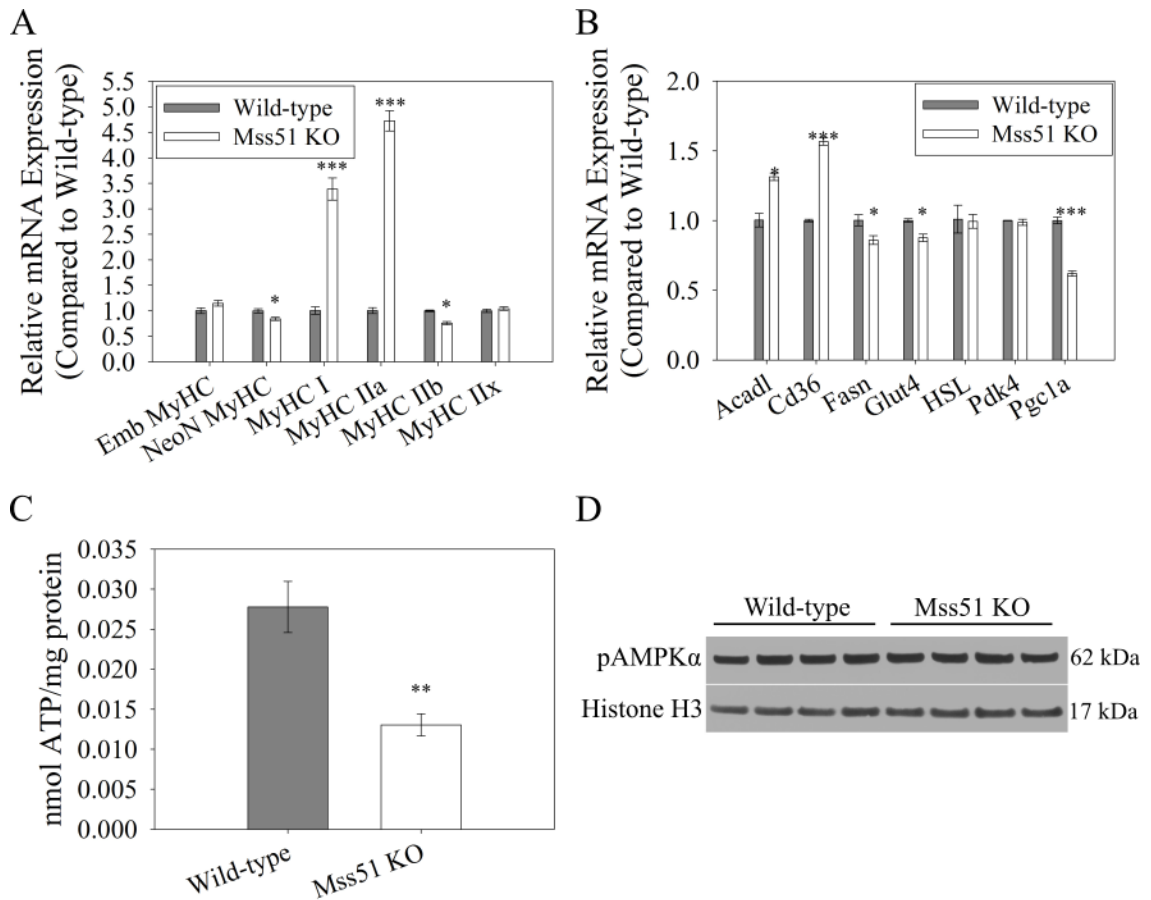


Figure 4.5. *Mss51*^{-/-} mice do not differ in size from wild-type mice. (A) Female and (B) male mouse body weights from one week to six weeks postnatal (n=2 to 6 per group). (C) Muscle weights of EDL, gastrocnemius, soleus, triceps, and pectoralis, normalized to body weight, in wild-type and *Mss51*^{-/-} mice (n=2). (D) Weights of the gonadal white fat deposit and the subcutaneous brown fat deposit normalized to body weight, in wild-type and *Mss51*^{-/-} mice (n=2).

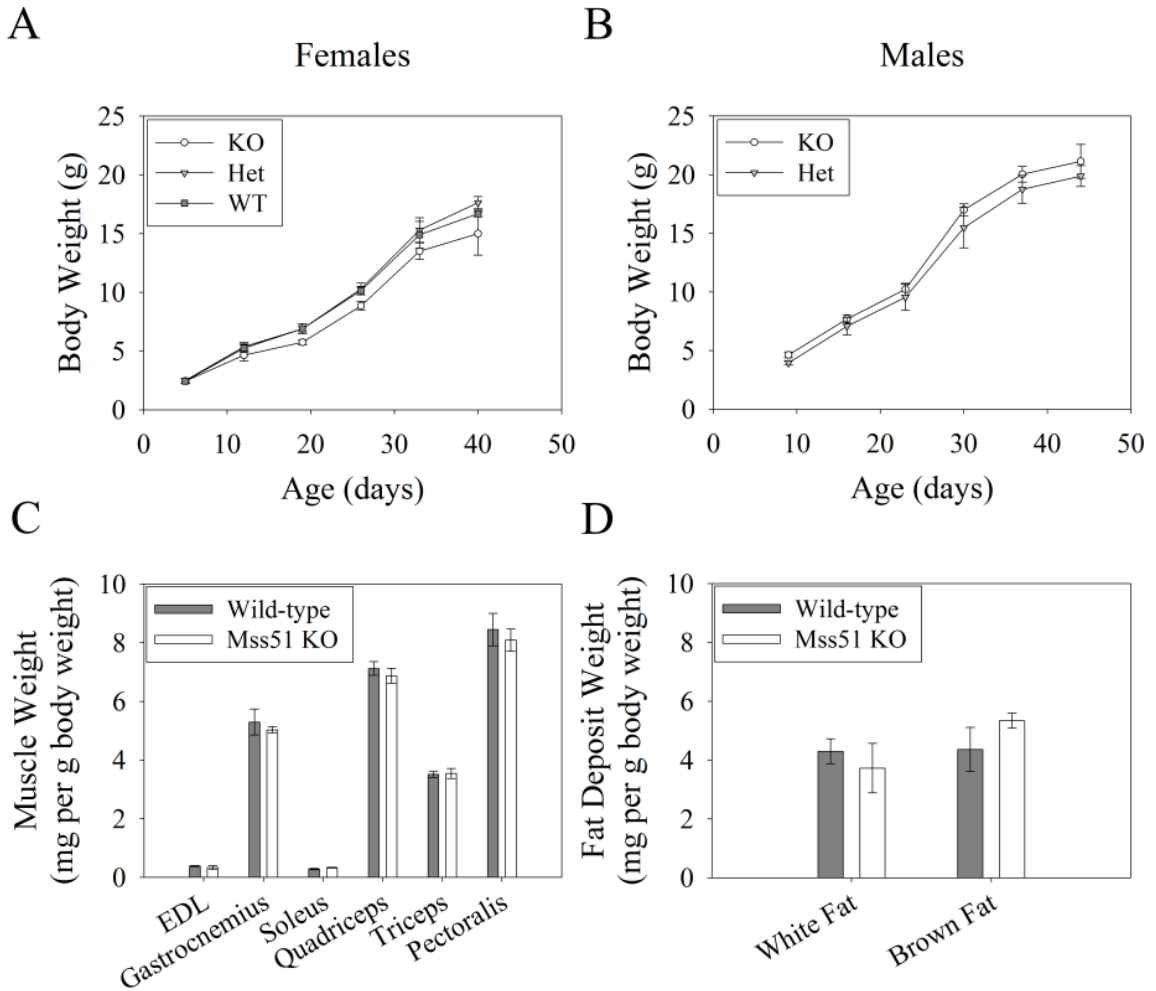
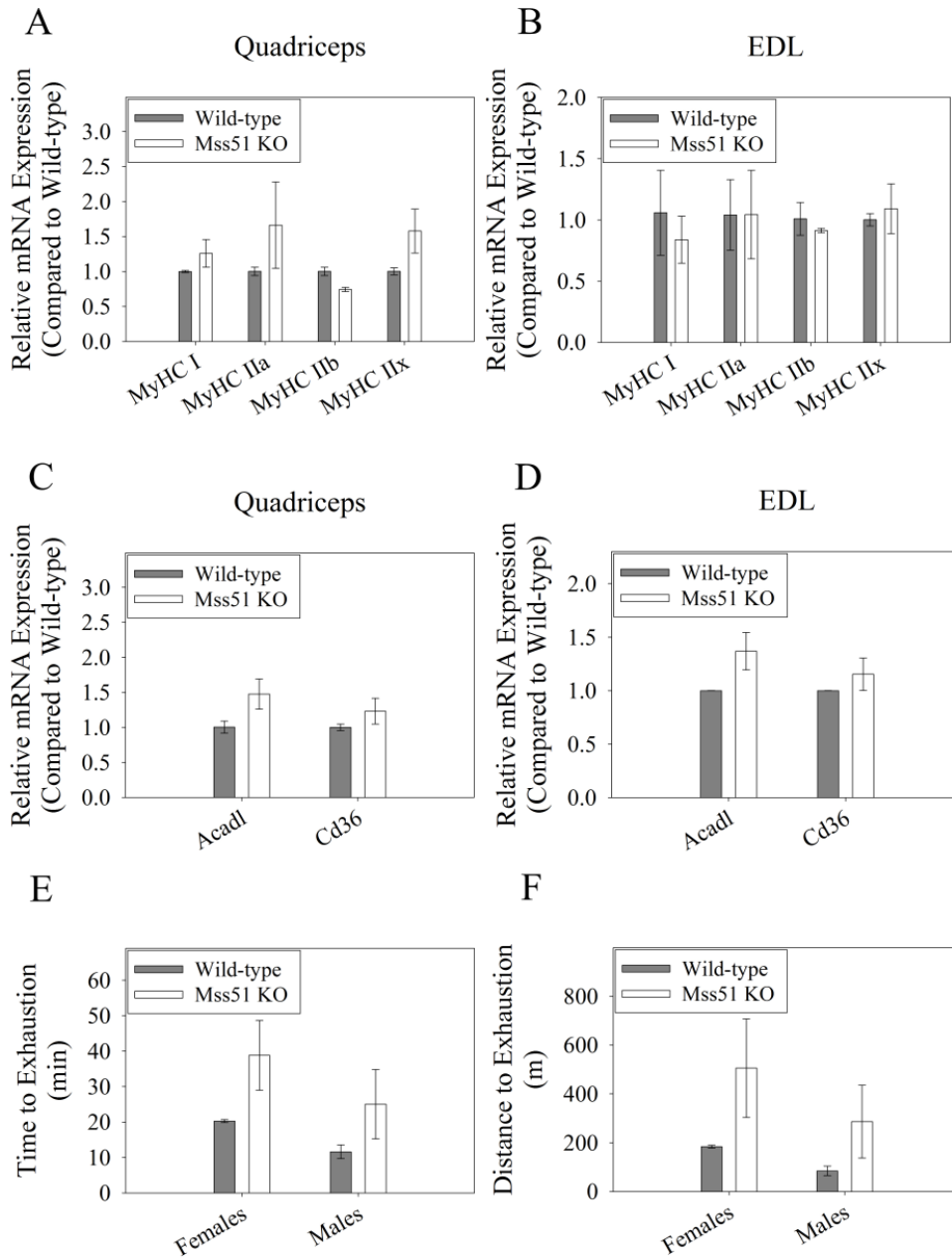


Figure 4.6. *Mss51*^{-/-} mice appear to differ metabolically from wild-type mice. (A) Myosin heavy chain gene expression profiling from the quadriceps and (B) from the EDL of wild-type and *Mss51*^{-/-} mice (n=2). (C) *Acadl* and *Cd36* gene expression in the quadriceps and (D) the EDL of wild-type and *Mss51*^{-/-} mice (n=2). (E) Time to exhaustion and (D) distance to exhaustion in treadmill endurance tests of female and male wild-type and *Mss51*^{-/-} mice (n=2 to 3).



References

- [1] Moyer AL, Wagner KR. Regeneration versus fibrosis in skeletal muscle. *Current Opinion in Rheumatology*. 2011. p. 568–73.
- [2] Brigitte M, Schilte C, Plonquet A, Baba-Amer Y, Henri A, Charlier C, et al. Muscle resident macrophages control the immune cell reaction in a mouse model of notexin-induced myoinjury. *Arthritis Rheum*. 2010;62(1):268–79.
- [3] Chazaud B, Brigitte M, Yacoub-Youssef H, Arnold L, Gherardi R, Sonnet C, et al. Dual and beneficial roles of macrophages during skeletal muscle regeneration. *Exerc Sport Sci Rev*. 2009;37(1):18–22.
- [4] Contreras-Shannon V, Ochoa O, Reyes-Reyna SM, Sun D, Michalek JE, Kuziel WA, et al. Fat accumulation with altered inflammation and regeneration in skeletal muscle of CCR2^{-/-} mice following ischemic injury. *Am J Physiol Cell Physiol*. 2007;292(2):C953–67.
- [5] Sun D, Martinez CO, Ochoa O, Ruiz-Willhite L, Bonilla JR, Centonze VE, et al. Bone marrow-derived cell regulation of skeletal muscle regeneration. *FASEB J*. 2009;23(2):382–95.
- [6] Lu H, Huang D, Ransohoff RM, Zhou L. Acute skeletal muscle injury: CCL2 expression by both monocytes and injured muscle is required for repair. *FASEB J*. 2011;25(10):3344–55.
- [7] Tidball JG, Villalta SA. Regulatory interactions between muscle and the immune system during muscle regeneration. *Am J Physiol Regul Integr Comp Physiol*. 2010;298(5):R1173–87.
- [8] Villalta SA, Nguyen HX, Deng B, Gotoh T, Tidball JG. Shifts in macrophage

phenotypes and macrophage competition for arginine metabolism affect the severity of muscle pathology in muscular dystrophy. *Hum Mol Genet.* 2009;18(3):482–96.

- [9] Villalta SA, Rinaldi C, Deng B, Liu G, Fedor B, Tidball JG. Interleukin-10 reduces the pathology of mdx muscular dystrophy by deactivating M1 macrophages and modulating macrophage phenotype. *Hum Mol Genet.* 2011;20(4):790–805.
- [10] Kafadar KA, Yi L, Ahmad Y, So L, Rossi F, Pavlath GK. Sca-1 expression is required for efficient remodeling of the extracellular matrix during skeletal muscle regeneration. *Dev Biol.* Elsevier Inc.; 2009;326(1):47–59.
- [11] Long KK, Pavlath GK, Montano M. Sca-1 influences the innate immune response during skeletal muscle regeneration. *Am J Physiol Cell Physiol.* 2011;300(2):C287–94.
- [12] Long KK, Montano M, Pavlath GK. Sca-1 is negatively regulated by TGF-beta1 in myogenic cells. *FASEB J.* 2011;25(4):1156–65.
- [13] Lagrota-Candido J, Canella I, Pinheiro DF, Santos-Silva LP, Ferreira RS, Guimarães-Joca FJ, et al. Characteristic pattern of skeletal muscle remodelling in different mouse strains. *Int J Exp Pathol.* 2010;91(6):522–9.
- [14] Boldrin L, Muntoni F, Morgan JE. Are human and mouse satellite cells really the same? *J Histochem Cytochem.* 2010;58(11):941–55.
- [15] Ono Y, Boldrin L, Knopp P, Morgan JE, Zammit PS. Muscle satellite cells are a functionally heterogeneous population in both somite-derived and branchiomeric muscles. *Dev Biol.* Elsevier Inc.; 2010;337(1):29–41.
- [16] Brack AS, Conboy MJ, Roy S, Lee M, Kuo CJ, Keller C, et al. Increased Wnt

signaling during aging alters muscle stem cell fate and increases fibrosis. *Science*. 2007;317(5839):807–10.

- [17] Conboy IM, Conboy MJ, Wagers AJ, Girma ER, Weissman IL, Rando T a. Rejuvenation of aged progenitor cells by exposure to a young systemic environment. *Nature*. 2005;433(7027):760–4.
- [18] Lu H, Huang D, Saederup N, Charo IF, Ransohoff RM, Zhou L. Macrophages recruited via CCR2 produce insulin-like growth factor-1 to repair acute skeletal muscle injury. *FASEB J*. 2011;25(1):358–69.
- [19] Madhala-Levy D, Williams VC, Hughes SM, Reshef R, Halevy O. Cooperation between Shh and IGF-I in promoting myogenic proliferation and differentiation via the MAPK/ERK and PI3K/Akt pathways requires smo activity. *J Cell Physiol*. 2012;227(4):1455–64.
- [20] McPherron AC, Lawler AM, Lee S-J. Regulation of skeletal muscle mass in mice by a new TGF-beta superfamily member. *Nature*. 1997;387(6628):83–90.
- [21] Li ZB, Kollias HD, Wagner KR. Myostatin directly regulates skeletal muscle fibrosis. *J Biol Chem*. 2008;283(28):19371–8.
- [22] Cadena SM, Tomkinson KN, Monnell TE, Spaits MS, Kumar R, Underwood KW, et al. Administration of a soluble activin type IIB receptor promotes skeletal muscle growth independent of fiber type. *J Appl Physiol*. 2010;109(3):635–42.
- [23] Lee S-J, Reed LA, Davies M V, Girgenrath S, Goad MEP, Tomkinson KN, et al. Regulation of muscle growth by multiple ligands signaling through activin type II receptors. *Proc Natl Acad Sci U S A*. 2005;102(50):18117–22.
- [24] Rahimov F, King OD, Warsing LC, Powell RE, Emerson CP, Kunkel LM, et al. Gene expression profiling of skeletal muscles treated with a soluble activin type

IIB receptor. *Physiol Genomics*. 2011;43(8):398–407.

- [25] Zhu J, Li Y, Lu A, Gharaibeh B, Ma J, Kobayashi T, et al. Follistatin improves skeletal muscle healing after injury and disease through an interaction with muscle regeneration, angiogenesis, and fibrosis. *Am J Pathol*. 2011;179(2):915–30.
- [26] Kota J, Handy CR, Haidet AM, Montgomery CL, Eagle A, Rodino-Klapac LR, et al. Follistatin gene delivery enhances muscle growth and strength in nonhuman primates. *Sci Transl Med*. 2009;1(6):6ra15.
- [27] Allen DL, Loh AS. Posttranscriptional mechanisms involving microRNA-27a and b contribute to fast-specific and glucocorticoid-mediated myostatin expression in skeletal muscle. *Am J Physiol Cell Physiol*. 2011;300(1):C124–37.
- [28] Joe AWB, Yi L, Natarajan A, Le Grand F, So L, Wang J, et al. Muscle injury activates resident fibro/adipogenic progenitors that facilitate myogenesis. *Nat Cell Biol*. Nature Publishing Group; 2010;12(2):153–63.
- [29] Natarajan A, Lemos DR, Rossi FM V. Fibro/adipogenic progenitors: A double-edged sword in skeletal muscle regeneration. *Cell Cycle*. 2010;9(11):2045–6.
- [30] Uezumi A, Fukada S, Yamamoto N, Takeda S, Tsuchida K. Mesenchymal progenitors distinct from satellite cells contribute to ectopic fat cell formation in skeletal muscle. *Nat Cell Biol*. Nature Publishing Group; 2010;12(2):143–52.
- [31] Olson LE, Soriano P. Increased PDGFRalpha Activation Disrupts Connective Tissue Development and Drives Systemic Fibrosis. *Dev Cell*. Elsevier Ltd; 2009;16(2):303–13.
- [32] Mathew SJ, Hansen JM, Merrell AJ, Murphy MM, Lawson JA, Hutcheson DA, et al. Connective tissue fibroblasts and Tcf4 regulate myogenesis. *Development*. 2011;138(2):371–84.

- [33] Bauersachs J. Regulation of myocardial fibrosis by MicroRNAs. *J Cardiovasc Pharmacol.* 2010;56(5):454–9.
- [34] Percival JM, Whitehead NP, Adams ME, Adamo CM, Beavo JA, Froehner SC. Sildenafil reduces respiratory muscle weakness and fibrosis in the mdx mouse model of Duchenne muscular dystrophy. *J Pathol.* 2012;228(1):77–87.
- [35] Hoffman EP, Brown RH, Kunkel LM. Dystrophin: the protein product of the Duchenne muscular dystrophy locus. *Cell.* 1987;51(6):919–28.
- [36] Nowak KJ, Davies KE. Duchenne muscular dystrophy and dystrophin: pathogenesis and opportunities for treatment. *EMBO Rep.* 2004;5(9):872–6.
- [37] Michele DE, Campbell KP. Dystrophin-glycoprotein complex: Post-translational processing and dystroglycan function. *J Biol Chem.* 2003;278(18):15457–60.
- [38] Froehner SC, Reed SM, Anderson KN, Huang PL, Percival JM. Loss of nNOS inhibits compensatory muscle hypertrophy and exacerbates inflammation and eccentric contraction-induced damage in mdx mice. *Hum Mol Genet.* 2015;24(2):492–505.
- [39] Kass DA. Res-erection of viagra as a heart drug. *Circ Heart Fail.* 2011;4(1):2–4.
- [40] Adamo C, Dai D, Percival J, Minami E, Willis MS, Patrucco E, et al. Sildenafil reverses cardiac dysfunction in the mdx mouse model of Duchenne muscular dystrophy. *Proc Natl Acad Sci U S A.* 2010;107(44):19079–83.
- [41] Leiria LO, Silva FH, Davel AP, Alexandre EC, Calixto MC, De Nucci G, et al. The soluble guanylyl cyclase activator BAY 60-2770 ameliorates overactive bladder in obese mice. *J Urol.* 2014;191(2):539–47.

- [42] Rojas-Moscoso JA, Antunes E, Figueira RR, Gonçalves FL, Simões ALB, Sbragia L. The soluble guanylyl cyclase activator BAY 60-2770 potently relaxes the pulmonary artery on congenital diaphragmatic hernia rabbit model. *Pediatr Surg Int.* 2014;30(10):1031–6.
- [43] Silva FH, Leiria LO, Alexandre EC, Davel APC, Mónica FZ, De Nucci G, et al. Prolonged Therapy with the Soluble Guanylyl Cyclase Activator BAY 60-2770 Restores the Erectile Function in Obese Mice. *J Sex Med.* 2014;11(11):2661–70.
- [44] Mónica FZ, Murad F, Bian K. Modulating cGMP levels as therapeutic drug targets in cardiovascular and non-cardiovascular diseases. *OA Biochem.* 2014;11:1–12.
- [45] Bilwes A, Rees B, Moras D, Menez R, Menez A. X-ray structure at 1.55 Å of toxin gamma, a cardiotoxin from *Naja nigricollis* venom. Crystal packing reveals a model for insertion into membranes. *J Mol Biol.* 1994. p. 122–36.
- [46] Partridge TA. The mdx mouse model as a surrogate for Duchenne muscular dystrophy. *FEBS J.* 2013;280(17):4177–86.
- [47] Bulfield G, Siller WG, Wight PA, Moore KJ. X chromosome-linked muscular dystrophy (mdx) in the mouse. *Proc Natl Acad Sci U S A.* 1984;81(4):1189–92.
- [48] Witting N, Kruuse C, Nyhuus B, Prahm K, Citirak G, Lundgaard S, et al. Effect of sildenafil on skeletal and cardiac muscle in Becker muscular dystrophy. *Ann Neurol.* 2014;1–8.
- [49] Leung DG, Herzka DA, Thompson WR, He B, Bibat G, Tennekoon G, et al. Sildenafil does not improve cardiomyopathy in Duchenne/Becker muscular dystrophy. *Ann Neurol.* 2014;76(4):541–9.

- [50] Sheffield-Moore M, Wiktorowicz JE, Soman K V, Danesi CP, Kinsky MP, Dillon EL, et al. Sildenafil increases muscle protein synthesis and reduces muscle fatigue. *Clin Transl Sci.* 2013;6(6):463–8.
- [51] Nelson MD, Rader F, Tang X, Tavyev J, Nelson SF, Miceli MC, et al. PDE5 inhibition alleviates functional muscle ischemia in boys with Duchenne muscular dystrophy. *Neurology.* 2014;82(23):2085–91.
- [52] Li ZB, Zhang J, Wagner KR. Inhibition of myostatin reverses muscle fibrosis through apoptosis. *J Cell Sci.* 2012;125(17):3957–65.
- [53] Wagner KR, Liu X, Chang X, Allen RE. Muscle regeneration in the prolonged absence of myostatin. *Proc Natl Acad Sci U S A.* 2005;102(7):2519–24.
- [54] Zhu J, Li Y, Shen W, Qiao C, Ambrosio F, Lavasani M, et al. Relationships between transforming growth factor- β 1, myostatin, and decorin: Implications for skeletal muscle fibrosis. *J Biol Chem.* 2007;282(35):25852–63.
- [55] Siritto V, Salerno MS, Berry C, Nicholas G, Bower R, Kambadur R, et al. Antagonism of myostatin enhances muscle regeneration during sarcopenia. *Mol Ther.* 2007;15(8):1463–70.
- [56] McCroskery S, Thomas M, Platt L, Hennebry A, Nishimura T, McLeay L, et al. Improved muscle healing through enhanced regeneration and reduced fibrosis in myostatin-null mice. *J Cell Sci.* 2005;118(Pt 15):3531–41.
- [57] McPherron AC. Metabolic functions of myostatin and GDF11. *Immunol Endocr Metab Agents Med Chem.* 2010;10(4):217–31.
- [58] Girgenrath S, Song K, Whittemore LA. Loss of myostatin expression alters fiber-type distribution and expression of myosin heavy chain isoforms in slow- and fast-type skeletal muscle. *Muscle and Nerve.* 2005;31(1):34–40.

- [59] Amthor H, Macharia R, Navarrete R, Schuelke M, Brown SC, Otto A, et al. Lack of myostatin results in excessive muscle growth but impaired force generation. *Proc Natl Acad Sci U S A*. 2007;104(6):1835–40.
- [60] Mouisel E, Relizani K, Mille-Hamard L, Denis R, Hourde C, Agbulut O, et al. Myostatin is a key mediator between energy metabolism and endurance capacity of skeletal muscle. *AJP Regul Integr Comp Physiol*. 2014;307(4):R444–54.
- [61] Guo T, Jou W, Chanturiya T, Portas J, Gavrilova O, McPherron AC. Myostatin inhibition in muscle, but not adipose tissue, decreases fat mass and improves insulin sensitivity. *PLoS One*. 2009;4(3):1–11.
- [62] Zhang C, McFarlane C, Lokireddy S, Bonala S, Ge X, Masuda S, et al. Myostatin-deficient mice exhibit reduced insulin resistance through activating the AMP-activated protein kinase signalling pathway. *Diabetologia*. 2011;54(6):1491–501.
- [63] Qiu S, Mintz JD, Salet CD, Han W, Giannis a., Chen F, et al. Increasing Muscle Mass Improves Vascular Function in Obese (db/db) Mice. *J Am Heart Assoc*. 2014;3(3):e000854–e000854.
- [64] McPherron AC, Lee SJ. Suppression of body fat accumulation in myostatin-deficient mice. *J Clin Invest*. 2002;109(5):595–601.
- [65] Guo T, Bond ND, Jou W, Gavrilova O, Portas J, McPherron AC. Myostatin inhibition prevents diabetes and hyperphagia in a mouse model of lipodystrophy. *Diabetes*. 2012;61(10):2414–23.
- [66] Koncarevic A, Kajimura S, Cornwall-Brady M, Andreucci A, Pullen A, Sako D, et al. A novel therapeutic approach to treating obesity through modulation of TGF β signaling. *Endocrinology*. 2012;153(7):3133–46.

- [67] Akpan I, Goncalves MD, Dhir R, Yin X, Pistilli EE, Bogdanovich S, et al. The effects of a soluble activin type IIB receptor on obesity and insulin sensitivity. *Int J Obes (Lond)*. Nature Publishing Group; 2009;33(11):1265–73.
- [68] Welle S, Cardillo A, Zanche M, Tawil R. Skeletal muscle gene expression after myostatin knockout in mature mice. *Physiol Genomics*. 2009;38(3):342–50.
- [69] Welle S, Burgess K, Mehta S. Stimulation of skeletal muscle myofibrillar protein synthesis, p70 S6 kinase phosphorylation, and ribosomal protein S6 phosphorylation by inhibition of myostatin in mature mice. *Am J Physiol Endocrinol Metab*. 2009;296(3):E567–72.
- [70] Miao Y, Yang J, Xu Z, Jing L, Zhao S, Li X. RNA Sequencing Identifies Upregulated Kyphoscoliosis Peptidase and Phosphatidic Acid Signaling Pathways in Muscle Hypertrophy Generated by Transgenic Expression of Myostatin Propeptide. *Int J Mol Sci*. 2015;16(4):7976–94.
- [71] Accornero F, Kanisicak O, Tjondrokoesoemo A, Attia A, McNally E, Molkentin J. Myofiber-specific inhibition of TGF β signaling protects skeletal muscle from injury and dystrophic disease in mice. *Hum Mol Genet*. 2014 Dec 20;23(25):6903–15.
- [72] Perez-Martinez X, Butler CA, Shingu-Vazquez M, Fox TD. Dual functions of Mss1 couple synthesis of Cox1 to assembly of cytochrome c oxidase in *Saccharomyces cerevisiae* mitochondria. *Mol Biol Cell*. 2009;20(20):4371–80.
- [73] Soto IC, Fontanesi F, Myers RS, Hamel P, Barrientos A. A heme-sensing mechanism in the translational regulation of mitochondrial cytochrome c oxidase biogenesis. *Cell Metab*. Elsevier Inc.; 2012;16(6):801–13.
- [74] Szklarczyk R, Wanschers BF, Cuypers TD, Esseling JJ, Riemersma M, van den Brand MA, et al. Iterative orthology prediction uncovers new mitochondrial proteins and identifies C12orf62 as the human ortholog of COX14, a protein

involved in the assembly of cytochrome c oxidase. *Genome Biol. BioMed Central Ltd*; 2012;13(2):R12.

- [75] Ran FA, Hsu PD, Wright J, Agarwala V, Scott DA, Zhang F. Genome engineering using the CRISPR-Cas9 system. *Nat Protoc.* 2013 Nov;8(11):2281–308.

- [76] Wilson KA, Chateau ML, Porteus MH. Design and Development of Artificial Zinc Finger Transcription Factors and Zinc Finger Nucleases to the hTERT Locus. *Mol Ther Nucleic Acids.* 2013;2(April):e87.

- [77] Dimauro I, Pearson T, Caporossi D, Jackson MJ. A simple protocol for the subcellular fractionation of skeletal muscle cells and tissue. *BMC Res Notes. BMC Research Notes*; 2012;5(1):513.

- [78] Schmidt EK, Clavarino G, Ceppi M, Pierre P. SUnSET, a nonradioactive method to monitor protein synthesis. *Nat Methods.* 2009;6(4):275–7.

- [79] Watkins PA, Ferrell E V, Pedersen JI, Hoefler G. Peroxisomal fatty acid beta-oxidation in HepG2 cells. *Arch Biochem Biophys.* 1991;289(2):329–36.

- [80] Lowry OH, Rosebrough NJ, Farr AL RR. Protein measurement with the Folin phenol reagent. *J Biol Chem.* 1951;193(1):265–75.

- [81] Wu M, Neilson A, Swift AL, Moran R, Tamagnine J, Parslow D, et al. Multiparameter metabolic analysis reveals a close link between attenuated mitochondrial bioenergetic function and enhanced glycolysis dependency in human tumor cells. *Am J Physiol Cell Physiol.* 2007;292(1):C125–36.

- [82] Song YH, Song JL, Delafontaine P, Godard MP. The therapeutic potential of IGF-I in skeletal muscle repair. *Trends Endocrinol Metab. Elsevier Ltd*; 2013;24(6):310–9.

- [83] Bloemberg D, Quadrilatero J. Rapid determination of myosin heavy chain expression in rat, mouse, and human skeletal muscle using multicolor immunofluorescence analysis. *PLoS One*. 2012;7(4).
- [84] Mathewson MA, Chapman MA, Hentzen ER, Fridén J, Lieber RL. Anatomical, architectural, and biochemical diversity of the murine forelimb muscles. *J Anat*. 2012;221(5):443–51.
- [85] Green HJ, Reichmann H, Pette D. Inter- and intraspecies comparisons of fibre type distribution and of succinate dehydrogenase activity in type I, IIA and IIB fibres of mammalian diaphragms. *Histochemistry*. 1984;81(1):67–73.
- [86] GTEx Consortium. The Genotype-Tissue Expression (GTEx) pilot analysis: Multitissue gene regulation in humans. *Science* (80-). 2015;348(6235):648–60.
- [87] Musarò A, McCullagh K, Paul A, Houghton L, Dobrowolny G, Molinaro M, et al. Localized IGF-1 transgene expression sustains hypertrophy and regeneration in senescent skeletal muscle. *Nat Genet*. 2001;27(2):195–200.
- [88] Christoffolete MA, Silva WJ, Ramos GV, Bento MR, Costa MO, Ribeiro MO, et al. Muscle IGF-1-Induced Skeletal Muscle Hypertrophy Evokes Higher Insulin Sensitivity and Carbohydrate Use as Preferential Energy Substrate. *Biomed Res Int*. 2015;2015.
- [89] Lynch GS, Cuffe SA, Plant DR, Gregorevic P. IGF-I treatment improves the functional properties of fast- and slow-twitch skeletal muscles from dystrophic mice. *Neuromuscul Disord*. 2001;11(3):260–8.
- [90] Messi ML, Delbono O. Target-derived trophic effect on skeletal muscle innervation in senescent mice. *J Neurosci*. 2003;23(4):1351–9.

- [91] Lin J, Wu H, Tarr PT, Zhang C-Y, Wu Z, Boss O, et al. Transcriptional co-activator PGC-1 alpha drives the formation of slow-twitch muscle fibres. *Nature*. 2002;418(6899):797–801.
- [92] Suwa M, Nakano H, Radak Z, Kumagai S. Short-term adenosine monophosphate-activated protein kinase activator 5-aminoimidazole-4-carboxamide-1- β -D-ribofuranoside treatment increases the sirtuin 1 protein expression in skeletal muscle. *Metabolism*. Elsevier B.V.; 2011;60(3):394–403.
- [93] Garcia-Roves PM, Osler ME, Holmström MH, Zierath JR. Gain-of-function R225Q mutation in AMP-activated protein kinase γ 3 subunit increases mitochondrial biogenesis in glycolytic skeletal muscle. *J Biol Chem*. 2008;283(51):35724–34.
- [94] Hardie DG. AMP-activated/SNF1 protein kinases: conserved guardians of cellular energy. *Nat Rev Mol Cell Biol*. 2007;8(10):774–85.
- [95] Lipina C, Kendall H, McPherron AC, Taylor PM, Hundal HS. Mechanisms involved in the enhancement of mammalian target of rapamycin signalling and hypertrophy in skeletal muscle of myostatin-deficient mice. *FEBS Lett*. Federation of European Biochemical Societies; 2010;584(11):2403–8.
- [96] Izumiya Y, Hopkins T, Morris C, Sato K, Zeng L, Viereck J, et al. Fast/Glycolytic Muscle Fiber Growth Reduces Fat Mass and Improves Metabolic Parameters in Obese Mice. *Cell Metab*. 2008;7(2):159–72.
- [97] McPherron AC, Guo T, Bond ND, Gavrilova O. Increasing muscle mass to improve metabolism. *Adipocyte*. 2013;2(2):92–8.
- [98] Bernardo BL, Wachtmann TS, Cosgrove PG, Kuhn M, Opsahl AC, Judkins KM, et al. Postnatal PPAR δ activation and myostatin inhibition exert distinct yet complimentary effects on the metabolic profile of obese insulin-resistant mice. *PLoS One*. 2010;5(6).

- [99] McPherron A, Guo T, Wang Q, Portas J. Soluble activin receptor type IIB treatment does not cause fat loss in mice with diet-induced obesity. *Diabetes Obes Metab.* 2012;14(3):279–82.
- [100] Moyer AL, Wagner KR. Mammalian Mss51 is a skeletal muscle-specific gene modulating cellular metabolism. *J Neuromuscul Dis.* 2015;preprint(preprint):1–15.
- [101] Su J, Ekman C, Oskolkov N, Lahti L, Ström K, Brazma A, et al. A novel atlas of gene expression in human skeletal muscle reveals molecular changes associated with aging. *Skeletal Muscle.* *Skeletal Muscle*; 2015;5(1):35.
- [102] Gross CT, McGinnis W. DEAF-1, a novel protein that binds an essential region in a Deformed response element. *EMBO J.* 1996;15(8):1961–70.
- [103] Melnick AM, Westendorf JJ, Polinger A, Carlile GW, Arai S, Ball HJ, et al. The ETO protein disrupted in t(8;21)-associated acute myeloid leukemia is a corepressor for the promyelocytic leukemia zinc finger protein. *Mol Cell Biol.* 2000;20(6):2075–86.
- [104] Lutterbach B, Westendorf JJ, Linggi B, Patten A, Moniwa M, Davie JR, et al. ETO, a target of t(8;21) in acute leukemia, interacts with the N-CoR and mSin3 corepressors. *Mol Cell Biol.* 1998;18(12):7176–84.
- [105] Lutterbach B, Sun D, Schuetz J, Hiebert SW. The MYND motif is required for repression of basal transcription from the multidrug resistance 1 promoter by the t(8;21) fusion protein. *Mol Cell Biol.* 1998;18(6):3604–11.
- [106] Masselink H, Bernards R. The adenovirus E1A binding protein BS69 is a corepressor of transcription through recruitment of N-CoR. *Oncogene.* 2000;19(12):1538–46.

- [107] Jinek M, Chylinski K, Fonfara I, Hauer M, Doudna JA, Charpentier E. A Programmable Dual-RNA– Guided DNA Endonuclease in Adaptive Bacterial Immunity. *Science* (80-). 2012;337(August):816–21.
- [108] Mali P, Esvelt KM, Church GM. Cas9 as a versatile tool for engineering biology. *Nat Methods*. 2013;10(10):957–63.
- [109] Wang H, Yang H, Shivalila CS, Dawlaty MM, Cheng AW, Zhang F, et al. One-step generation of mice carrying mutations in multiple genes by CRISPR/Cas-mediated genome engineering. *Cell*. Elsevier Inc.; 2013 May 9;153(4):910–8.
- [110] Partridge TA. Tissue culture of skeletal muscle. *Methods Mol Biol*. 1997;75:131–44.
- [111] DeBalsi KL, Wong KE, Koves TR, Slentz DH, Seiler SE, Wittmann AH, et al. Targeted metabolomics connects thioredoxin-interacting protein (TXNIP) to mitochondrial fuel selection and regulation of specific oxidoreductase enzymes in skeletal muscle. *J Biol Chem*. 2014;289(12):8106–20.
- [112] Collins S, Martin TL, Surwit RS, Robidoux J. Genetic vulnerability to diet-induced obesity in the C57BL/6J mouse: physiological and molecular characteristics. *Physiol Behav*. 2004;81(2):243–8.
- [113] Taicher GZ, Tinsley FC, Reiderman A, Heiman ML. Quantitative magnetic resonance (QMR) method for bone and whole-body-composition analysis. *Anal Bioanal Chem*. 2003;377(6):990–1002.
- [114] Kobilko T, Guerrieri D, Zhang Y, Collica SC, Becker KG, van Praag H. AMPK agonist AICAR improves cognition and motor coordination in young and aged mice. *Learn Mem*. 2014;21(2):119–26.
- [115] Rozman J, Klingenspor M, Hrabě de Angelis M. A review of standardized

metabolic phenotyping of animal models. *Mamm Genome*. 2014;25(9-10):497–507.

- [116] Wagner KR, McPherron AC, Winik N, Lee SJ. Loss of myostatin attenuates severity of muscular dystrophy in mdx mice. *Ann Neurol*. 2002;52:832–6.

- [117] Bogdanovich S, Krag TOB, Barton ER, Morris LD, Whittemore L-A, Ahima RS, et al. Functional improvement of dystrophic muscle by myostatin blockade. *Nature*. 2002;420(November):418–21.

- [118] Lee Y-S, Lehar A, Sebald S, Liu M, Swaggart KA, Conover C, et al. Muscle hypertrophy induced by myostatin inhibition accelerates degeneration in dysferlinopathy. 2015;24(20):5711–9.

Curriculum Vitae

ADAM LANDES MOYER

1129 Hollins Street, Baltimore, MD 21223 | 215-896-7945 | moyer.adam@gmail.com

EDUCATION

2015 (Expected) Ph.D. in Cellular and Molecular Medicine, Johns Hopkins University School of Medicine, Thesis Adviser: Kathryn Wagner, M.D./Ph.D.

2007 B.S. in Biology, Ecology concentration, The Pennsylvania State University

2007 B.S. in International Studies, The Pennsylvania State University

2007 B.A. in Spanish, The Pennsylvania State University

RESEARCH EXPERIENCE

National Cancer Institute, Laboratory of Cellular Oncology (2008-2009)

Adviser: Chris Buck, Ph.D.

- Studied human papillomavirus capsid assembly and maturation
- Performed molecular biology techniques including vector cloning, one- and two-dimensional PAGE, and mammalian tissue culture

Smithsonian Tropical Research Institute, Gamboa, Panama (2007-2008)

Adviser: Hermógenes Fernández-Marín, Ph.D.

- Examined social evolution and symbiotic relationships in fungus-growing ants of the tribe *Attini*
- Collected three species of ants in Soberanía National Park, maintained colonies in the laboratory, and studied their defense mechanisms against the fungal parasite *Escovopsis*
- Worked collaboratively with Panamanian college students to collect specimens and analyze data

Penn State University, Department of Veterinary and Biomedical Sciences (2004-2007)

Adviser: Bhushan Jayarao, M.V.Sc., Ph.D., M.P.H.

- Examined prevalence of antibiotic-resistant *Staphylococcus* bacteria in canine nasal cavities to complete an undergraduate honors thesis
- Established relationships with local veterinary hospitals and implemented sample collection protocols during routine veterinary visits

HONORS, FELLOWSHIPS, AND GRANTS

- Johns Hopkins Computational Biology Consulting Core RNA-seq Analysis Grant, 2015
- NIH Cancer Research Training Award (CRTA) Postbaccalaureate Fellowship, Tumor Virus Molecular Biology Section of Laboratory of Cellular Oncology, 2008-2009
- Fulbright U.S. Student Fellowship to Smithsonian Tropical Research Institute, 2007-2008

PUBLICATIONS

1. **Moyer AL** and Wagner KR. (2015). Mammalian Mss51 is a skeletal muscle-specific gene modulating cellular metabolism. *J Neuromuscul Dis.* 2(4):371-385. doi:10.3233/JND-150119
2. Cardone G*, **Moyer AL***, Cheng N, Thompson CD, Dvoretzky I, Lowry DR, Schiller JT, Steven AC, Buck CB, and Trus BL. (2014). Maturation of the human papillomavirus 16 capsid. *MBio.* 5(4):e01104-14. (* joint first author)
3. **Moyer AL** and Wagner KR. (2012). Incomplete degeneration versus enhanced regeneration in skeletal muscle. *J Biol Chem.* 287(30):25549. (Letter to the Editor)
4. **Moyer AL** and Wagner KR. (2011). Regeneration versus fibrosis in skeletal muscle. *Curr Opin Rheumatol.* 23(6):568-73. (Review)
5. Schowalter RM, Pastrana DV, Pumphrey KA, **Moyer AL**, and Buck CB. Merkel cell polyomavirus and two previously unknown polyomaviruses are chronically shed from human skin. *Cell Host Microbe.* 7(6):509-15.

POSTERS AND ABSTRACTS

1. **Moyer AL** and Wagner KR. Mss51 is a newly-described, skeletal muscle-specific gene. Poster session presented at: 3rd Ottawa International Conference on Neuromuscular Biology, Disease & Therapy; 2015 September 24-26; Ottawa, ON, Canada.

MENTORSHIP EXPERIENCE

- Courtney Young (JHU Undergraduate, 2010-2012)
- Jessica Miciak (JHU Undergraduate, 2011-2012)
- Margaret McClary (Washington College Undergraduate, Summer 2013)
- Michelle Brown (JHU Undergraduate, Spring 2014)
- Arjun Ramesh (Gilman School intern, Summer 2014)
- Gwynn Marsh-Armstrong (Middle River High School G&T intern, 2014-2015)
- Pankhuri Jha (JHU Undergraduate, Fall 2015-present)
- Christopher Moad (JHU CMM rotation student, Fall 2015)
- Derrell Frazier (Thread student, 2009-2011)
- Keith Clary (Thread student, 2010-2013)

SERVICE AND LEADERSHIP

Treasurer, Thread Volunteer Alumni Association (2014-present)

- Founding board member involved in creating a network of the hundreds of volunteer alumni from the organization Thread
- Managed the organization's budget with transparency and created an electronic reimbursement request protocol
- Worked on a team to plan events and recruit volunteers and new board members

Tutor and Head of Household, Thread (formerly Incentive Mentoring Program, 2009-2013)

- Served as a family member and a head of household for two underperforming high school students in a family-style mentorship program at a Baltimore City Public School
- Worked to overcome barriers outside of the classroom and increase access to resources, culminating with high school graduation and college enrollment
- Managed a team of volunteers to ensure adequate tutoring coverage, liaised with teachers and parents to facilitate the passage of crucial information

Matchmaker, Baltimore Animal Rescue and Care Shelter (BARCS, 2012-2014)

- Guided members of the public through a high volume city animal shelter, managing introductions and interactions with adoptable dogs
- Attended public events with adoptable dogs to promote the animal shelter and engage community members

Secretary, Mt. Clare Street Community Garden (2012-2013)

- Kept organized minutes and maintained the website for an urban community garden as it underwent significant structural changes including its incorporation in a Baltimore land trust

Finance Committee Member, Hollins Roundhouse, Inc. (2015)

- Filed non-profit tax forms and made decisions by consensus regarding neighborhood association budgets and processes of a neighborhood association

Secretary, Hollins Roundhouse, Inc. (2015-2016)

- Recorded and disseminated meeting minutes for the board and general body of a neighborhood association
- Reduced number of communications by implementing a weekly newsletter of events and announcements relevant to community members, shared by email as well as by posting on the organization's website and Facebook page